DISSERTATIONES
CHIMICAE
UNIVERSITATIS
TARTUENSIS
236

JAN-MICHAEL C. CAYME

Organic-inorganic interactions in experimental and archaeological ceramics

DISSERTATIONES CHIMICAE UNIVERSITATIS TARTUENSIS
236

DISSERTATIONES CHIMICAE UNIVERSITATIS TARTUENSIS
236

JAN-MICHAEL C. CAYME

Organic-inorganic interactions in experimental and archaeological ceramics

UNIVERSITY OF TARTU
Press
1632

Institute of Chemistry, Faculty of Science and Technology, University of Tartu, Estonia

Dissertation is accepted for the commencement of the degree of *Doctor Philosophiae* (PhD) in Analytical Chemistry on December 10th, 2024 by the Council of Institute of Chemistry, Faculty of Science and Technology, University of Tartu

Supervisors:	Associate Professor Ester Oras, PhD Institute of Chemistry, University of Tartu, Estonia Institute of History and Archaeology, University of Tartu, Estonia
	Associate Professor Signe Vahur, PhD Institute of Chemistry, University of Tartu, Estonia
	Professor Ivo Leito, PhD Institute of Chemistry, University of Tartu, Estonia
Opponent:	Dr. Léa Drieu, PhD Université Côte d'Azur-National Centre for Scientific Research (CNRS), France
Commencement:	February 10th, 2025 at 14.15, Auditorium 1020, Ravila 14A (Chemicum), Tartu and Microsoft Teams

Publication of this dissertation is granted by University of Tartu, Estonia.

This work has been partially supported by Estonian Research Council (Grant PSG492, PRG1198), ASTRA project PER ASPERA Graduate School of Functional Materials and Technologies receiving funding from the European Regional Development Fund under project in University of Tartu, Estonia, as well as by the Estonian Ministry of Education and Research (TK210). This work was carried out using the instrumentation at the Estonian Center of Analytical Chemistry (TT4, https://www.akki.ee) and Centers of Excellence, TK141 'Advanced materials and high-technology devices for energy recuperation systems'.

ISSN 1406-0299 (print)
ISBN 978-9916-27-788-1 (print)

ISSN 2806-2159 (pdf)
ISBN 978-9916-27-789-8 (pdf)

University of Tartu Press
www.tyk.ee

TABLE OF CONTENTS

LIST OF ORIGINAL PUBLICATIONS

I. Vahur, S., Kiudorv, L., Somelar, P., **Cayme, J.-M.**, Retrato, M.D.C., Remigio, R.J., Sharma, V., Oras, E., Leito, I. (2021). Quantitative mineralogical analysis of clay-containing materials using ATR-FT-IR spectroscopy with PLS method. *Analytical and Bioanalytical Chemistry*, 413, 6535–6550. https://doi.org/10.1007/s00216-021-03617-9

II. **Cayme, J.-M.C.**, Palm, R., Somelar, P., Vahur, S., Leito, I., Oras, E. (2024). Influence of mineral composition and firing temperature on the micro- and mesoporosity of replicate archaeological ceramics. *Clays and Clay Minerals*, 72, e13, 1–14. https://doi.org/10.1017/cmn.2024.18

III. **Cayme, J.-M.C.**, Vahur, S., Teearu, A., Oras, E., Leito, I. (2024). The impact of mineral composition on the yield and preservation of selected fatty acids in replicate archaeological ceramics. *Journal of Chemical Metrology*, 18(2), 95–113. http://doi.org/10.25135/jcm.117.2409.3336

Author's contribution

I. Coauthor in preparing the manuscript; prepared some of the selected clay samples for ATR-FT-IR and XRD analysis; performed ATR-FT-IR measurements on some of the selected clay samples.

II. Lead author in preparing the manuscript; prepared the clay briquettes for XRD and N_2 porosimeter analysis; performed N_2 porosimeter measurements on the clay briquettes; partially interpreted the N_2 adsorption data; created the clay briquettes used for testing.

III. Lead author in preparing the manuscript; performed extraction, derivatization, optimization and GC-MS analysis; interpreted the GC-MS data; created the clay briquettes used for testing.

ABBREVIATIONS

ACM	acid-catalyzed methylation
ATR-FT-IR	attenuated total reflection Fourier transform infrared
BET	Brunauer-Emmett-Teller
CI	confidence interval (at 95%)
DA	discriminant analysis
DSC	differential scanning calorimeter
EI	electron ionization
EIC	extracted ion chromatogram
FAME	fatty acid methyl esters
FT-ICR-MS	Fourier transform ion cyclotron resonance mass spectrometry
GC-C-IRMS	gas chromatography-combustion-isotope mass spectrometry
GC-FID	gas chromatography-flame ionization detector
GC-MS	gas chromatography-mass spectrometry
IUPAC	International Union of Pure and Applied Chemistry
LA-ICP-MS	laser ablation-inductively coupled plasma-mass spectrometry
LC-MS	liquid chromatography-mass spectrometry
LIBS	laser-induced breakdown spectroscopy
MALDI	matrix assisted laser desorption/ionization
m	slope
MethPrep II	methanolic solution of TMTFTH
NLDFT	non-local density function theory
ORA	organic residue analysis
PCA	principal component analysis
PIXE	particle-induced X-ray emission
PLS	partial least squares
R^2	squared correlation coefficient
RMSEC	root mean square error of calibration
RMSECV	root mean square error of cross-validation
RMSEP	root mean square error of prediction
S_{BET}	specific surface area using Brunauer-Emmett-Teller
S_{micro}	specific surface area of micropores
S_{NLDFT}	specific surface area using non-local density function theory
$S_{NLDFT,micro}$	specific surface area using non-local density function theory, micropores
SEM-EDX	scanning electron microscopy with energy dispersive X-ray spectroscopy
SNV	standard normal variate
TG-DTA	thermogravimetry differential thermal analysis
TIC	total ion chromatogram
TMTFTH	m-(trifluoromethyl)phenyltrimethylammonium hydroxide
ToF-SIMS	time-of-flight secondary ion mass spectrometry
UHPLC	ultra-high-performance liquid chromatography

$V_{0.95}$	volume of pores calculated from the amount of adsorbed nitrogen gas at $p/p° = 0.95$
V_{micro}	volume of micropores
V_{NLDFT}	pore volume using non-local density function theory
$V_{NLDFT,micro}$	pore volume using non-local density function theory, micropores
XRD	X-ray diffraction
XRF	X-ray fluorescence

1 INTRODUCTION

Clay is the fundamental raw material used for manufacturing traditional artefacts commonly encountered in daily life, such as ceramic containers (i.e., pottery), decorative elements, figurines, and masonry materials (i.e., bricks). It is ideal for these purposes due to its natural abundance, easy retrieval from the surrounding environment, and suitability for large-scale production. Preparation of the material is also relatively straightforward, involving the shaping of raw clay in its wet state, allowing them to dry, and then firing at elevated temperatures. The physical and chemical properties of ceramic artefacts depend on the type of clay used and the specific firing temperature. Due to the ease of manufacture and durability, clay ceramics have become an essential resource for human societies throughout history, serving as tangible links to understanding past cultures (Santacreu 2014; Eramo 2020).

In most archaeological finds, pottery, a type of ceramic vessel produced from raw clay, is the most abundant artefact. Analyzing pottery assemblages provides valuable insights into various activities and behaviours of past communities, which include trade networks, socio-economic developments, production techniques, and technological and cultural exchanges (Tite et al. 2001; Barone et al. 2005; İssi et al. 2011; Povlsen 2013; Sanjurjo-Sánchez et al. 2018; Papakosta et al. 2020). Pottery is an ideal artefact for such analysis because it was widely used in daily life, often produced locally to meet specific needs, and is well-preserved in terms of archaeological contexts. Although the physical shape, form, and the manufacturing technology of pottery may suggest specific vessel functions, these attributes are often complicated to interpret and generally lead to determining broad functional categories rather than its intended use (Oudemans 2007).

Examining traces of direct usage, particularly organic residues left on the pottery, whether absorbed within the pottery matrix or visible as food crusts on the surface, can reveal remnants of the vessel's original contents, offering more direct evidence of its intended function (Evershed 2008a; Regert 2011; Craig et al. 2012; Roffet-Salque et al. 2017). Extracting and characterizing these preserved organic compounds in the pottery to determine their origin involves analytical techniques jointly called Organic Residue Analysis (ORA). Through the application of ORA, various classes of organic compounds, or archaeological biomarkers, have been identified in ancient pottery, which includes lipids, waxes, resinous materials (Regert et al. 2003; Lucquin et al. 2007; Craig et al. 2011; Roffet-Salque et al. 2015; Dunne et al. 2016; Rageot et al. 2021; Chen et al. 2024), and proteinaceous compounds (Barker et al. 2012; Hendy et al. 2018; Evans et al. 2023). While extensive degradation during past cooking events and subsequent post-depositional processes have altered the structures of the original parent compounds, a significant amount of molecular information can remain detectable (Dudd et al. 1998; Regert et al. 1998; Evershed 2008b). Based on the class of compounds identified through ORA, insights into the original use of pottery can be determined, contributing to a wider archaeological understanding

of ancient food ways and subsistence strategies (Evershed 2008b; Salque et al. 2013; Šoberl et al. 2014; Roffet-Salque et al. 2017; Chasan et al. 2022; Evershed et al. 2022; Manoukian et al. 2022; Oras et al. 2023).

Lipids have been the primary focus of most ORA studies due to their chemical stability as archaeological biomarkers and the possibility to differentiate between animal and plant sources in both food and non-food commodities. Many factors can influence the accumulation of lipids in pottery, including vessel use, cooking methods, the nature of the food or non-food products processed, and the properties of the clay material. Several rigorous methodological discussions focussing on identifying lipid compounds from pottery have been previously published (Evershed 2008b; Roffet-Salque et al. 2017; Whelton et al. 2021). However, the role of the inorganic components in clay pottery for overall lipid preservation and yield remains largely unexplored (Steele 2013). Thus far, investigations into the interactions between organic compounds and the clay matrix have primarily focused on the porosity analyses of archaeological pottery (Matlova et al. 2017; Drieu et al. 2019) and the use of experimental pottery prepared from a single mixture of clay and temper (Goldenberg et al. 2014; Hammann et al. 2020). Establishing how different clay types, tempers, and firing temperature affect the physiochemical properties of pottery and how these influence the binding of organic compounds could yield significant insights into the mechanism of lipid retention in ancient ceramics. This information could contribute to better informed sample selection that would maximize the possible lipid yield and acknowledging analytical limitations in archaeological pottery ORA.

In this doctoral study, the crucial role of the inorganic clay matrix in relation to the preservation and retention of selected lipid compounds was investigated. A comprehensive set of replicate briquettes mimicking variations in archaeological ceramics were produced using varying amounts and different types of clays (i.e., illite/illite-smectite and kaolinite), tempers (i.e., sand and chalk), and fired at different temperatures of 600°C and 800°C, respectively. The resulting changes in the mineral structure and the development of micro- and mesopores within the briquettes were analyzed to tackle the correlations between lipid binding and porosity of the clay material. Two sets of these briquettes were used to investigate the quantitative yield of selected fatty acids, specifically palmitic acid ($C_{16:0}$) and oleic acid ($C_{18:1}$), which are common compounds extracted from archaeological pottery that are associated with food from animal or plant origin. Within these sets, one group of clay samples spiked with $C_{16:0}$ and $C_{18:1}$ was allowed to adsorb and air dried without further treatments (non-degraded), while another group was subjected to degradation at 100°C for 14 h to mimic cooking events (degraded). The methodology developed in this study, was further tested on real-life 12th–13th century AD archaeological pottery samples, excavated from Kukruse cemetery, Estonia, and the results were compared to the experimental briquettes.

Various analytical techniques were utilized in this doctoral study to investigate the potential interactions between the inorganic clay matrix and the organic compounds in both the replicate experimental clay briquettes and the archaeological samples. These techniques included attenuated total reflection Fourier transform

infrared (ATR-FT-IR) spectroscopy, X-ray diffraction (XRD), nitrogen (N_2) porosimeter, and gas chromatography-mass spectrometry (GC-MS).

This doctoral study focused on two primary directions:

(1) The quantitative analysis of clay and non-clay minerals, and the determination of clay micro- and mesoporosity (**Paper 1** and **Paper 2**).
(2) The quantification of organic compounds, namely $C_{16:0}$ and $C_{18:1}$ fatty acids retained on the replicate pottery briquettes (**Paper 3**), and a case study using archaeological pottery.

For the characterization of the clay components, a rapid and minimally invasive quantitative method was utilized, employing an ATR-FT-IR with Partial Least Squares (PLS) technique. This analytical method demonstrated mostly good comparability with XRD and enabled quantifying groups of mineral phases in the samples, although in some cases at semiquantitative level. The ATR-FT-IR-PLS method was able to quantify well the groups of minerals to which the organic residues may possibly bind − calcium carbonate and specific clay mineral groups (e.g. kaolinite, illite, and illite-smectite) that have been associated with lipid retention in archaeological pottery. Furthermore, this method is very suitable for analysing cultural heritage and archaeological materials because it requires minimal amount of sample.

Having established a method for quantifying the mineral phases in clays, the porosity of the replicate ceramic pottery and archaeological case study samples were investigated using the N_2 porosimeter. Porosity is considered as one of the key factors in the preservation of organic compounds within ancient pottery, as pores can act as protective barriers against microbial attack and environmental degradation across archaeological timescales (Drieu et al. 2019). This doctoral research investigated the formation of micro- and meso-sized pores (with widths < 50 nm), resulting from various combinations of clay types, tempers, and firing temperatures, and also for real-life archaeological pottery. It has been reported that smaller-sized pores, such as micropores, seem to better protect the organic residues due to their nanometer sizes (Matlova et al. 2017). The results of this part of the study would contribute to a better understanding of the development of pores within clay ceramics and served as a baseline information for further investigations of lipid adsorption.

After determining the mineral content and the micro- and mesoporosity of the replicate clay ceramics, a representative set of samples with diverse compositions were spiked with $C_{16.0}$ and $C_{18.1}$. One part of the set underwent heat degradation, while the other remained untreated. Two derivatization techniques were evaluated to determine the most effective method for quantifying the organic compounds present in the spiked clay briquettes. These methods are acid catalyzed methylation (ACM) compared with a methanol and dichloromethane extraction, followed by TMTFTH methylation. Absolute quantification of the methylated $C_{16.0}$ and $C_{18.1}$ was achieved using a FAME standard calibration curve and GC-MS.

Building on the above, this doctoral study addresses the following research questions:

- What is the progression of the changes in the mineral structure of clay ceramics, with various amounts of clay types and sand or chalk temper, fired at 600°C and 800°C?
- How do these mineralogical changes influenced the formation of micro- and mesoporosity in the clay, which is relevant for determining the pottery composition that would produce more pores?
- How does the clay composition – temper type and amount – and the resulting micro- and mesoporosity affected the extraction yield of $C_{16:0}$ and $C_{18:1}$ fatty acids?

Relying on these experimental settings and analytical approaches, the overarching aim of this doctoral study is to highlight the major mineralogical and porosity related physio-chemical characteristics affecting the adsorption and retention of lipid compounds, using two representative archaeological fatty acids ($C_{16:0}$ and $C_{18:1}$) as model residues. The results have further implications for selecting ceramic samples and interpreting lipid quantities in the fields of archaeology and cultural heritage, specifically pottery organic residue analysis, but also wider environmental and geological studies including clay minerology and organic components.

2 LITERATURE OVERVIEW

2.1 Clays

Clays are one of the natural constituents of soil, classified as fine-grained with particle sizes smaller than 2 μm, and formed through the erosion and weathering of sedimentary rocks over geological timescales. Soils that contain clays exhibit cohesive properties and become plastic when water is added (Velde and Meunier 2008; Schroeder 2018). These properties allow clays to act as binders for larger, coarse-grained particles in soil, which makes it an ideal raw material for manufacturing ceramics since ancient times. While clay minerals are the primary components of clay fractions in soils, these fractions also consist of various associated phases in clay (i.e. non-clay minerals) that do not impart plasticity (Guggenheim and Martin 1995). Depending on the geological location, these would include silicates (e.g. quartz and feldspars), carbonates (e.g. calcite and dolomite), sulfates (e.g. gypsum), oxides and hydroxides (e.g. hematite and gibbsite), sulfides, phosphates, and halides.

2.1.1 Clay mineralogy

Clay minerals are crystalline hydrous aluminum silicates or phyllosilicates which are arranged in thin sheets of repeating tetrahedral and octahedral units. The tetrahedral sheets are formed by the linkage of the basal O^{2-} anions in each tetrahedral unit, either SiO_4^{4-} or AlO_4^{5-}, sharing a cation pair. A continuous octahedral sheet, with central atoms of Al^{3+} or Mg^{2+}, is formed by the sharing of the O^{2-} or OH^- anions at the six vertices of each octahedral unit. These structural units are stacked together in repeating layers. The way these units are layered, as well as the different bonding interaction of various metallic ions within the crystal lattice, determines the formation of distinct clay mineral types (Brigatti et al. 2006; Velde and Meunier 2008).

The general crystal structure of phyllosilicates is derived from two basic layer types, the 1:1 group (two-layer structure) and the 2:1 group (three-layer structure), which differ in the number and arrangement of the tetrahedral and octahedral sheets (Figure 2.1.1.1). Mixed layer minerals can also develop through the stacking of two or more of these basic layer types, such as combinations of different 2:1 groups or 2:1:1 and 1:1 groups. Due to the similarities in the presence of Si-O and Al-O bonds, as well as the closely packed arrangement of these layers, variations in the orientations of clay minerals can readily occur in mixed layers.

In the 1:1 group, one tetrahedral sheet is bonded to one octahedral sheet through shared oxygen atoms, coming from the apical of the tetrahedra and one of the vertices of the octahedra. Strong hydrogen bonds hold together the successive layers of the 1:1 group, making it less plastic compared to the other clay minerals and resulting in the formation of larger, stacked crystals. Kaolinite ($Al_2Si_2O_5(OH)_4$) is an example of a clay mineral belonging to the 1:1 group and

is utilized as a raw material in making porcelain ceramics (Schroeder and Erickson 2014).

The 2:1 group consists of two tetrahedral sheets positioned on either side of a central octahedral sheet. These sheets are connected through the apical oxygens of the two tetrahedra, which are shared within different vertices of the octahedra. With this layered arrangement, water molecules and other exchangeable ions such as Ca^{2+}, Mg^{2+}, Na^{+} and K^{+} can enter the interlayer space between stacked 2:1 layers and expand them (swelling), which is made possible by the weak van der Waals forces between the stacked layers and a deficient net negative charge in the octahedral sheet. These properties contribute to the structural diversity of the 2:1 group, resulting in various clay mineral types within this category. Examples of 2:1 group minerals include illite and montmorillonite (i.e. main component of smectites), which differ in the types of exchangeable cations bonding their interlayer (Velde and Meunier 2008). These clay minerals are widely used in pottery and brick ceramics, often recognizable by their red color (Ferrari and Gualtieri 2006; Mahmoudi and Bennour 2022).

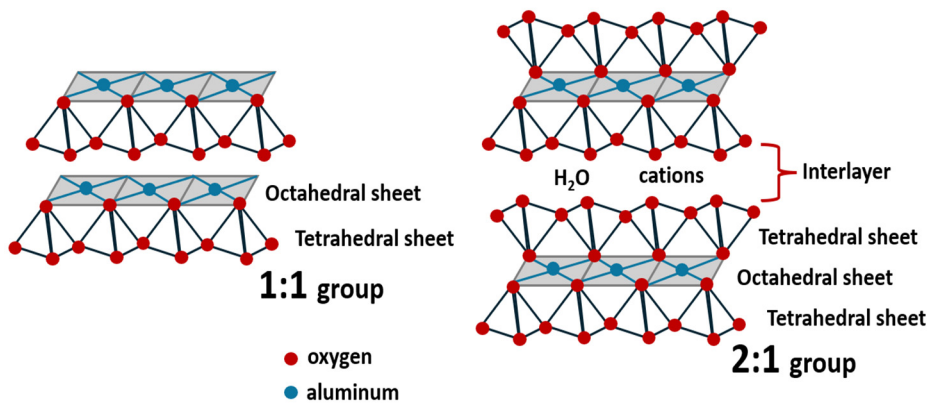

Figure 2.1.1.1. Schematic representation of a 1:1 (two-layer structure, like kaolinite) and 2:1 (three-layer structure, such as illite and montmorillonite) groups. The layer stacking is also represented.

2.1.2 Post-firing mineralogical changes

The application of heat to natural clays to create ceramic materials has been a well-established practice since ancient times (Rice 2015). Early methods of ceramic production typically involved firing in open pits or primitive kilns, often resulting in uneven heat distributions and contributing to the variability in the final properties of the material. Firing alters the clay's original microstructure, forming a complex set of mineralogical transformations that depend on the maximum temperature reached (Moropoulou et al. 1995; El Ouahabi et al. 2015).

Mineral phase transformations in clays during firing generally occur in three thermal stages: dehydration, dehydroxylation, and recrystallization (Hanein et al.

2022). Several factors can influence the formation of post-firing minerals, including the specific types of clay mineral groups present (i.e., 1:1 group, 2:1 group and mixed layer) (Moropoulou et al. 1995; McConville and Lee 2005), the degree of order or disorder of the layer stackings (Wolters and Emmerich 2007; Ptáček et al. 2013; Izadifar et al. 2020), and the addition of tempers such as non-clay mineral inclusions (i.e., crushed rocks and shells) and organic additives (i.e., hair and plant fibers) (Santacreu 2014; Maritan et al. 2019). The presence of fluxing agents, such as oxides of K^+ and Na^+, also affects phase transformations by lowering the melting point of the minerals, facilitating the vitrification process (Trindade et al. 2010; Msinjili et al. 2019).

Dehydration takes place when the clay is heated from room temperature to about 300°C, during which adsorbed molecular water on the outer clay surface, as well as the interlayer water in 2:1 clay mineral group, is removed from the pores of the clay matrix (Kubliha et al. 2017; Derkowski and Kuligiewicz 2022). This stage is followed by dehydroxylation, wherein the structural hydroxyl groups in the clay lattice collapse between 400°C and 900°C (Frost and Vassallo 1996; Hanein et al. 2022). Generally, 1:1 group clays dehydroxylate at a lower and narrower temperature range compared to 2:1 group, converting to amorphous phases at a lower temperature (Escalera et al. 2012). Depending on the bond strengths, crystal purity and stackings, kaolinite, a 1:1 group, usually transforms into its meta-form from 400°C to 600°C (Frost et al. 2003; Xue et al. 2023), while 2:1 group, such as illite and smectite, can persist until 900°C (Wolters and Emmerich 2007; Msinjili et al. 2019; Derkowski and Kuligiewicz 2022). Within this temperature range, non-clay minerals such as calcite ($CaCO_3$) will also start undergoing decomposition at around 700°C until it reaches 850°C (Allegretta et al. 2015; Karunadasa et al. 2019). An increase in temperature above 950°C will eventually lead to the collapse of the crystalline structure of clay minerals and recrystallization will develop, resulting in the formation of more stable high-temperature phases from structurally disordered clay minerals and the thermal modifications of non-clay minerals (Santacreu 2014; Hanein et al. 2022). Certain non-mineral phases, such as quartz, plagioclase and hematite, can also retain its mineral form at temperatures exceeding 1000°C (Laita and Bauluz 2018; Miras et al. 2018).

Understanding the thermal transformations of minerals in clays is relevant in archaeological contexts, particularly for estimating the firing temperature achieved during ceramic production (Cultrone et al. 2001; Daghmehchi et al. 2018; Botticelli et al. 2020; Rahman et al. 2024) and in determining whether the firing process took place in a kiln or open pits (Gliozzo 2020). These insights are crucial for assessing how the raw clay material and the temper additions may have influenced the physical properties of ceramics (i.e. pottery). One example of a physical property influenced by the degree of firing is the formation of different sized pores, resulting from changes in the mineralogical structures (Musthafa et al. 2010; Mondelli et al. 2020; Cayme et al. 2024a). The development of porosity in pottery also has significant implications in organic residue preservation (Evershed 2008a; Matlova et al. 2017; Drieu et al. 2019). In general, knowledge

of the firing temperature can provide direct evidence for evaluating technological capabilities of past societies, tracing the provenance of ceramic materials, and in reconstructing possible trade networks (Chatfield 2010; Damjanović et al. 2014; Mentesana et al. 2019; Thér et al. 2019; Casale et al. 2022).

2.1.3 Identification of clay and non-clay minerals in ceramics

Clay ceramics, specifically pottery materials, can be viewed as a combination of the compositional factors (i.e. original clay and temper materials), mechanical process (i.e. kneading and moulding), and the thermal transformation of the raw material (Eramo 2020). In the case of archaeological pottery, additional physical and chemical alterations may also result from use-wear during its functional lifetime and from post-depositional processes (Golitko et al. 2012; Vieugué 2014; Sanchez-Garmendia et al. 2021). Use-wear related alterations, such as surface carbonation, is a result of soot deposition associated with cooking fires and charring of food during cooking events (Skibo 2015; Forte et al. 2018). An example of post-depositional processes is the dissolution of calcite in carbonate-rich ceramics, which can alter the bulk elemental composition of the pottery, particularly when buried in acidic soil environments or exposed to groundwater seepage (Maritan 2020; Gilstrap et al. 2021).

Various analytical techniques (see below) are available for analyzing and characterizing the mineral composition of pottery, with the choice of method depending on the specific type of information being investigated and availability. These techniques are often used in combination with one other to achieve a more comprehensive understanding of the material properties. Statistical methods have significantly improved the accuracy of mineral quantification, particularly in the context of cultural heritage and archaeological clay artefacts, where sample availability is often limited (Madariaga 2015). Furthermore, the advancement of analytical techniques in the cultural heritage and archaeology field in the past decades has primarily focused on the development of non-invasive to minimally invasive techniques (Holakooei et al. 2019; Bruni et al. 2023; Pérez et al. 2024).

Frequently employed analytical techniques in clay identification and characterization include: (1) spectroscopy methods, such as Raman spectroscopy (Bersani and Lottici 2016; Carter et al. 2017), Fourier transform infrared spectroscopy (FT-IR) including attenuated total reflection (ATR) sampling method (Tarhan et al. 2021, 2024; Vahur et al. 2021), and laser-induced breakdown spectroscopy (LIBS) (Melessanaki et al. 2002; Genc Oztoprak et al. 2016); (2) X-ray techniques, including X-ray diffraction (XRD) (Moon et al. 2021; Singh et al. 2021), X-ray fluorescence (XRF) (Tanasi et al. 2017; Liritzis et al. 2020), and particle-induced X-ray emission (PIXE) (Bakraji et al. 2015; Roumie et al. 2019); (3) mass spectrometry techniques, which includes laser ablation-inductively coupled plasma-mass spectrometry (LA-ICP-MS) (Gehres and Querré 2018; Vannoorenberghe et al. 2020); (4) microscopy technique coupled with spectroscopy method, specifically scanning electron microscopy with energy dispersive X-ray spectroscopy (SEM-EDX) (Knappett et al. 2011; Dey et al. 2020); and (5)

thermal methods, such as differential scanning calorimetry (DSC) (Drebushchak et al. 2005; Giordana et al. 2004) and thermogravimetry differential thermal analysis (TG-DTA) (Ravisankar et al. 2014; Tamilarasi and Chandrasekaran 2023).

Chemometric methods, also referred to as multivariate statistical methods, are often applied for analyzing quantitative data, particularly when large datasets are available from a specific analytical technique (Akyuz et al. 2019; Festa et al. 2019; Ferri et al. 2020; Papageorgiou 2020). These statistical methods have greatly improved the accuracy of the quantitative results and facilitates the comparison of unknown samples with reference datasets. In the field of cultural heritage and archaeology, the common chemometric applications include principal component analysis (PCA), partial least squares (PLS), and correlation analysis, with PCA being the most widely used method (Hayes et al. 2014; Bitetto et al. 2016; Peets et al. 2017, 2019; Vahur et al. 2019, 2021; Işik and Tarhan 2021; Chen et al. 2022).

Among the analytical techniques mentioned, XRD is the most reliable method for quantitative analysis of clay minerals due to their regular and repeating crystal structures, which enable them to diffract X-rays and produce distinct patterns based on their crystal arrangement (Bunaciu et al. 2015). The XRD data can reveal the changes in the mineral composition that occurred in the pottery, including the remnants of the raw materials used (i.e. clay and temper), the thermal transformations as a result of firing, and the post-depositional effects during burial (Eramo 2020). However, the effectiveness of XRD for quantitative analysis is limited by various factors, examples of which are variations in clay orientations, crystal defects in clay minerals, and the presence of mixed-layer phases and amorphous phases (Dohrmann et al. 2009; Zhou et al. 2018; Ali et al. 2022; Xiao et al. 2023a). Furthermore, XRD is not a sensitive technique for trace level analysis of mixed minerals which has a detection limit of approximately 2 wt. % of the sample (Ali et al. 2022).

FT-IR, on the other hand, has been a complementary analytical technique to XRD for mineral quantification of clays (Craddock et al. 2017; Hahn et al. 2018; Vahur et al. 2021) and has gained increasing use due to its non-destructive to minimally destructive approach, making it particularly suitable for archaeological and cultural heritage materials (Monnier 2018; Liu and Kazarian 2022; Macchia et al. 2023). FT-IR can detect poorly crystalline clay mineral phases and other inorganic minerals, since each mineral exhibits a unique absorption pattern in the infrared region (Shoval 2017). Various application techniques, such as ATR, have been employed for mineral quantification of clays using chemometric techniques, which greatly enhanced the quantitative ability of FT-IR, especially when the model is built with more calibration sets (Müller et al. 2014; Heath et al. 2016; Vahur et al. 2021). Furthermore, FT-IR offers the added benefits of fast analysis, minimal sample preparation, and small (i.e. few milligrams) sample size (Jordá et al. 2015; Işik and Tarhan 2021). Portable FT-IR instruments are also widely available on the market, allowing for *in situ* analysis (Bouchard et al. 2019; Izzo et al. 2020).

2.1.4 Formation of porosity in clays

The formation of pores is a fundamental characteristic of nearly all pottery microstructures (Rice 2015). These pores, which are pockets of empty spaces or voids, are distributed in-between or within the individual mineral grains of the clay or non-clay components. It may occur in various shapes and types and are generally categorized as open or closed pores. Open pores refer to networks of channels that are connected to the ceramic surface, whereas closed pores are isolated from the surface (Harry and Johnson 2004). Depending on the sizes of pores formed, the International Union of Pure and Applied Chemistry (IUPAC) classifies it as micropores (width < 2 nm), mesopores (width from 2 nm to 50 nm) and macropores (width > 50 nm) (Sing et al. 1985). The ratio between the pore volume, which is derived from the various sizes and types of pores, and the total volume of the sample pottery material defines the porosity (Sobott et al. 2014).

The pore structure of pottery is quite complex, because it reflects the cumulative effect of the potter's choices regarding raw materials, forming techniques, and production technologies (Lindahl and Pikirayi 2010; Gomart et al. 2017; Beltrame et al. 2020; Thér 2020; Cutillas-Victoria and Day 2022). It is possible to alter and introduce pores on the ceramic matrix at any stage of the manufacturing process (Neumannová et al. 2017; Kozatsas et al. 2018). For instance, kneading the clay paste have been shown to eliminate air bubbles, producing smaller and more uniform pores compared to the larger and irregular pores found in unkneaded clays (Drieu 2020).

The physical characteristics of the clay material itself, including the presence of coarse- and fine-grained mineral sizes and the type of temper additives, also contribute significantly to the pore structure of the final pottery product (Van Doosselaere at el. 2014; Kramar and Lux 2015; Cayme et al. 2024a). For instance, low combustion organic-based tempers can result in more open pores as the firing temperature increases (Eramo 2020). Similarly, calcareous clays (Ca > 5%) or calcium-based tempers, such as the addition of limestones or marine shells, also increases the formation of bloated pores due to the release of CO_2 from the decomposition of $CaCO_3$ at a high temperature (T > 600°C) (Maniatis and Tite 1981; Chatfield 2010). Furthermore, as the temperature reaches the vitrification or the glass phase stage (T > 1000°C), the minerals become more amorphous and begin to fuse together, producing a pottery with low porosity (Hein et al. 2007; Dey et al. 2020).

The presence of pores of less than 1μm (1,000 nm) and generally abundant micropores (< 2 nm) in pottery were considered essential for preserving organic residues (Namdar et al. 2009; Drieu et al. 2019). During cooking, prolonged food storage, or the application of sealants, organic residues are physically absorbed into the unglazed pottery matrix and subsequently trapped within these pores (Heron and Evershed 1993; Oudemans 2007). Similarly, glazed ceramics have also been found to retain organic residues, attributed to adsorption within microcracks from use-wear and pores from possible manufacturing flaws (Pecci et al. 2015, 2016). This entrapment eventually protects the residues from post-

depositional processes in harsh burial environments, such as microorganism degradation, pH changes, and water seepage (Dudd et al. 1998; Regert et al. 1998; Evershed 2008b). Studies have shown that organic residues can be extracted from pores of varying sizes in potsherds, which includes micro- to mesopores (< 2 nm to 50 nm) (Cayme et al. 2024b), and meso- to macropores (2 nm to > 50 nm) (Matlova et al. 2017; Drieu et al. 2019; Namdar et al. 2009).

Several characterization methods have been developed to determine the porosity and characterize the pore structures of archaeological pottery. These include direct methods, in which porosity is determined using imaging techniques such as scanning electron microscopy (SEM), thin section optical microscopy, computed tomography, and neutron scattering and imaging techniques. There are also the indirect methods, where gas (i.e. N_2) or liquid (Hg) probes are utilized to obtain data on the porosity of the material, such as N_2 adsorption and mercury intrusion porosimetry (Aili and Maruyama 2020). Each method has its advantages and disadvantages depending on the level of data needed, sample preparation and the scarcity of samples (Klobes et al. 2006).

For direct methods, producing thin section slides and examining them under an optical microscope has traditionally been used as a general visualization tool. This technique not only provides an idea of the mineral inclusions but also describes the pore structure and its association with other minerals (De Vito et al. 2014; Cohen et al. 2018; Fabrizi et al. 2020).

More advanced and accurate non-invasive techniques include SEM (Moraru and Szendrei 2010; Moraru et al. 2011), X-ray computed microtomography (μCT) (Larreina-García et al. 2021; Coli et al. 2022; Reedy and Reedy 2022), and neutron techniques (Barone et al. 2009; Barbera et al. 2013). These techniques provide a wholistic interpretation of the pore sizes and their distribution in the sample, the orientation and connectivity of the pore structures, and the nature of the mineral inclusions. Noteworthy is the ability of these techniques to determine the closed pores which the indirect methods will not be able to detect (Barone et al. 2011; Kahl and Ramminger 2012). The pore structure of pottery is typically dominated by open pores when the pottery is originally fired at lower temperatures ($T < 950°C$). However, if fired at higher temperatures above 950°C, vitrification becomes more extensive, leading to a significant rise in the proportion of closed pores (Rye 1976; Martín-Márquez et al. 2008).

The indirect methods are particularly suited for quantifying the surface area, volume, and the size distribution of open pores. Porosity analysis can be performed using N_2 gas adsorption, where a known amount of N_2 gas is physically adsorbed onto the open pores of the pottery at a subcritical temperature, eventually forming weak intermolecular attraction with the pore surface. When the saturation pressure is achieved, N_2 gas is gradually removed (desorption) until fully evacuated. The gas adsorption isotherm, which represents the amount of gas adsorbed and desorbed, are then used to calculate the pore parameters in the pottery, particularly in the micro- and mesopore regions (Zouridakis and Tzevelekos 1999; Espinal 2012; Cayme et al. 2024a).

Mercury intrusion works similarly as the gas adsorption method but uses non-wetting liquids (i.e Hg) instead of gas, which is forcibly introduced into the pores under applied pressure. The volume of mercury intruded and extruded as a function of pressure is analyzed to determine the open pore parameters in the meso- and macropore regions (Espinal 2012; Volzone and Zagorodny 2014; Daghmehchi et al. 2023).

2.2 Organic residue analysis (ORA)

Organic compounds are often present in various archaeological and cultural heritage artifacts, including those found in or on pottery (Cramp and Evershed 2014; Heron and Craig 2015; Oras et al. 2017a; Bondetti et al. 2021; Hopper et al. 2023; Oras et al. 2023), mummified remains (Ménager et al. 2014; Oras et al. 2020), textiles (Peets et al. 2020; Lantos et al. 2024), and art works (Rella et al. 2006; Sarmiento et al. 2011). Despite the susceptibility of organic compounds to degradation, residues can still be preserved for millennia within pottery, stone tools, or other mineral matrices (Langejans 2010; Craig et al. 2013).

ORA as a methodological approach has significantly improved, evolving from classical wet chemistry methods in the early 1900s, that required large amounts of archaeological pottery samples (Regert 2011), to the application of advanced chromatography techniques at the beginning of the 1980s that needed only small sample sizes and provided more detailed characterization (Patrick et al. 1985; Needham and Evans 1987). By the 1990s, gas chromatography (GC) with either a flame ionization detector (GC-FID) or mass spectrometry (GC-MS), became a standard equipment for ORA in knowing the molecular identity of biomarkers and the concentration of different lipid compounds from e.g. food sources or other organic substances (Evershed et al. 1990). In archaeology, this technique is often used in parallel with the gas chromatography-combustion-isotope mass spectrometry (GC-C-IRMS) to further determine the origin of analyzed food substances, usually through the isotopic analysis of fatty acids (Evershed et al. 1994, 1997). There have been several additional mass spectrometry based advancements since the 2000s, with the more recent ones focusing on increasing the sensitivity of the instruments to identify and distinguish food residues, like e.g. the matrix-assisted laser desorption/ionization (MALDI) ionization in tandem with Fourier transform-ion cyclotron resonance mass spectrometry (MALDI-FT-ICR-MS) (Oras et al. 2017a; Drieu et al. 2024), and ultra-high-performance liquid chromatography coupled with Orbitrap mass analyzer (UHPLC/Orbitrap MS) techniques (Doliente et al. 2024).

2.2.1 Organic residue analysis from archaeological pottery

A widely recognized application of ORA is in the analysis of food residues, specifically the recovery of lipids from archaeological potsherds (Evershed 2008a-b; Roffet-Salque et al. 2017; Whelton et al. 2021; Irto et al. 2022). Lipids are

excellent targets for ORA due to their hydrophobic properties, making it less soluble in water, and gets better preserved within the artifacts by limiting their loss during diagenesis (Heron and Evershed 1993). Proteins, one of the most commonly occurring biological molecules, can be also recovered from archaeological ceramics despite being more sensitive to degradation (Craig et al. 2005; Pavelka et al. 2016; Hendy et al. 2018; Chowdhury et al. 2021; Tanasi et al. 2021).

Biomarkers are the main target analytes in lipid-based ORA (Evershed et al. 1991; Evershed 2008a).These are chemically stable organic compounds that can be diagnostic of specific food substances derived from plants and animals, and are usually detected using GC-MS in archaeological pottery, and less often with liquid chromatography-mass spectrometry (LC-MS) (Krueger et al. 2018; Doliente et al. 2024) and tandem mass spectrometry (NanoESI MS and MS/MS) techniques (Mirabaud et al. 2007). The analysis of these residues can infer the original functions of ceramic vessels, whether for cooking, storage or tableware, as well as the type of organic products processes within them (Heron and Evershed 1993; Evershed et al. 1999; Roffet-Salque et al. 2017). Biomarker compounds are indicative of possible animal fats of terrestrial (Evershed et al. 1997, 2002; Mottram et al. 1999) or aquatic (Hansel et al. 2004; Oras et al. 2018; Dolbunova et al. 2022) origin, plant-derived lipids (Dunne et al. 2016; Shoda et al. 2018; Chen et al. 2024), and products processed or derived from natural sources such as dairy (Salque et al. 2013; Carrer et al. 2016; Evans et al. 2023), honey (Oliveira et al. 2019; Dunne et al. 2021), and adhesives including tars (Mitkidou et al. 2008; Stacey et al. 2020; Chen et al. 2022) and beeswax (Regert et al. 2001; Roffet-Salque et al. 2015; Roumpou et al. 2021), respectively.

Understanding the intended function and use of pottery through chemical evidence has provided insights into the daily lifestyles and practices of ancient communities. Among them are mortuary practices (Namdar et al. 2017; Van de Velde et al. 2019; Vykukal et al. 2021; Roumpou et al. 2023), dairy innovations (Dunne et al. 2019; Cubas et al. 2020; Demirci et al. 2021; Evershed et al. 2022), adoption of pottery technologies (Taché and Craig 2015; Oras et al. 2017b; Admiraal et al. 2020; Craig 2021), farming practices (Heron et al. 2016; Cramp et al. 2019; Lucquin et al. 2023; Oras et al. 2023) and trade networks (Steele and Stern 2017; Drieu et al. 2021).

2.2.2 Effects of mineralogical component on organic residues

The recovery of lipids in archaeological pottery is influenced by several factors, which include the physical and chemical properties of the pottery, the intended functional use during its lifetime, and the burial environment (Colombini et al. 2005a). Among these factors, the mineral component of the pottery has the most important effect on the long-term preservation of lipid residues because it facilitates adsorption during cooking events and serves as a protective barrier during burial (Evershed 2008b).

In the first factor, the type of clay (e.g., 1:1 group, 2:1 group, or mixed layer types), the added temper (e.g., mineral, shell, or plant and animal materials), and

the firing conditions (e.g., low or high fired, and oxidizing or reducing atmosphere) contributes to the physical and chemical properties of the final pottery material (Moropoulou et al. 1995; Sanjurjo-Sánchez et al. 2018). The variability in the raw materials and manufacturing processes is dictated by technological expertise, raw material availability, and regional traditions (Tite 2008; Povlsen 2013; Woolsey 2018). The formation of different sized pores in pottery is a direct outcome of the mineral content in the clay and temper mixture, and the formation of specific post-firing minerals depending on the firing temperature attained. These pores can enhance the adsorption of organic residues on the pottery surfaces, effectively trapping and preserving them over time (Evershed et al. 1990; Drieu et al. 2019; Drieu 2020). Studies have shown that unglazed pottery typically have higher lipid yields compared to those with surface treatments such as burnishing or glazing (Pecci et al. 2016; Drieu 2020). This difference is attributed to the higher porosity of unglazed ceramics, which facilitated the adsorption and retention of more organic residues, in contrast to surface-treated pottery, where porosity is limited (Pecci et al. 2016).

The presence of specific mineral groups in clay can enhance lipid retention in pottery. In particular, clays containing calcium-rich inclusions, such as calcite, has been reported to contribute to this preservation. Unsaturated compounds, particularly oleic acid bonded to iodine through its double bond, appeared to preferentially come together within the calcite inclusions in clays, as demonstrated through elemental mapping employing a scanning electron microscopy with energy dispersive spectrometer (SEM-EDS) (Goldenberg et al. 2014). This finding is supported by studies using time-of-flight secondary ion mass spectrometry (ToF-SIMS), which revealed significant lipid accumulations surrounding calcium-rich inclusions in pottery (Hammann et al. 2020). This binding of fatty acids to calcium is attributed to the formation of calcium salts of fatty acids, which are insoluble and resistant to leaching, thus protecting lipids during post-depositional processes. Besides calcite, clay minerals also adsorb moderate amounts of oleic acid (bonded to iodine), while quartz exhibited no detectable adsorption, as evidenced by SEM-EDS elemental mapping analysis (Goldenberg et al. 2014).

Macroscopically, calcified deposits consisting of $CaCO_3$, lining the interiors of archaeological pottery, have been found to preserve not only lipids but also proteins (Hendy et al. 2018). Similarly, dental calculus, which also contains calcium minerals, can effectively preserve both protein and lipid residues (Velsko et al. 2017; Hendy et al. 2018).

In addition to lipid preservation, metal oxides within the clay matrix have been reported to catalyze the formation of long mid-chain ketones in archaeological pottery. These ketones are formed through the ketonic decarboxylation of fatty acids, with fatty acid metal salts acting as reaction intermediates. Experimental investigations using replicate pottery materials have demonstrated that metal oxides and salts, such as CaO, Al_2O_3, SiO_2, $CaCO_3$, MgO, and FeO, can facilitate this catalytic process (Raven et al. 1997; Evershed et al. 2008c).

Secondly, lipid accumulation is also related to the original function of the pottery, with cooking pots generally having more adsorbed lipids compared to storage pots (Matlova et al. 2017). Cooking, which in ancient times normally involved boiling in liquid or roasting, facilitates the breakdown of organic molecules in food which enables the residues to penetrate deeper into the pottery matrix (Evershed 2008b; Charters et al. 1993,1997; Dunne et al. 2020). This process also produces more degradation products that can eventually react with the clay matrix and become bound to it, resulting to better preservation in the pottery. Furthermore, charred food remains (food crusts) formed during cooking, can also be a source of preserved organic residues (Craig et al. 2007; Evershed 2008b; Miller et al. 2020).

Lastly, the combined effect of the mineral composition and the processes the pottery underwent during its lifetime of use can either induce further degradation or prevent it once buried in the ground (Colombini et al. 2005b). It has been reported that lipids are better preserved from water leaching and the harmful effects of microorganisms in arid surroundings and anoxic waterlogged deposits (Regert et al. 1998; Evershed 2008a; Dunne et al. 2012; Drieu 2020). Additionally, soils characterized by low pH can alter the mineral composition of pottery, particularly those containing calcium, leading to the formation of calcified mineral deposits that may affect the surface porosity of the pottery (Cau Ontiveros et al. 2002; Gilstrap et al. 2021). Such changes in porosity, if significant, may in turn, also affect the retention of organic residues.

2.2.3 Quantification methods of organic residues

Typical ORA protocols are generally designed to evaluate the presence and relative concentration of lipid compounds (i.e. fatty acids, acylglycerols, sterols) and its degradation products in the pottery, rather than determining their absolute amount with precise quantification. The quantification of lipid components in ORA usually involves adding a known concentration of an internal standard to an unknown sample and then comparing the peak areas of the standard and target analytes to calculate the concentration of the unknown analyte (Charters et al. 1993; Olsson and Isaksson 2008; Kałużna-Czaplińska et al. 2016). For the internal standard to be effective, it should be of high purity, possess properties similar to those of the analytes, and should measure accurately. The most widely used internal standards in archaeological ORA are long chain *n*-alkanes, like C_{34} or C_{36} alkanes. Internal standards are usually introduced to the lipid extracts prior to GC-MS analysis, although standards can also be added to the ceramic powder before extraction to assess the efficiency of the extraction method (Baeten et al. 2013; Cramp et al. 2014).

Ensuring the reliability of results requires incorporating blank samples during extraction to monitor possible contamination, performing multiple sample analysis for improved repeatability when necessary, employing internal standards, and including reference materials as part of the protocol (Kałużna-Czaplińska et al. 2016). Furthermore, it has been established that the total lipid extracted from

archaeological pottery in order for it to be considered representative of its original contents should be above 5µg/g of clay powder (Evershed 2008b; Reber et al. 2019; Suryanarayan et al. 2021). This threshold value ensures reliable interpretation of its organic residue contents.

3 EXPERIMENTAL SECTION

The general methodology employed in this doctoral study is presented in Figure 3.1. Specifically, analyses were conducted on the inorganic compounds and organic components of the clay samples, which included the experimental pottery briquettes and the 12th–13th century archaeological pottery from Kukruse, Estonia, to determine their mineral composition, porosity, and yields of two archaeologically relevant fatty acids ($C_{16:0}$ and $C_{18:1}$).

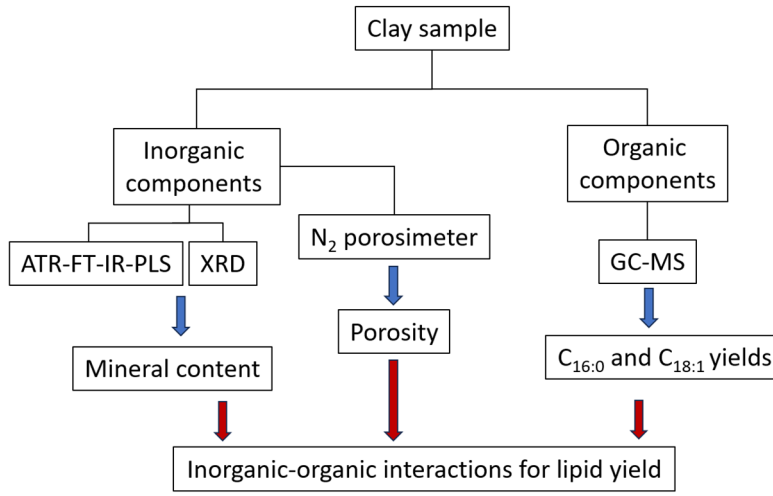

Figure 3.1. General flow of experiments.

3.1 Replicate clay pottery briquettes

The reference pottery briquettes were manufactured using two distinct clay types: predominantly illite and mixed-layered illite-smectite red clay (RC), and kaolinite white clay (WC). The aim was to test and compare the physical and chemical properties and their influence on lipid yield of two different, archaeologically relevant clay types. RC was sourced from a Quaternary clay formation in southeastern Estonia while WC was obtained commercially from Bang & Bonsomer Group Oy in Helsinki, Finland. Additionally, natural Quaternary sand (S) from Toome Hill in Tartu, Estonia, was used as sand temper. The sand was first sieved on a 0.500 mm mesh screen (#35 US Standard Mesh Number) to ensure uniform grain size, and then the finer fraction was mixed with the clays. Commercial powdered chalk (CH) purchased from Bang & Bonsomer Group Oy in Helsinki, Finland, was used to represent shell debris temper, which is commonly found in archaeological pottery from the eastern Baltic region (Kriiska et al. 2017). The production process, including the firing temperatures employed in the manufacturing of the replicate clay briquettes, were designed following the practices

identified in prehistoric pottery production (Dumpe and Stivrins 2015; Spataro et al. 2021).

Table 3.1.1 presents the proportions by mass of the clay type and temper additives used in the manufacture of each briquettes having an individual total weight of 30 g. Briquettes made entirely from RC and WC, representing 100% clay without temper, were also produced. Both the pure clays and the clay-temper mixtures were thoroughly hand-mixed, and approximately 8 to 10 mL of ultra-pure water (Milli-Q® Advantage A10 system, Merck Millipore, Darmstadt, Germany) was added to achieve plasticity. The resulting paste was then shaped into rectangular forms with dimensions of 3.0–3.5 cm x 5.0–6.0 cm and a thickness of 0.8–1.0 cm. The formed briquettes were air-dried at room temperature for 12 h and oven-dried at 105°C for an additional 24 h. Two equivalent sets of briquettes were prepared, which was fired separately at 600°C and 800°C. A total of 44 briquettes were produced.

A muffle furnace (KL-22, Kerako, Tallinn, Estonia) with an electronic programmable controller (ST315A, Stafford 129 Instruments, Stafford, United Kingdom) was utilized to fire the prepared briquettes in an oxidizing atmosphere. The temperature program for the furnace was as follows: room temperature equilibration for 10 min, followed by a temperature increase within 90 min to either 600°C or 800°C, and finally, a 120 min soaking time at the final temperature.

Table 3.1.1. Mass percentage of different clay types, tempers, and firing temperature used to form the replicate briquettes.

Composition	**RC**		**WC**	
	600°C	**800°C**	**600°C**	**800°C**
Clay:15% Sand (S): 85%	 RC600-S1	 RC800-S1	 WC600-S1	 WC800-S1
Clay: 20% Sand (S): 80%	 RC600-S2	 RC800-S2	 WC600-S2	 WC800-S2
Clay: 25% Sand (S): 75%	 RC600-S3	 RC800-S3	 WC600-S3	 WC800-S3

Clay: 50% Sand (S): 50%				
	RC600-S4	RC800-S4	WC600-S4	WC800-S4
Clay: 75% Sand (S): 25%				
	RC600-S5	RC800-S5	WC600-S5	WC800-S5
Clay: 100% Sand (S): 0%				
	RC600-S6	RC800-S6	WC600-S6	WC800-S6

Composition	**RC**		**WC**	
	600°C	**800°C**	**600°C**	**800°C**
Clay:20% Sand (S): 32% Chalk (CH): 48%				
	RC600-CH1	RC800-CH1	WC600-CH1	WC800-CH1
Clay: 25% Sand (S): 30% Chalk (CH): 45%				
	RC600-CH2	RC800-CH2	WC600-CH2	WC800-CH2
Clay: 50% Sand (S): 20% Chalk (CH): 30%				
	RC600-CH3	RC800-CH3	WC600-CH3	WC800-CH3

Clay: 75% Sand (S): 10% Chalk (CH): 15%				
	RC600-CH4	RC800-CH4	WC600-CH4	WC800-CH4
Clay: 90% Sand (S): 5% Chalk (CH): 5%				
	RC600-CH5	RC800-CH5	WC600-CH5	WC800-CH5

3.2 Inorganic clay components

3.2.1 ATR-FT-IR analysis

A Thermo Scientific Nicolet 6700 FT-IR spectrometer with a Smart Orbit diamond micro-ATR accessory (active sampling a 1.5 mm diameter), was utilized to acquire the ATR-FT-IR spectra of the 236 reference clay samples, 28 mineral standards, and the 11 case study samples in the 4000–225 cm^{-1} region. The FT-IR spectrometer is equipped with a DLaTGS (deuterated L-alanine doped triglycine sulphate) detector, CsI (Cesium Iodide) beamsplitter, and Vectra Aluminium interferometer. A constant purging of dry air protects the FT-IR spectrometer from atmospheric moisture.

For obtaining ATR-FT-IR spectrum, small amount of grounded sample was placed on the ATR crystal and initially pressed on a micro-ATR crystal utilizing a pressure applicator. The FT-IR operating parameters were set as follows: $4cm^{-1}$ resolution, 128 and 256 scans, zero filling factor was 0, and Happ-Genzel apodization window. Afterwards, the spectra were recorded and processed using the Thermo Electron's OMNIC 9 software.

To ensure homogeneous results, 2 to 4 recorded ATR-FT-IR spectra were made for every individual monomineralic samples and clay-related reference samples, while 1 to 3 ATR-FT-IR spectra were acquired for the case study samples. The resulting IR spectra were averaged, and the statistical average ATR-FT-IR spectra were obtained. Atmospheric suppression correction was applied to all the recorded ATR-FT-IR spectra using Thermo Fisher Scientific Inc. OMNIC Specta 2.0 software. The smoothing function of the OMNIC software was employed for some noisier ATR-FT-IR spectra.

Details on the development of the discriminant analysis (DA) classification model and the PLS partial least squares model for quantification can be found in Paper 1. For these techniques, Thermo Scientific TQ Analyst™ Professional Edition 9.0 software was used.

The compositions of the calibration and validation standards for creating the ATR-FT-IR-PLS quantification model were based on the XRD data. For evaluating the PLS model the following parameters were used: root mean square error of calibration (RMSEC), root mean square error of predication (RMSEP), squared correlation coefficient (R^2), root mean square error of cross-validation (RMSECV), and modified Willmott performance index.

3.2.2 X-ray diffraction analysis

A Bruker D8 Advance (Germany) X-ray diffractometer (XRD) was employed to identify the mineral content of the raw clay materials used for the replicate briquettes, the fired clay briquettes, and the archaeological samples from Kukruse Estonia. The sample preparation process included drying the samples at 105°C in an oven for 24 h, followed by grinding into fine powder with an agate mortar and pestle, and then transferring them into aluminum sample holders, which were flattened with a glass side. The XRD measurements were performed using Ni-filtered CuKα radiation in the 3–70°2θ range. The resulting XRD data were interpreted and modeled using Siroquant-3 software, which utilizes a Rietveld algorithm-based code. The XRD analysis was conducted in collaboration with the Department of Geology, University of Tartu, Estonia.

3.2.3 Porosity: Nitrogen gas adsorption

The N_2 adsorption of the raw clay materials used for the replicate briquettes, the fired clay briquettes, and the archaeological case study samples at different relative pressures were measured using a Micromeritics 3Flex adsorption analyser (Norcross, GA, USA). The samples, each weighing approximately 1.0 g, were first degassed under vacuum for about 24 h at 300°C in a VacPrep 061 Micromeritics sample degas system (Norcross, GA, USA) prior to analysis. The total specific micro- and mesopore volume ($V_{0.95}$) and the total specific surface area (S_{BET}) were computed from the amount of N_2 adsorbed at $p/p° = 0.95$ for $V_{0.95}$, and in the $p/p°$ range from 0.05 to 0.2 for S_{BET}, respectively. The Brunauer–Emmett–Teller (BET) method was used to determine the S_{BET}.

The non-local density functional theory (NLDFT) model for pillared clays was used to derive the pore size distribution, the cumulative values for the specific surface area (S_{NLDFT}) and specific pore volume (V_{NLDFT}), and the percentage of micropores, S_{micro} and V_{micro}, using the Micromeritics 3Flex software (version 6.01, Norcross, GA, USA). Further details on the computations are reported in Paper 2. The N_2 adsorption analysis was conducted in collaboration with the Chair of Physical Chemistry, Institute of Chemistry, University of Tartu, Estonia.

3.3 Organic residue analysis from experimental and archaeological samples

3.3.1 Chemical standards and solvents used in ORA

All sample solutions were prepared by weighing and expressed in mass units. The fatty acid standards used for spiking on the powdered clay samples are palmitic acid ($C_{16:0}$) (certified reference material, TraceCERT®, 99.6%, Sigma-Aldrich, Switzerland) and oleic acid ($C_{18:1}$) (ROTICHROM® GC, ≥ 99%, Carl Roth GmbH + Co. KG, Karlsruhe, Germany). Each standard was dissolved in hexane (puriss p.a. ACS reagent, ≥ 99% (GC), Sigma-Aldrich, Co. St. Louis, MO, USA) to produce solutions with concentrations of approximately 1 µg/µL. The internal standard used for quantification was a 10% hexadecane (≥ 99.0%, Sigma-Aldrich, USA) in toluene (puriss p.a., ACS reagent, ≥ 99.7%, Honeywell) solution with a concentration of 0.4 mg g^{-1}. Additionally, a stock solution of fatty acid methyl esters (FAME) standard, consisting of 14 different fatty acid methyl esters ranging from C8-C24 (CRM18918, Supelco, Sigma-Aldrich, USA) was prepared by diluting in toluene to a concentration of 6.1 mg g^{-1}. From this stock solution, the series of standard solutions for the calibration curves were prepared.

The following reagents were used in the derivatization and extraction process: TMTFTH (m-(trifluoromethyl)phenyltrimethylammonium hydroxide, 5% w/v in methanol, Thermo Scientific, Kandel, Germany), concentrated sulfuric acid (analytical reagent, AnalaR NORMAPUR, 98%, VWR Chemicals BDH Prolabo, Leuven, Belgium), potassium carbonate (ACS reagent, ≥ 99.0%, Sigma-Aldrich, USA), dichloromethane (puriss p.a., ACS reagent, ≥ 99.9%, Honeywell, USA), and methanol (Chromasolv™ for HPLC, ≥ 99.9%, Honeywell, USA).

3.3.2 Spiking of palmitic and oleic acid standards

Standard solutions of $C_{16:0}$ and $C_{18:1}$ were spiked on homogenized clay briquettes, according to the amounts presented in Table 3.3.2.1. Homogenization was carried out using a mini ball mill (Mini-mill Pulverisette 23, Fritsch GmbH, Germany). Two equivalent sets of spiked clay briquette powders were prepared, one set was air-dried without additional treatment (non-degraded), while the other set was heated (100°C) in a laboratory oven (ECOCELL® 22-ECO line, MMM Group, München, Germany) for 14 h (degraded). The degradation temperature and time settings were selected based on the starting point of degradation of pure $C_{16:0}$ and $C_{18:1}$ (Charuwat et al. 2018; Xiao et al. 2023b), with the purpose of investigating whether the clay influences the oxidation of these fatty acids. Furthermore, the parameters reflect potential low-heat cooking events.

Additionally, out of the sets prepared, one batch underwent acid catalyzed methylation (ACM), and another batch was designated for the TMTFTH methylation. ACM is a conventional method used for one step extraction and methylation (Correa-Ascencio and Evershed 2014; Oras et al. 2017b) of lipids, while TMTFTH was used for comparison, since it is largely unexplored on clay pottery

ORA (Stern et al. 2000). The spiked amount of $C_{16:0}$ and $C_{18:1}$ and the mass of clay used were adjusted between the two methylation methods to ensure that sufficient amount was quantified. Spiking was performed by first diluting both $C_{16:0}$ and $C_{18:1}$ in 1.0 mL hexane in a separate vial, then uniformly distributing this solution onto the clay powder. Afterwards, the hexane was allowed to evaporate completely, leaving the $C_{16:0}$ and $C_{18:1}$ at their original concentrations on the clay briquettes. Each sample was placed in clear glass test tubes with PTFE-lined screw caps.

Table 3.3.2.1. The amount of fatty acids and the mass of clay utilized in the ACM and TMTFTH methylation methods.

Fatty acid and clay	Methylation methods	
	ACM	TMTFTH
$C_{16:0}$	25 µL	50 µL
$C_{18:1}$	25 µL	50 µL
Clay powder	0.25 g	0.50 g

3.3.3 Derivatization methods

The methodology discussed in the subsequent sections was applied to both degraded and non-degraded powdered clay samples spiked with $C_{16:0}$ and $C_{18.1}$. Each batch extraction included a blank that contained no clay powders and no spiked $C_{16:0}$ and $C_{18.1}$. Additionally, test tubes containing only $C_{16:0}$ and $C_{18.1}$were extracted in parallel with each batch run to correct and improve the accuracy of the fatty acid percentage yield computations. Representative clay powders without any spiked fatty acids (blank samples) were also derivatized and extracted to confirm the absence of organic compounds. The archaeological Kukruse pottery used as case study samples was also subjected to the ACM method, but not with the TMTFTH methylation method. The amount of homogenized Kukruse clay powders extracted and derivatized by ACM was around 0.50 g.

3.3.3.1 Acid-catalyzed methylation (ACM)

The extraction protocol was followed from previously published ACM procedure (Correa-Ascencio and Evershed 2014; Papakosta et al. 2015; Oras et al. 2017b). Briefly, the powdered clay samples were treated with methanol (4 mL), sonicated for 15 min, and then concentrated sulfuric acid (800 µL) was added dropwise before sealing. The mixture was heated in a dry heating block at 70°C for 4 h, then allowed to cool at room temperature. Once cooled, the heterogenous mixture were centrifuged for 5 min at 3000 rpm and extracted three times with hexane (2 mL) while filtering through a glass pipette plugged with silanized glass wool containing potassium carbonate. Each hexane extracts were combined and evaporated to dryness under a stream of N_2 gas. The dried lipid extracts were

reconstituted in 10% hexadecane in toluene (15 µL), further diluted with toluene (140 µL), and analyzed by GC-MS.

3.3.3.2 Solvent extraction and TMTFTH derivatization

The DCM:MeOH extraction (Evershed et al. 1990) and modified TMTFTH derivatization (Tammekivi et al. 2019) protocols, were adapted from previously reported studies. Using another set of powdered clay samples, the spiked lipids were extracted three times with a solution of 2:1 dichloromethane: methanol (DCM:MeOH, v/v, 5 mL), sonicated for 15 min and centrifuged for 15 min at 3000 rpm. The DCM:MeOH extracts were combined and evaporated to dryness under a stream of N_2 gas. The dried lipid extracts were then treated with a solution of 5% TMTFTH in methanol (50 µL) and sonicated for 30 min. To complete the derivatization, the mixture was allowed to stand at room temperature for 24 h. After derivatization, 10% hexadecane in toluene (30 µL) was added, followed by dilution of toluene (230 µL), and analyzed in GC-MS.

3.3.4 GC-MS instrumentation and parameters

Methylated samples from ACM and TMTFTH, together with the prepared FAME calibration standards, were analyzed by injecting a 1 µL aliquot into an Agilent Technologies 6890N gas chromatography system coupled with a 5973 mass spectrometer (MS). The instrument was operated using an Agilent GC-MSD/ Enhanced software. Helium (purity 6.0, 99.9999%) served as the carrier gas for the samples. The GC inlet temperature was set to 300°C, and the samples were split at a ratio of 2:1, with a 2.3 mL/min flow rate. Separation was achieved using an Agilent J&W HP-5ms capillary column composed of (5%-phenyl)-methylpolysiloxane, with the following specifications: 30 m length, 0.25 µm film thickness, and 0.25 mm internal diameter.

The temperature program for the GC analysis was as follows: the oven was initially held at 80°C for 2 min, then ramped to 200°C at 10°C/min, held at 200°C for 1 min, increased to 220°C at 5°C/min, held again for 1 min, and further raised to 280°C at 30°C/min with a 3 min hold. Finally, the temperature was increased to 300°C at 30°C/min, resulting in a total run time of 25.67 min.

For the MS, the electron ionization (EI) energy was at 70 eV, the ion source temperature was set at 230°C, and the transfer line was maintained at 280°C. The total ion chromatogram (TIC) was recorded within the mass range of 30-600 *m/z* in scan mode and a 4.00 min solvent delay. The target analytes have the following mass ratios: 226.0 *m/z* for hexadecane, 239.2 *m/z* for methyl palmitate, and 264.2 *m/z* for methyl oleate. For the data analysis, an Agilent Technologies MassHunter Workstation, Qualitative Analysis Version 10.0 and the NIST 23 Mass Spectral Library was used to evaluate the peak areas in the extracted ion chromatogram (EIC) mode.

3.3.5 Quantification by GC-MS

A series of standard solutions with varying concentrations of the fatty acid methyl ester (FAME) stock solution was prepared, each containing a fixed amount (60 μL) of internal standard (10% hexadecane in toluene). The solutions were diluted with a known volume of toluene depending on the target concentrations. Since only the $C_{16:0}$ and $C_{18:1}$ were quantified in this study, the dilutions were designed based on the relative amount of methyl palmitate (10.9%) and methyl oleate (4.98%) in the FAME solutions. The ratio of the peak areas relative to the concentration ratios between the analytes (methyl palmitate or methyl oleate) and the internal standard (10% hexadecane in toluene) was plotted, as shown in Figure 3.3.5.1. Two sets of calibration curves were prepared at different concentration ranges, a ten-point calibration curve for ACM, and a nine-point calibration curve for TMTFTH. The difference is due to the lower concentration of extracted compounds from TMTFTH. Linear equations derived from these calibration curves were used to calculate the unknown concentrations of $C_{16:0}$ and $C_{18:1}$ extracted from the clay powder samples. The percentage yields of $C_{16:0}$ and $C_{18:1}$ were then calculated as follows:

$$\%\ \text{yield} = \frac{\text{concentration of C16: 0 or C18: 1 extracted}}{\text{concentration of pure C16: 0 or C18: 1}}\ \text{x}\ 100$$

Calibration curves were constructed for each batch of GC-MS run, with calibration solutions made from stock solutions of fatty acid methyl esters (FAME) producing very good linearity for the target fatty acids, $C_{16:0}$ and $C_{18:1}$. The observed linearity was reproducible across a range of concentrations, including low concentrations for the TMTFTH methylation ($R^2 \geq 0.998$), mid-range concentrations for the acid-catalyzed methylation ($R^2 \geq 0.998$), and high concentrations ($R^2 \geq 0.999$) used for the archaeological pottery. Data analysis was performed on the briquette powders by computing the average yields from the two replicate analyses conducted on separate days. The data was organized to reflect the changes in the concentrations of $C_{16:0}$ and $C_{18:1}$ between the different amounts of clay and temper types, and whether the samples were degraded or non-degraded. The detailed data analysis employed is discussed in Paper 3. The amount of selected fatty acids investigated in the Kukruse pottery samples were expressed in μg/g clay instead of the percentage yield.

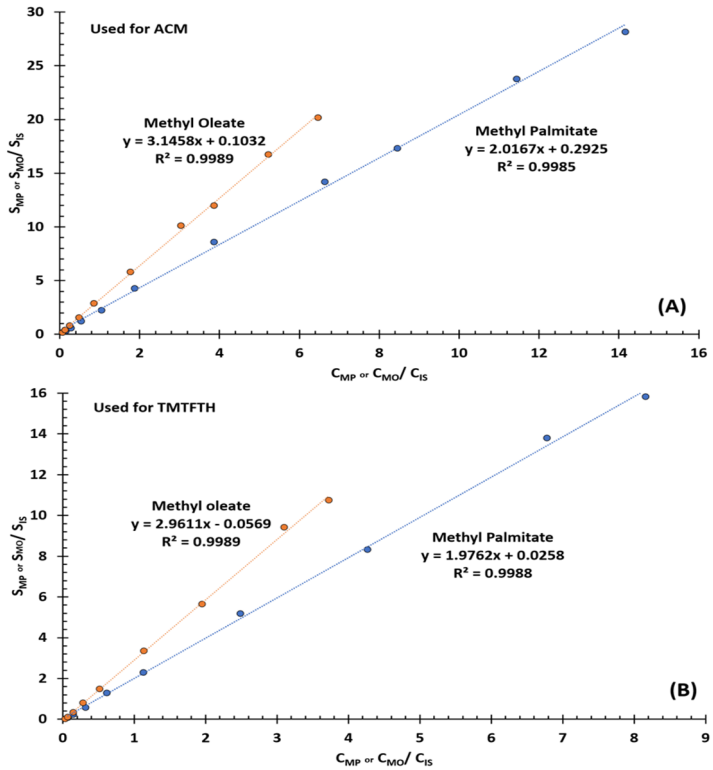

Figure 3.3.5.1. Representative calibration curves used for quantifying the extracts from (A) ACM, and for (B) TMTFTH. The peak area ratios of methyl palmitate (S_{MP}) or methyl oleate (S_{MO}), relative to the area of the internal standard, 10% hexadecane in toluene (S_{IS}) was plotted relative to the concentration ratios of the analytes (C_{MP}) or (C_{MO}), and the internal standard (C_{IS}).

4 RESULTS AND DISCUSSION

4.1 Characterization of mineralogical components of clay minerals

The mineralogical composition of clays provides important information about the possible type of raw materials used in the production of pottery, including the addition of non-clay mineral tempers, and its thermal mineral transformations after the firing process. ATR-FT-IR-PLS method and XRD were employed in this study to determine the mineralogical composition of archaeological pottery which will be presented in the Case Study section.

4.1.1 Quantitative ATR-FT-IR-PLS method

An ATR-FT-IR-PLS quantitative method was developed to address the need for rapid and efficient quantitative analysis when sample size is limited. This method serves as an alternative to XRD, which requires larger sample sizes and cannot determine amorphous components. Section 4.1.1.1 provides a summary of the advantages of the ATR-FT-IR-PLS method compared to the conventional XRD technique.

Paper 1 describes a quantitative method that demonstrates the effectiveness of ATR-FT-IR-PLS (using spectral range of 3720-275 cm^{-1}) in quantifying seven different mineral groups in clays. These groups include: (1) silica varieties (quartz and cristobalite), (2) feldspars (plagioclase and K-feldspar), (3) clay minerals, group 1 (kaolinite and halloysite), (4) clay minerals, group 2 (micas, illite, illite-smectite, smectite, vermiculite), (5) clay minerals, group 3 (chlorite, chlorite-smectite), (6) carbonates (calcite, dolomite, siderite, ankerite), and (7) iron-oxyhydroxides (hematite and goethite). The PLS model was developed using the largest calibration and validation datasets ever collected for clay minerals, containing 222 clay-related reference standards with known and diverse compositions. Different natural clays were used as standards, as well as archaeological, cultural heritage and geological materials that were of different types, age and origin, to cover a broad and extensive range of mineral components in the model (see Paper 1).

During this work, it was also evaluated how effectively it was possible to differentiate between various monomineralic minerals usually present in most clays based on their ATR-FT-IR spectral features. For that, discriminant analysis (DA) classification were used, which is based on principal component analysis (PCA) (Fig. 4.1.1.1).

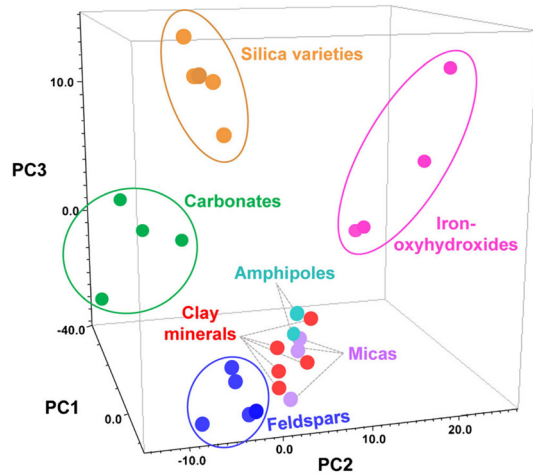

Figure 4.1.1.1. The classification results of the individual minerals presented by the three principal components (source: Vahur et al. 2021).

In Fig. 4.1.1.1, it can be seen that the silica varieties, feldspars, carbonates and iron-oxyhydroxides were distributed in separate groups. Micas, clay minerals and amphiboles were grouped more together. The DA classification results demonstrate that the ATR-FT-IR spectra of analysed minerals are different enough and can be utilized for quantification by the PLS model. The ATR-FT-IR spectra interpretation and the detailed discussions are provided in Paper 1.

The overall performance index, which indicated how accurately the created PLS model can quantify the validation standards, was 82.6%. The average performance index of 7 classes of minerals in clays was 84.8%. Carbonates (i.e. calcite, dolomite) showed the highest accuracy at 96.4% performance largely due to their well-resolved ATR-FT-IR peaks compared to the other mineral groups. The clay mineral groups, specifically group 2 (i.e. illite, illite-smectite), have the lowest performance index at 79.7% due to their overlapping bands in the ATR-FT-IR that are difficult to separate. However, the R^2 values for the calibration and validation standards are all > 0.9, signifying satisfactory to good accuracy. RMSEC values of main components were between 1.7 to 6.1 g/100g and RMSEP values 0.9 and 5.1 g/100g. These results are satisfactory. The ATR-FT-IR-PLS method developed in Paper 1 has demonstrated its usefulness as a starting point for determining the clay components of archaeological pottery. The PLS method shows that carbonates (i.e. calcite and dolomite) were the most accurately quantified group of minerals. The clay minerals in the sample were separated into three groups. Group 1 (i.e. kaolinite and halloysite) was quantified well, while Group 2 (i.e. illite, illite-smectite) was quantified satisfactorily.

4.1.1.1 Advantages and disadvantages of ATR-FT-IR-PLS method

Applying the ATR-FT-IR-PLS method to eleven real-life archaeological and cultural heritage case study samples, as described in detail in Paper 1, have shown its effectiveness in quantifying the seven mineral groups selected in the PLS model. The method is particularly well-suited for small sample amounts, for its fast data acquisition, minimal sample preparation requirements, and in some cases, the ability to obtain usable data from a single FT-IR spectrum. However, improving the precision and reducing the uncertainties in quantitative analysis would require at least three replicate IR measurements. These features make the ATR-FT-IR-PLS method especially valuable for cultural heritage and archaeological materials, where preserving the sample's integrity is very relevant. While the ATR-FT-IR-PLS method performed well in determining the amount of the silicate varieties, feldspars, and iron-oxyhydroxides in some case study samples, it was less effective in quantifying the clay minerals 1 and 2 groups compared to the XRD technique.

The XRD has the advantage in identifying crystalline mineral phases and provides greater accuracy in quantifying their amounts. However, its limitations become apparent in the presence of amorphous mineral phases, as seen in one of the case study samples in Paper 1. XRD is unable to identify non-crystalline phases, which can lead to overestimation in the amount of the crystalline phases at the expense of the amorphous phases. In contrast, ATR-FT-IR can identify amorphous, semi-crystalline, and crystalline phases, with the potential for more improved quantification through the addition of new calibration standards in the PLS model. Although the XRD has the advantage of more detailed and accurate mineral phase analysis, the ATR-FT-IR-PLS method is a more practical alternative when semi-quantitative data is already sufficient to address the research question or when sample amounts are very limited.

4.1.2 Analysis by X-ray diffraction (XRD)

The comprehensive XRD analysis of the mineral composition of the briquette raw materials (i.e. RC and WC clays, sand, and chalk) and their corresponding thermal transformations at 600°C and 800°C were provided in detail in Paper 2. Furthermore, the mineralogical characterization of the Kukruse pottery and its potential implications for lipid yield from those potsherds will also be discussed in detail on the Case Study section of this dissertation.

In general, RC contains 64 wt.% average clay minerals, mainly 50 wt.% average of 2:1 clay type (illite, illite-smectite, mica), with fractions (14 wt.% average) of 1:1 clay type (kaolinite). WC, on the other hand, consisted of 91 wt.% average clay minerals, composed primarily of kaolinite (74 wt.% average) and 18 wt.% average of 2:1 clay type. The rest of the minerals in the raw clays are non-clay minerals, which included quartz and K-feldspar in both RC (31 wt.% average) and WC (9 wt.% average). In addition, hematite is also present in RC at about 4 wt.% average.

For the tempers, sand (S) has quartz (74 wt.% average) as its major component, along with K-feldspar (8 wt.% average) and plagioclase (8 wt.% average). It also contained minor amounts of 2:1 clay type (5 wt.% average) and carbonates (4 wt.% average). The ground chalk (CH) was composed of relatively pure calcite (99 wt.% average), with 1.0 wt. % average dolomite. The mineral composition of raw clays varies depending on their geographical origin and the geological processes that shaped its environment.

4.1.2.1 Mineralogical changes after firing

The behavior of phyllosilicates or clay minerals during firing was related to their specific types (i.e. 1:1 clay, 2:1 clay, or mixed-layer clay) and their interactions with other non-clay minerals within the clay matrix. These processes are further influenced by firing conditions made in either oxidizing or reducing environment, the firing duration, and the maximum temperature attained. Despite these different factors, the briquettes used in this doctoral study exhibited mineralogical transformations consistent with those typically observed at firing temperatures of 600°C and 800°C.

At a firing temperature of 600°C, the phyllosilicates in RC and WC have already underwent dehydroxylation, losing both interlayer water and structural hydroxyl groups. In particular, kaolinite in RC and WC was fully transformed into amorphous metakaolinite as shown in equation [1] and is no longer identifiable by XRD (Trindade et al. 2009; Izadifar et al. 2020). This transformation occurred consistently across all the briquettes, regardless of whether sand or chalk was used as temper. Figure 4.1.2.1.1 shows an example of this transformation, where at 800°C, the kaolinite is already absent.

$$Al_2O_3 \cdot 2SiO_2 \cdot 2H_2O_{\text{(kaolinite)}} \rightarrow Al_2O_3 \cdot 2SiO_{2\ \text{(metakaolinite)}} + 2H_2O \quad [1]$$

However, the 2:1 clay group (i.e. illite, illite-smectite) in both RC and WC were not fully dehydroxylated and still stable at 800°C (Gualtieri an d Ferrari 2006).

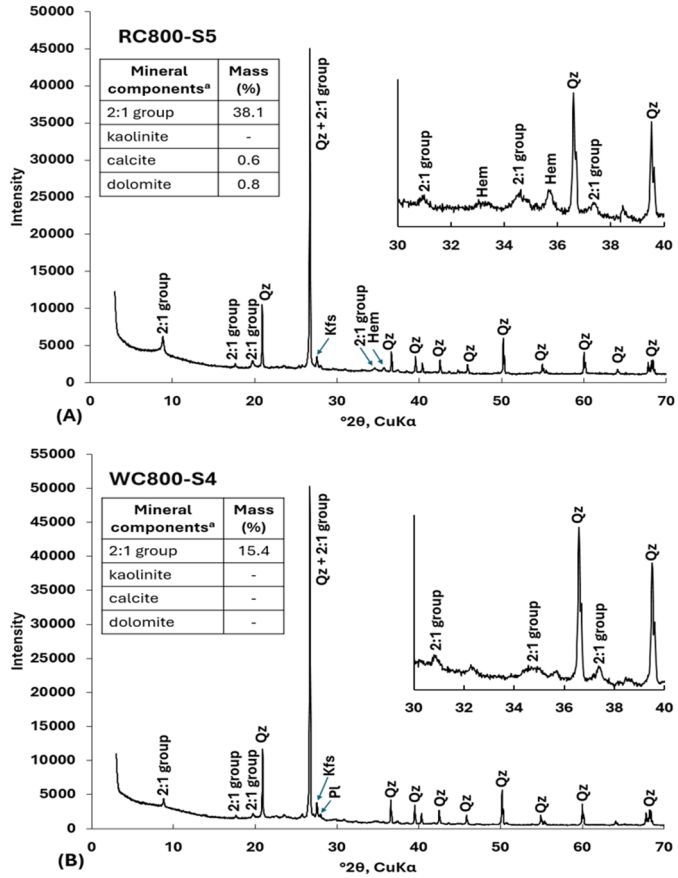

Figure 4.1.2.1.1. Representative XRD patterns of (A) RC, and (B) WC sand-tempered briquettes both fired at 800°C. Kaolinite, which is present in the original raw material in both clays, have already dehydroxylated at this temperature. Selected mineral phases are tabulated in (a). The mineral symbols are as follows (Warr 2021): Hem = hematite, Kfs = K-feldspar, Pl = plagioclase, Qz = quartz.

At 800°C, the carbonate minerals calcite and dolomite, originally present in the chalk temper, have largely decomposed, releasing CO_2 from their molecular structure, as described in equations [2] and [3] (Cultrone et al. 2001; İssi et al. 2011). Similarly, the sand temper, which also contained small amounts of carbonates, will also undergo decomposition at this temperature. This decomposition is evident from the comparison of the XRD data of the chalk-tempered clay briquettes fired at 600°C (i.e., RC600-CH and WC600-CH series) with those fired at 800°C (i.e. RC800-CH and WC800-CH series), where a consistent and very large decrease in the amount of calcite and dolomite was observed (Figure 4.1.2.1.2).

$$CaCO_{3\,(calcite)} \rightarrow CaO_{\,(lime)} + CO_2(g) \quad [2]$$

$$CaMg(CO_3)_{2\,(dolomite)} \rightarrow CaO_{\,(lime)} + MgO + 2CO_2(g) \quad [3]$$

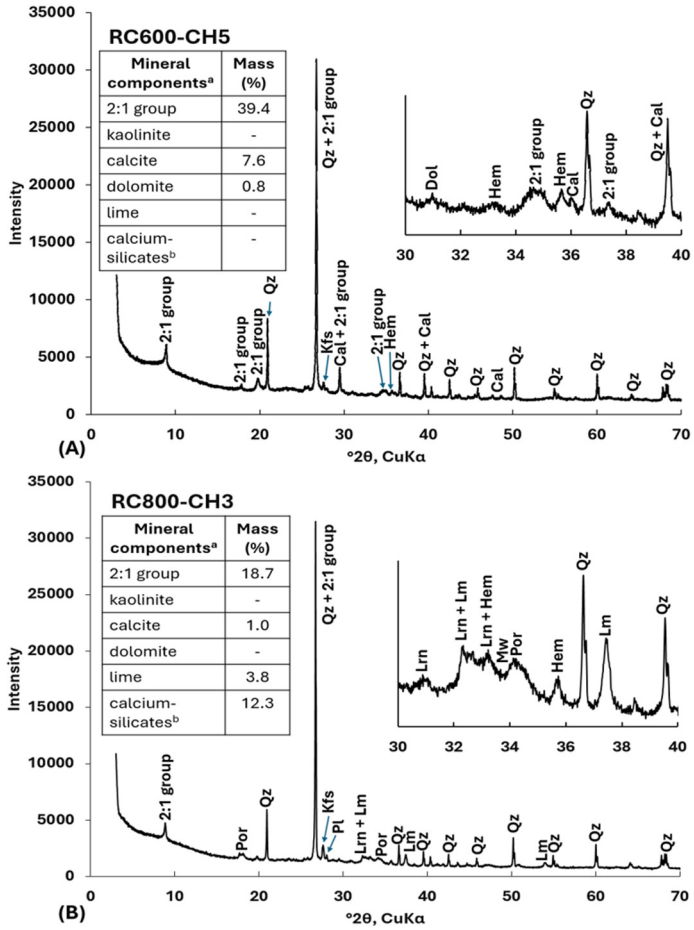

Figure 4.1.2.1.2. Representative XRD patterns of RC chalk-tempered briquettes fired at (A) 600°C, and (B) 800°C. Selected mineral phases are tabulated in (a). The amount of calcite has reduced, and the formation of calcium-silicate minerals (i.e. Lrn and Mw) are evident in (b). The mineral symbols are as follows (Warr 2021): Cal = calcite, Dol = dolomite, Hem = hematite, Kfs = K-feldspar, Lm = lime, Lrn = larnite, Mw = merwinite, Pl = plagioclase, Por = portlandite, Qz = quartz.

The XRD profiles of the chalk-tempered briquettes fired at 800°C (i.e. RC800-CH and WC800-CH series) showed the formation of stable calcium-silicate mineral phases such as larnite and merwinite (González-García et al. 1990; Trindade et al. 2010). At this temperature, CaO, a decomposition product of calcite, reacts with the clay minerals to form the calcium-silicate mineral phases (Fabbri et al. 2014). These mineralogical transformations were not observed in the chalk-tempered briquettes fired at 600°C (i.e. RC600-CH and WC600-CH series) or in the sand-tempered briquettes (i.e. RC600-S, RC800-S, WC600-S, and WC800-S series).

4.1.2.2 Relationship between mineralogy and micro- and mesoporosity development

Although a pottery can contain broad range of pore sizes from micro- to macropores, the assumption is that the smaller sized pores, such as the micropores, should be more effective at preserving organic residues (Matlova et al. 2017). Paper 2 provided an extensive characterization of the micro- and mesopores in the RC and WC, sand- and chalk-tempered briquettes used in this doctoral study.

From the XRD data, the firing temperature employed during the manufacturing process has a significant influence on the thermal transformation products of both clay (i.e. kaolinite) and non-clay minerals (i.e. $CaCO_3$ in chalk) in the pottery briquettes, directly affecting the development of micro- and mesosized pores (Mondelli et al. 2020). When different proportions of RC and WC raw clays with sand temper were fired at 600°C and 800°C, the specific surface area (S_{NLDFT}) and specific pore volume (V_{NLDFT}) exhibited very good proportionality with the initial amount (in %) of clay used to manufacture the different briquettes, with coefficients of determination (R^2) $\geq$ 0.993. This shows that both RC and WC clays were the primary contributors of porosity (Kuila and Prasad 2013), and that the sand temper did not directly alter the micro- and mesoporosity of the briquette despite being fired (Kilikoglou et al. 1998). Furthermore, the presence of dolomite in the sand-temper, which is prone to thermal decomposition as shown in equation [3], caused the differences in pore parameters between the lower mass clay fractions compared to the higher mass clay fractions in both RC and WC (see Figure 4.1.2.2.1).

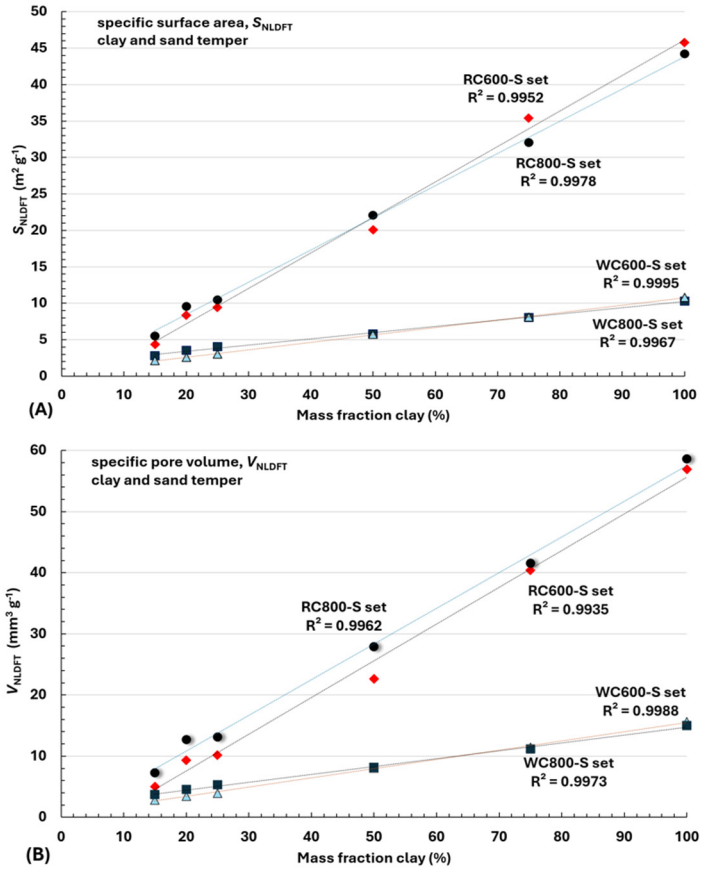

Figure 4.1.2.2.1. Graph of the (A) specific surface area (S_{NLDFT}), and the (B) specific pore volume (V_{NLDFT}), both vs the added clay mass fraction. Samples are shown for both RC and WC sand-tempered briquettes.

The addition of chalk temper caused a significant deviation from proportionality between the pore parameters and the initial amount of RC and WC, particularly in briquettes fired at 800°C. At this temperature, the WC briquettes were more affected by the addition of chalk, with pore parameters of $R^2 \geq 0.564$, compared to the RC briquettes, which exhibited an $R^2 \geq 0.843$ (see Figure 4.1.2.2.2). This deviation highlights the important effect of $CaCO_3$ decomposition in the clay matrix, as described in equation [2], which can produce highly porous CaO. Some of the formed CaO has reacted with the clay minerals, forming non-porous calcium-silicate minerals. In comparison, the chalk-tempered RC and WC briquettes fired at 600°C, where $CaCO_3$ decomposition products were not present, both exhibited an $R^2 \geq 0.959$.

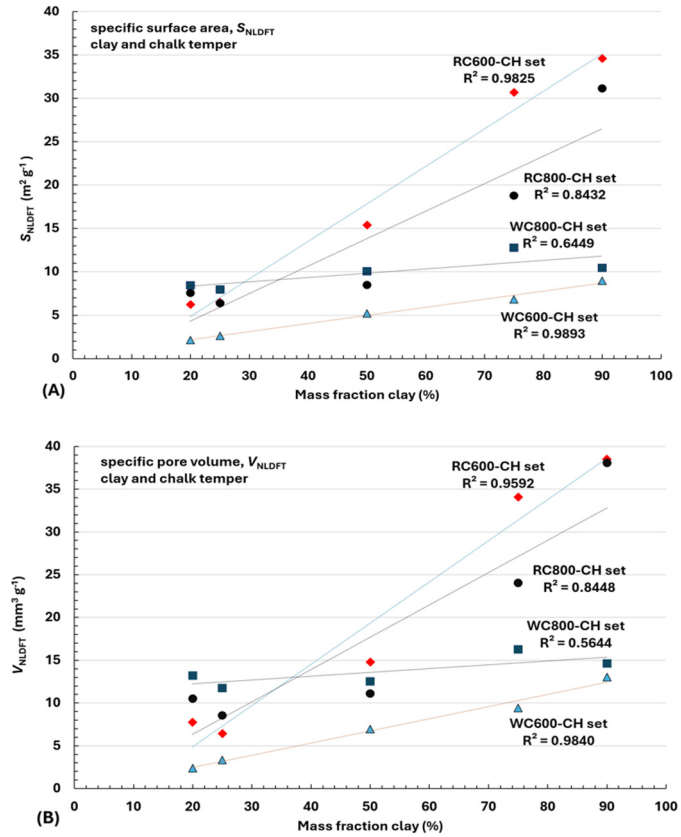

Figure 4.1.2.2.2. Graph of the (A) specific surface area (S_{NLDFT}), and the (B) specific pore volume (V_{NLDFT}), both vs the added clay mass fraction. Samples are shown for both RC and WC chalk-tempered briquettes.

In general, pottery fired at a higher temperature, 800°C, would form smaller percentage of microporosity parameters (S_{micro} and V_{micro}) compared to those fired at a lower temperature, 600°C, regardless of the clay type used or the temper added. The S_{micro} data also indicated that the replicate briquettes are mostly composed of micropores. The extent of the reduction in microporosity across the two firing temperatures used in this study was influenced by the sintering of illitic clay in the case of sand-tempered briquettes and by the formation of $CaCO_3$ decomposition products that would eventually react with clay, in the case of the chalk-tempered briquettes.

The pore size distribution of the fired RC and WC sand-tempered briquettes closely resembled that of the original raw clay materials and varied proportionally with the amount of clay used. At 800°C, a significant shift towards higher micropore widths is observed in both clay types.

The porosity data obtained from the replicate RC and WC clay briquettes in this doctoral study revealed that there are multiple factors that can influence the

development of porosity. Based on the experimental parameters employed, these factors include the type of clay, mineralogical transformations occurring at varying temperature, and the composition of the non-clay minerals or the added temper, which can react with clay minerals during the manufacturing process. The results also indicate the substantial presence of micro- and mesopores within the briquettes, which are likely sufficient to entrap organic residues and enhance long-term preservation.

4.2 Quantitative analysis of palmitic and oleic acids

Out of the 44 sets of replicate pottery briquettes described in Paper 2, that were utilized for the XRD and porosity analysis, eight (RC-800-S3, RC-800-S4, RC-800-S5, RC-800-S6, RC-800-CH2, RC-800-CH3, RC-800-CH4, and RC-800-CH5) were selected and spiked with $C_{16:0}$ and $C_{18:1}$ to evaluate the extraction yield both with and without degradation. These sets of briquettes were chosen due to the prevalence of illitic clays in unglazed archaeological pottery and the occurrence of $CaCO_3$ thermal transformations at 800°C.

Paper 3 showed that ACM derivatization method consistently achieved higher fatty acid yields, more than two-fold recovery, compared to those obtained using a combination of solvent extraction followed by TMTFTH methylation. Hence, the quantitative yield of $C_{16:0}$ and $C_{18:1}$ from using the ACM was used to evaluate its effect on the briquettes. A discussion on the comparison of the extraction recoveries from ACM and TMTFTH methods are found in Paper 3. Since the absolute yields of $C_{16:0}$ and $C_{18:1}$ is important for determining the recovery relative to the mineral composition of the briquette samples, as demonstrated in this thesis, the FAME calibration curve method is the most appropriate approach for quantification. The archaeological samples will be further discussed in the Case Study section of this doctoral study.

4.2.1 Relationship between mineralogy and preservation of organic residues

4.2.1.1 Sand-tempered clay briquettes

The amount of clay and sand in the replicate pottery briquettes have minimal effect on the recovery of the spiked $C_{16:0}$ and $C_{18:1}$ when no heat was applied (non-degraded). Table 4.2.1.1.1 shows that the average (two replicates) recoveries of 90% (4%) for $C_{16:0}$ and 88% (4%) for $C_{18:1}$, wherein the values in parenthesis represent the half-widths at 95% confidence intervals (CI), have overlapping standard deviations across the samples indicating no significant differences in the recoveries despite the variations in the clay and sand content. The half-widths of the 95% CI are the measured uncertainties.

Degradation, i.e. applying heat on the briquettes containing the adsorbed fatty acids (100°C for 14 h) decreased the average recovery of $C_{16:0}$ to 87% (5%) and also yielded no significant differences in recovery across the briquettes. However,

the unsaturated $C_{18:1}$ was more affected by heating. Its recovery decreased significantly to an average of 61% (5%). A statistically significant correlation was identified between the recovered yield of $C_{18:1}$ and the mineral content of the briquettes.

The reported reduction of degraded $C_{18:1}$ yield compared to $C_{16:0}$ is attributed to the formation of an isomer of $C_{18:1}$. Isomers of $C_{18:1}$, such as *trans* $C_{18:1}$, have been reported as possible diagnostic biomarker for ruminant fats (Mottram et al. 1999; Baeten et al. 2013). However, considering that only two fatty acids were analyzed in this study, the presence of these isomers cannot be ascribed to the direct degradation from food stuffs. Rather, it is more likely the result of the $C_{18:1}$ heat degradation, generated from the catalytic effect of metals (flux elements) within the illitic clay matrix (Poulain et al. 2016). The GC-MS chromatographs in Paper 3 illustrated the progressions of isomer formation, with briquettes containing more clays (less sand) exhibiting lower $C_{18:1}$ yield, while those with less clay (more sand) showed higher $C_{18:1}$ yield. This indicated that sand remains chemically inert under the experimental conditions employed (Kilikoglou et al. 1998), and that the observed isomer formation was influenced by the amount of clay. Similarly, the non-degraded samples show that $C_{16:0}$ and $C_{18:1}$ can be absorbed in the clay matrix and retained even without the application of heat (Drieu et al. 2022).

4.2.1.2 Chalk-tempered clay briquettes

Unlike the sand-tempered briquettes, the recovery of $C_{16:0}$ and $C_{18:1}$ was strongly influenced by the amount of chalk originally added in the briquettes and its decomposition products, even in the absence of heat. A statistically significant correlation was observed between the chalk content and the recovery of both fatty acids (Table 4.2.1.2.1). For the non-degraded samples, the briquettes with more clay (5% and 15% chalk) content, have resulted in more $C_{16:0}$ and $C_{18:1}$ recovery. As the amount of chalk temper increases (30% and 45% chalk), the recovery of these fatty acids decreases. This suggests that, even without heat, interactions between the fatty acids and $CaCO_3$, along with its calcium-containing mineral transformation products, such as CaO, portlandite and calcium-silicate minerals, facilitated the formation of calcium salts of the fatty acids. These salts were only partially converted back into free acids and extracted by the ACM procedure. Furthermore, the structural similarities between the carbonate group and the carboxylate in the fatty acid may have also contributed to the additional stability of the fatty acid salts (Goldenberg et al. 2014). This would have made it more strongly bound to the clay matrix and decreased the ability of the ACM to extract efficiently.

A comparison of the slope (m) and the half-width of its 95% CI in Table 4.2.1.2.1 shows a similar trend was also observed for the degraded $C_{16:0}$, where a statistically significant correlation was also found between the chalk content and the fatty acid recovery. For the degraded $C_{18:1}$, the recovery was not statistically significant, and there is no clear relationship between the amount of clay or chalk and its yield. Despite this, the general trend among the samples remains consistent for the degraded $C_{18:1}$, with higher chalk content associated with reduced recovery.

Table 4.2.1.1.1. Percentage yield of $C_{16:0}$ and $C_{18:1}$ in clay and sand-tempered briquettes for non-degraded and degraded samples.

Clay with sand temper (S)		Non-Degraded						Degraded					
		$C_{16:0}$			$C_{18:1}$			$C_{16:0}$			$C_{18:1}$		
Paper 2[a]	Paper 3[b]	Replicate 1	Replicate 2	Average[c]	Replicate 1	Replicate 2	Average[c]	Replicate 1	Replicate 2	Average[c]	Replicate 1	Replicate 2	Average[c]
RC-800-S3	S-75	93.7	89.4	91.6 (3.0)	91.2	87.4	89.3 (2.7)	90.6	87.1	88.8 (2.5)	75.3	76.0	75.6 (0.5)
RC-800-S4	S-50	94.6	89.4	92.0 (3.7)	95.0	84.5	89.7 (7.4)	92.7	85.5	89.1 (5.1)	67.9	68.2	68.1 (0.2)
RC-800-S5	S-25	82.5	88.8	85.6 (4.5)	85.3	84.4	84.8 (0.6)	86.9	84.7	85.8 (1.6)	52.0	67.5	59.8 (11.0)
RC-800-S6	S-0	88.0	94.4	91.2 (4.5)	83.7	92.9	88.3 (6.6)	91.8	77.4	84.6 (10.2)	28.3	39.3	33.8 (7.8)
Average[d]				90 (4)			88 (4)			87 (5)			61 (5)
m[e]				-0.030			-0.032			-0.064			-0.436
95% CI of m[e]				0.269			0.186			0.079			0.294
Pooled standard deviation					4.6					6.3			

[a] Sample codes used in Paper 2; [b] Sample codes used in Paper 3; [c] Average percentage yield of the two replicates. Values in parentheses represent the standard deviations of the two replicate measurements; [d] Half-width of the 95% confidence interval in parentheses; [e] Slope (m) of the regression line between the average yield of $C_{16:0}$ or $C_{18:1}$ relative to the percentage of clay in the briquettes and its half-width of 95% confidence interval.

Table 4.2.1.2.1. Percentage yield of $C_{16:0}$ and $C_{18:1}$ in clay and sand-tempered briquettes for non-degraded and degraded samples.

Clay with chalk temper (CH)		Non-Degraded						Degraded					
		$C_{16:0}$			$C_{18:1}$			$C_{16:0}$			$C_{18:1}$		
Paper 2[a]	Paper 3[b]	Replicate 1	Replicate 2	Average[c]	Replicate 1	Replicate 2	Average[c]	Replicate 1	Replicate 2	Average[c]	Replicate 1	Replicate 2	Average[c]
RC-800-CH2	CH-45	71.1	64.3	67.7 (4.8)	66.0	61.0	63.5 (3.6)	64.9	57.8	61.4 (5.0)	47.8	51.2	49.5 (2.4)
RC-800-CH3	CH-30	84.4	76.7	80.6 (5.4)	82.0	74.2	78.1 (5.6)	77.7	75.7	76.7 (1.4)	76.5	74.3	75.4 (1.6)
RC-800-CH4	CH-15	89.0	83.6	86.3 (3.8)	88.0	82.2	85.1 (4.1)	85.5	79.7	82.6 (4.1)	83.0	77.6	80.3 (3.9)
RC-800-CH5	CH-5	90.3	88.2	89.2 (1.5)	86.5	90.8	88.6 (3.1)	84.5	83.6	84.1 (0.7)	73.2	82.1	77.6 (6.3)
Average[d]				81 (3)			79 (3)			76 (3)			71 (3)
m[e]				0.326			0.380			0.345			0.427
95% CI of m[e]				0.233			0.249			0.341			0.789
Pooled standard deviation					4.2					3.7			

[a] Sample codes used in Paper 2; [b] Sample codes used in Paper 3; [c] Average percentage yield of the two replicates. Values in parentheses represent the standard deviations of the two replicate measurements; [d] Half-width of the 95% confidence interval in parentheses; [e] Slope (m) of the regression line between the average yield of $C_{16:0}$ or $C_{18:1}$ relative to the percentage of clay in the briquettes and its half-width of 95% confidence interval.

4.2.2 Relationship of micro- and mesoporosity with organic residues

The specific surface area (S_{NLDFT}) of the sand-tempered briquettes used for the recovery of $C_{16:0}$ and $C_{18:1}$ ranged from 44 $m^2 g^{-1}$ for S-0 (100% clay) to 10 $m^2 g^{-1}$ for S-75 (25% clay). The proportion of micropores (S_{micro}) within this range accounts for 48 to 51%, while the rest are attributed to the mesopores. The chalk-tempered briquettes have lower overall S_{NLDFT}, ranging from 31 $m^2 g^{-1}$ for CH-5 (90% clay) to 6.4 $m^2 g^{-1}$ for CH-45 (25% clay), with S_{micro} ranging from 53 to 56% (see Paper 2). Even with the lowest S_{NLDFT} observed in S-75 and CH-45, as well as the lowest fatty acid recovery for the sand tempered briquettes at 33.8%, for the degraded $C_{18:1}$ from S-0, and 49.5% for the degraded $C_{18:1}$ from CH-45 for the chalk tempered briquettes, there is no clear indication that the micro- and meso-sized pores may have influence the amount of $C_{16:0}$ and $C_{18:1}$ recovery. This holds true regardless of whether the fatty acids are non-degraded or degraded, or the type of temper used.

Given the substantial amount of micro- and mesopores in the briquettes, it is likely that the spiked amounts of $C_{16:0}$ and $C_{18:1}$ were sufficiently absorbed into the clay matrix. Furthermore, the larger grain size of sand, primarily composed of quartz and K-feldspars as indicated by XRD data in Paper 2, or the decomposition of chalk at 800°C, likely contributed to the expansion of pores to the macropore (pore width > 50 nm) region within the clay briquettes. These macropores would be undetectable by the N_2 porosimeter due to its measurement limitations in the micro- and mesopore regions. These findings suggest that mineral interactions with the fatty acids may have a more direct role in the initial retention of organic residues, while pore adsorption may contribute to their long-term preservation.

4.3 Applied case study: Kukruse 12th to 13th century AD pottery

To further test the methodologies presented above for disentangling organic-inorganic interactions in archaeological pottery (Figure 4.3.1), a selection of archaeological pottery excavated from the 12th–13th century AD Kukruse cemetery, in northeastern Estonia (Lõhmus et al. 2011), was subjected to ATR-FT-IR-PLS method developed for quantifying the mineralogical composition, N_2 porosimeter for the analysis of the micro- and mesopore structures, and GC-MS for the absolute quantification of palmitic acid ($C_{16:0}$) and oleic acid ($C_{18:1}$). The excavated vessels exhibit diverse typologies, suggesting a combination of locally produced and potentially also imported wares. From the total assemblage of 14 vessels recovered, three – designated as Kukruse V, Kukruse XXXVII, and Kukruse XLIII – were selected for the analytical tests in this study (Oras et al. 2018).

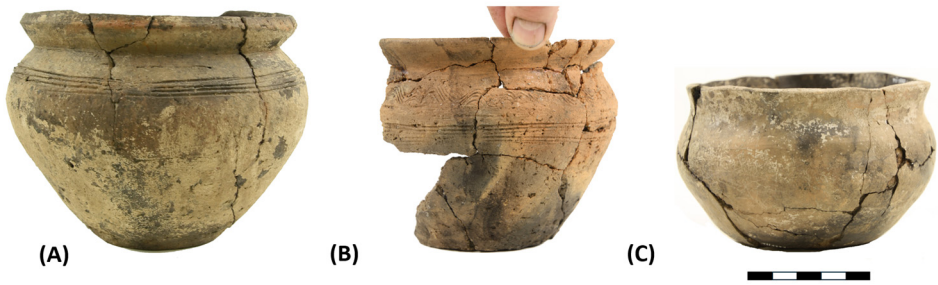

Figure 4.3.1. The archaeological pottery excavated at the Kukruse cemetery where the samples, (a) Kukruse V, (b) Kukruse XXXVII, and (c) Kukruse XLIII, were obtained (Photo by Ester Oras).

4.3.1 Analysis of clay and non-clay minerals using ATR-FT-IR-PLS

The mineralogical analysis of the selected Kukruse vessels (see Table 4.3.1.1) using the ATR-FT-IR-PLS model in Paper 1 identified Clay Minerals group 2 (i.e. 2:1 clay mineral type) as the most abundant clay mineral in the three samples. Kukruse XXXVII exhibited the highest Clay Mineral group 2 content at (40.1±5.1) g/100g, while Kukruse V had the lowest at (10.6±5.1) g/100g. Kukruse XLIII has the median amount of (35.6±5.1)g/100g. Clay minerals grouped under 1 (i.e. kaolinite/halloysite) and 3 (i.e. chlorite/chlorite-smectite) were not detected in the XRD data.

For the non-clay minerals, Kukruse XLIII was found to have the highest amount of silica varieties, with (41.1±3.6)g/100g identified by the PLS model. Kukruse XXXVII has the most abundant feldspar content at (24.6± 4.0)g/100g, while Kukruse V has the lowest amount of both silicate varieties (7.2±3.6)g/100g and feldspars (11.6± 4.0)g/100g, respectively. This trend aligns well with the results of the XRD, which similarly identified the distribution of silica varieties and feldspars across the samples. Regarding the carbonates (i.e. calcite, aragonite, dolomite, siderite, ankerite), Kukruse V exhibited the highest amount quantified by the PLS method at (81.2±0.9)g/100g. The XRD analysis supported this, identifying 76.5g/100g of carbonates in Kukruse V, while no carbonates were detected from Kukruse XXXVII and Kukruse XLIII.

However, the PLS model has overestimated the amount of iron-oxyhydroxides in Kukruse V, quantifying it at (6.4±1.9)g/100g, which resulted to a total mineral content exceeding 100g/100g (i.e. (111.1±8.3)g/100g). This overestimation may have likely resulted from this mineral group due to the XRD not able to detect any iron-oxyhydroxides in Kukruse V or any of the other samples, despite the PLS model predicting that Kukruse XLIII and Kukruse XXXVII containing (0.9±1.90)g/100g and (0.7±1.9)g/100g of iron-oxyhydroxides, respectively.

Based on the results of the ATR-FT-IR-PLS method, the selected Kukruse vessels can be classified according to their mineralogical composition as represen-

Table 4.3.1.1. Quantitative mineral contents of the Kukruse archaeological pottery samples using the ATR-FT-IR-PLS method.[a]

Pottery sample	Content (g/100g) of the compound														Total quantified (g/100g)	
	Silica varieties [b]		Feldspars [c]		Clay minerals 1 [d]		Clay minerals 2 [e]		Clay minerals 3 [f]		Carbonates [g]		Iron-oxy-hydroxides [h]			
	XRD	PLS	XRD	PLS	XRD	PLS	XRD	PLS	XRD	PLS	XRD	PLS	XRD	PLS	XRD	PLS
Kukruse V	6.5	7.2 ±3.6	2.6	11.6±4.0	0.0	-3.7±2.6	12.7	10.6±5.1	0.0	-2.2±1.8	76.5	81.2±0.9	0.0	6.4±1.9	100 [i]	111.1±8.3
Kukruse XXXVII	34.1	32.8±3.6	19.1	24.6±4.0	0.0	-2.4±2.6	46.8	40.1±5.1	0.0	-1.7±1.8	0.0	1.6 ±0.9	0.0	0.7±1.9	100	95.7 ±8.3
Kukruse XLIII	56.2	41.1±3.6	12.6	16.1±4.0	0.0	-0.8±2.6	30.3	35.6±5.1	0.0	0.3±1.8	0.0	1.5 ±0.9	0.0	0.9±1.9	99.7 [j]	94.7 ±8.3

[a] Samples from the University of Tartu archaeology collection; site ID no. TÜ1777, roman number indicates burial/pot number. Uncertainties of the mineral contents correspond to the RMSEP values. The uncertainty of the total quantified amount was found as the square root of sums of squares of individual component of the RMSEP values. [b] quartz, cristobalite. [c] K-feldspar, plagioclase. [d] kaolinite, halloysite. [e] smectite, illite, mica, illite-semectite, vermiculite. [f] chlorite, chlorite-smectite. [g] calcite, aragonite, dolomite, siderite, ankerite. [h] hematite/goethite. [i] contains apatite (1.7g/100g). [j] contains Ti-oxides (anatase/ rutile) (0.6g/100g).

tatives of different clay and temper types in pottery: Kukruse V with higher carbonate (chalk) content, Kukruse XXXVII with higher clay mineral content, and Kukruse XLIII with higher quartz (sand) content. These vessels were found to approximate the composition of the replicate clay briquettes used in this study, with varying proportions of clay and tempers such as sand or chalk ($CaCO_3$), and to test the implications of these clay compositions to pottery porosity and subsequent quantification of $C_{16:0}$ and $C_{18:1}$ yield from those sherds.

4.3.2 Micro- and mesoporosity

4.3.2.1 Pore characteristics

The Kukruse V pottery, which consists of 76.5 g/100 g carbonates (74.4 g/100g calcite and 2.1 g/100g dolomite), by XRD analysis, had greater porosity parameters (S_{NLDFT} and V_{NLDFT}) compared to the Kukruse XLIII and Kukruse XXXVII, which primarily composed of quartz most likely from added sand temper or naturally found in the clays (Table 4.3.2.1.1). Specifically, the S_{NLDFT} (15 $m^2\ g^{-1}$) and the V_{NLDFT} (20 $mm^3\ g^{-1}$) of Kukruse V are both higher compared to Kukruse XLIII and Kukruse XXXVII. Two possibilities may account for the greater formation of micro- and mesopores in Kukruse V. First is the possibility that the abundant $CaCO_3$ identified from the XRD data was a product of the recarbonation process of lime (CaO) (Shoval 2003; Shoval et al. 2011), produced during high temperature (T > 800°C) firing of pottery and have reacted with atmospheric CO_2 over hundreds of years, following the lime cycle reaction (Fabbri et al. 2014; Herrick and Berna 2024). CaO could have been produced if the firing temperature exceeded 800°C, leading to the thermal decomposition of $CaCO_3$, as observed in this study's model chalk-tempered clay briquettes fired at 800°C (RC800-CH and WC800-CH series). The second possibility is that the $CaCO_3$ was originally present in the clay matrix, described as a primary calcite, and was not fully decomposed during firing, suggesting a lower firing temperature likely T < 650°C in an oxidizing atmosphere or T < 750°C in a reducing atmosphere (Tite et al. 2001; Fabbri et al. 2014). Hence, the release of CO_2 during the production process and the aggregation of $CaCO_3$ may have contributed to the increased micro- and mesoporosity observed in the Kukruse V pottery compared to the other two samples (Trindade et al. 2009).

Table 4.3.2.1.1. Surface area and pore volume parameters of the Kukruse archaeological samples determined from the N_2 adsorption isotherms.

Archaeological samples	Specific surface area			Specific pore volume		
	S_{BET} ($m^2\ g^{-1}$)	S_{NLDFT} ($m^2\ g^{-1}$)	S_{micro} (%)	$V_{0.95}$ ($mm^3\ g^{-1}$)	V_{NLDFT} ($mm^3\ g^{-1}$)	V_{micro} (%)
Kukruse V	12	15	47	24	20	12
Kukruse XXXVII	8	9	40	19	16	9
Kukruse XLIII	7	8	48	16	12	12

The pottery with the highest clay mineral content, as quantified by XRD in Paper 1, is Kukruse XXXVII, which contained 46.8 g/100g of Clay Minerals 2 group (or 2:1 clay mineral type). The results show that Kukruse XXXVII exhibited a slightly higher S_{NLDFT} of 9 m^2 g^{-1}, compared to the Kukruse XLIII which has a higher sand content, with 56.2 g/100g of silica varieties (mainly quartz in sand) and a lower S_{NLDFT} value of 8 m^2 g^{-1}. Additionally, Kukruse XXXVII formed a greater V_{NLDFT} of 16 mm^3 g^{-1}, in contrast to Kukruse XLIII, which has a V_{NLDFT} of 12 mm^3 g^{-1}.

A similar general trend was observed in the replicate sand-tempered briquettes made from an illitic/illite-smectitic clay type (RC clay) in Paper 2. The clay content increased proportionally with both the S_{NLDFT} and V_{NDLFT}, or consequently, these pore parameters change inversely with the amount of added sand temper in the briquettes. These results are comparable with the findings for Kukruse XXXVII and Kukruse XLIII, regardless of the firing temperatures of the replicate briquettes at either 600°C or 800°C. Sand, in its raw material form, has an almost negligible contribution to porosity (Kilikoglou et al. 1998), resulting in lesser micro- and mesopores in pottery with higher sand content such as in Kukruse XLIII.

4.3.2.2 Pore-size distribution

The pore-size distribution of the three Kukruse vessels revealed the presence of significant volume of micropores (width < 2 nm) ranging from 1.4 to 2.4 mm^3 g^{-1}. This level of porosity is sufficient to protect the absorbed food residues within the pottery matrix. As shown in Figure 4.3.2.2.1, Kukruse V exhibited a peak maximum at 1.5 nm, accompanied by a peak shoulder at about 1.1 nm, which is characteristic of the chalk-tempered briquettes with an illite/illite-smectite clay group (RC clay) used as replicate archaeological ceramics in this study. A slight shift of the peak distribution maximum to about 1.6 nm was observed for both Kukruse XLIII and XXXVII. This suggests that the relatively higher clay content in Kukruse XXXVII, and the higher sand content in Kukruse XLIII, did not significantly alter the micropore volumes.

In addition to the microporosity, the $CaCO_3$-rich Kukruse V also displayed a larger volume of mesopores (width between 2 nm to 50 nm) compared to the clay-rich Kukruse XXXVII and sand-rich Kukruse XLIII. The presence of mesopores may also enhance the capacity of the ceramic matrix to absorb more lipids and other food residues. Direct comparisons between the Kukruse vessels and the model sand- and chalk-tempered briquettes remain complicated due to the differences in the manufacturing processes, firing temperatures, and uncertainties regarding the extent of diagenetic changes in the archaeological pottery. Despite these limitations, the model briquettes made in this study provided a useful basis for comparison with the archaeological Kukruse pottery samples.

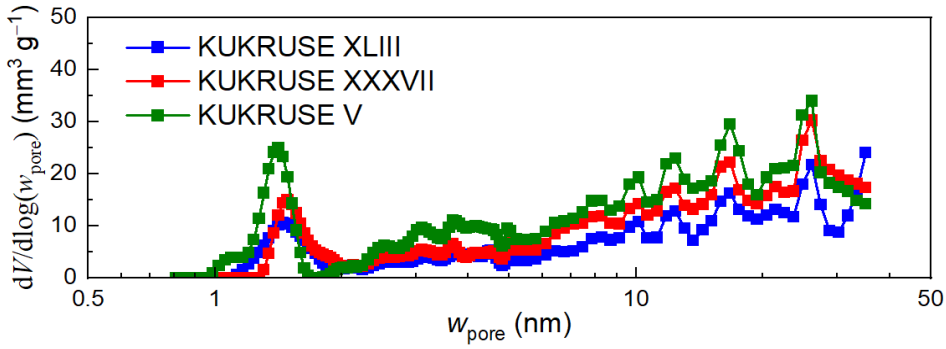

Figure 4.3.2.2.1. Pore-size distributions, as differential pore volumes (dV/dlog(w_{pore})) vs pore widths (w_{pore}) of the Kukruse archaeological samples.

4.3.3 Absolute quantification of palmitic and oleic acids

Calibration curves were prepared for $C_{16:0}$ and $C_{18:1}$ from the same FAME stock solution used for the replicate pottery briquettes. The concentration range was adjusted to account for the higher absolute abundance of fatty acids, particularly $C_{16:0}$, in the archaeological pottery compared to the spiked concentrations in the briquettes. The resulting calibration curves produced very good linearity for both $C_{16:0}$ and $C_{18:1}$, with coefficients of determination (R^2) of 0.9986 and 0.9995, respectively (Figure 4.3.3.1). This indicated that the calibration curves remained replicable and robust, even with an increase concentration of FAME solution.

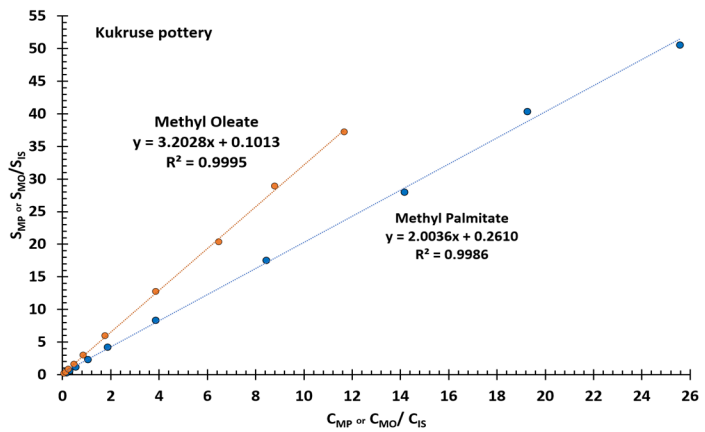

Figure 4.3.3.1. Calibration curves used to quantify the amount of $C_{16:0}$ as methyl palmitate, and $C_{18:1}$ as methyl oleate extracted using ACM. The peak area ratios of methyl palmitate (S_{MP}) or methyl oleate (S_{MO}), relative to the area of the internal standard, 10% hexadecane in toluene (S_{IS}) was plotted relative to the concentration ratios of the analytes (C_{MP}) or (C_{MO}), and the internal standard (C_{IS}).

Among the archaeological samples analyzed, Kukruse V, which has the highest carbonate composition of (81.2±0.9) g/100 g based on the PLS method, exhibited the lowest amount of $C_{16:0}$ and $C_{18:1}$ extracted in ACM, with yields of 7.7 µg/g clay and 0.59 µg/g clay, respectively (Table 4.3.3.1). These findings are consistent with the general results from the chalk-tempered clay briquettes, which demonstrated a decreasing trend in $C_{16:0}$ and $C_{18:1}$ yields when the chalk content exceeded 30%, regardless of whether the briquette sample was degraded or non-degraded.

In contrast, Kukruse XXXVII and XLIII have significantly higher yields, with $C_{16:0}$ exceeding 100 µg/g clay and more than 17 µg/g clay for $C_{18:1}$. Specifically, the clay-rich Kukruse XXXVII exhibited the highest $C_{16:0}$ yield at 155 µg/g clay. As expected, the unsaturated $C_{18:1}$ consistently showed lower yields than $C_{16:0}$ across all the Kukruse samples, indicating that unsaturated compounds are indeed more susceptible to degradation, regardless of the mineral composition.

Furthermore, it appears that Kukruse XLIII, identified as the sample with the most silicate variety (i.e. quartz) content based on the PLS method, showed a generally higher $C_{18:1}$ extracted amount of 21 µg/g clay compared to Kukruse XXXVII. This observation correlates with the results from the sand-tempered briquettes, which suggests that an increase in sand content may favor the retention of relatively higher amounts of $C_{18:1}$.

Table 4.3.3.1. $C_{16:0}$ and $C_{18:1}$ yields from the Kukruse archaeological samples.

Archeological Samples	$C_{16:0}$ yield (µg/g clay)	$C_{18:1}$ yield (µg/g clay)
Kukruse V	7.7	0.59
Kukruse XXXVII	155	17
Kukruse XLIII	135	21

To further demonstrate the effectiveness of the FAME calibration curve in the absolute quantification of fatty acids in archaeological pottery, the same calibration solutions used for $C_{16:0}$ and $C_{18:1}$ were applied to quantify two additional fatty acids that are present in the Kukruse samples, specifically myristic acid ($C_{14:0}$) and stearic acid ($C_{18:0}$) (Figure 4.3.3.2). The calibration curves constructed for both $C_{14:0}$ and $C_{18:0}$ were linear and have an R^2 value of at least 0.998, making it suitable for accurate quantification.

The yields of $C_{14:0}$ and $C_{18:0}$ followed a pattern similar to that observed for $C_{16:0}$ and $C_{18:1}$. The calcium carbonate-rich Kukruse V, still had the lowest fatty acid yields, with 2.4 µg/g clay for $C_{14:0}$ and 1.7 µg/g clay for $C_{18:0}$. On the other hand, Kukruse XXXVII, which is composed of more clays, produced the highest yields, with 140 µg/g clay for $C_{14:0}$ and 31 µg/g clay for $C_{18:0}$. Kukruse XLIII, which contains the highest amount of silicates, showed intermediate yields, with 49 µg/g clay for $C_{14:0}$ and 43 µg/g clay for $C_{18:0}$.

The interpretation of the organic residues quantified from the Kukruse pottery requires caution since the usage and technical history of the vessels are unknown. It is also impossible to know whether the quantified fatty acids represent a single

cooking event or a series of such events over its lifetime of use. Additionally, post-depositional effects were not accounted for, which may have influenced or altered the concentration of the extracted fatty acids (Rice 2015). Consequently, the measured quantities may not accurately reflect the original contents of the archaeological pottery. Despite these uncertainties, the results of the quantification made on the pottery has demonstrated good consistency with the mineralogical content, as shown in Paper 3.

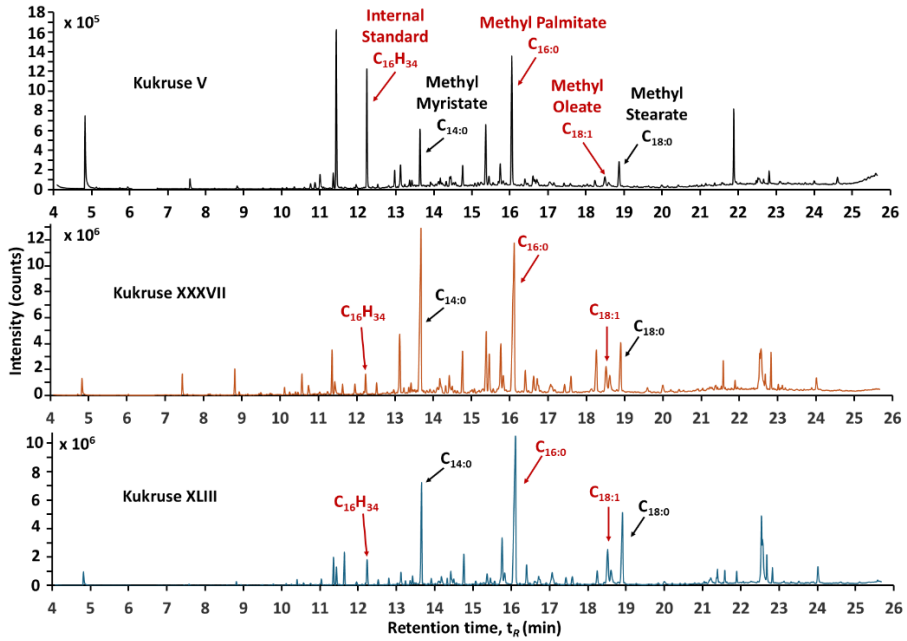

Figure 4.3.3.2. Total ion current (TIC) chromatogram of pottery samples from Kukruse V, XXXVII and XLIII obtained from ACM. The methylated fatty acids (i.e. $C_{14:0}$, $C_{16:0}$, $C_{18:1}$, and $C_{18:0}$), quantified in this study were labelled.

The amount of $C_{16:0}$ and $C_{18:1}$ quantified in the three Kukruse pottery samples far exceed the concentration of the same fatty acids spiked on the clay briquettes. Interestingly, Kukruse V, which exhibited the highest S_{NLDFT} value (15 $m^2\ g^{-1}$) yielded the lowest amount of $C_{16:0}$ and $C_{18:1}$, while the Kukruse XXXVII, which produced the median value of S_{NLDFT} (9 $m^2\ g^{-1}$) has the highest concentration of these fatty acids. This comparison clearly indicates that there is no direct correlation between the micro- and mesoporosity of the pottery and the quantity of fatty acids recovered, other than the assumption that these nanometer sized pores were sufficiently large to accommodate the organic residues and may have protected them from further degradation. However, the case study of these three archaeological vessels has shown that mineralogical composition can affect the preservation process.

SUMMARY

This PhD work has provided a quantitative baseline information into the factors influencing the retention and preservation of organic residues, particularly $C_{16:0}$ and $C_{18:1}$, in archaeological pottery. These factors are (1) the formation of pores in the clay matrix, which enhances the absorption of organic residues, and (2) the mineralogical composition, covering both initial clay and added tempers. These were investigated by creating 44 experimental replicate clay briquettes composed of different clays (illitic/illite-smectitic and kaolinite clay types), different tempers (sand and chalk), and fired at two different temperatures (600°C and 800°C). Within these sets, one group of clay samples spiked with $C_{16:0}$ and $C_{18:1}$ was allowed to adsorb and was thereafter air dried without further treatments (non-degraded), while another group was subjected to degradation at 100°C for 14 h to mimic cooking events (degraded). The analytical results from experimental material were compared with three selected archaeological pottery from a 12^{th}–13^{th} century AD burial site at Kukruse, Estonia.

Based on the porosity analysis of the experimental briquettes, the formation of micro- and meso-sized pores, are dictated by the initial porosity of the clay raw material, which is further modified by the type of temper added and the mineralogical transformations resulting from the firing temperature. The addition of sand has minimal effect on the porosity, while chalk, specifically at their decomposition at 800°C, can alter the development of micro- and mesopores depending if illitic/illite-smectitic or kaolinic clays. These are important considerations especially when choosing archaeological pottery that will most likely produce greater amounts of micro- and mesoporosity.

The yield of $C_{16:0}$ and $C_{18:1}$ spiked on selected briquettes were also found to be considerably influenced by the composition of the clay and temper. Absolute quantification using the FAME-based calibration curves was employed for more accurate quantification of $C_{16:0}$ and $C_{18:1}$ yield from the replicate briquettes. The results show that the unsaturated $C_{18:1}$ was particularly affected in sand-tempered briquettes, where heating with illitic clays catalyzed its conversion into an isomer. Sand in clay had a minimal effect on the yield of non-degraded fatty acids and degraded $C_{16:0}$. In contrast, a high proportion of chalk enhanced the binding of both $C_{16:0}$ and $C_{18:1}$ on the clay matrix, regardless of whether the fatty acids were degraded or non-degraded. Degraded $C_{18:1}$ was shown to bind more strongly to the mineral matrix as the chalk added increased. This effect is attributed to the formation of fatty acid calcium salts which enhances lipid preservation.

The key mineral components potentially influencing the retention of organic residues in pottery are the clay minerals, quartz from sand, and $CaCO_3$ from chalk. These minerals were identified effectively by the ATR-FT-IR-PLS method in the Kukruse archaeological pottery (Kukruse V, Kukruse XXXVIII and Kukruse XLIII). Furthermore, the archaeological pottery contained significant micro- and mesopores, with pore parameter values comparable to those of the replicate

pottery briquettes containing higher proportions of $CaCO_3$ (Kukruse V), clay (Kukruse XXXVIII), and sand (Kukruse XLIII), respectively.

Absolute quantification using the FAME calibration curves was also employed in the Kukruse samples to determine the yields of $C_{16:0}$ and $C_{18:1}$ and was found to have consistent results with that of the briquettes. Kukruse V, characterized by the highest $CaCO_3$ content, exhibited lower fatty acid yields, while the samples with relatively higher clay content (Kukruse XXXVII and Kukruse XLIII) produced the yielded fatty acid yields. Additionally, other fatty acids, such as myristic and stearic acids, were quantified, and their yields were found to correlate consistently with the mineral content.

All things considered, the results of this study have demonstrated that the mineralogical changes which occurred in clays upon heating, including the formation of micro- and mesoporosity have an impact on the amount of $C_{16:0}$ and $C_{18:1}$ that can be recovered from the pottery. These physical and chemical changes are essential for interpreting ORA data and future ORA methodologies should incorporate the influence of mineral composition on the preservation and yield of organic compounds.

REFERENCES

Admiraal, M.; Lucquin, A.; Von Tersch, M.; Craig, O. E.; Jordan, P. D. The Adoption of Pottery on Kodiak Island: Insights from Organic Residue Analysis. *Quat. Int.* **2020**, *554*, 128–142. https://doi.org/10.1016/j.quaint.2020.06.024.

Aili, A.; Maruyama, I. Review of Several Experimental Methods for Characterization of Micro- and Nano-Scale Pores in Cement-Based Material. *Int. J. Concr. Struct. Mater.* **2020**, *14* (1), 55. https://doi.org/10.1186/s40069-020-00431-y.

Akyuz, S.; Guliyev, F.; Celik, S.; Ozel, A. E.; Alakbarov, V. Investigations of the Neolithic Potteries of 6th Millennium BC from Göytepe-Azerbaijan by Vibrational Spectroscopy and Chemometric Techniques. *Vib. Spectrosc.* **2019**, *105*, 102980. https://doi.org/10.1016/j.vibspec.2019.102980.

Ali, A.; Chiang, Y. W.; Santos, R. M. X-Ray Diffraction Techniques for Mineral Characterization: A Review for Engineers of the Fundamentals, Applications, and Research Directions. *Minerals* **2022**, *12* (2), 205. https://doi.org/10.3390/min12020205.

Allegretta, I.; Eramo, G.; Pinto, D.; Kilikoglou, V. Strength of Kaolinite-Based Ceramics: Comparison between Limestone- and Quartz-Tempered Bodies. *Appl. Clay Sci.* **2015**, *116–117*, 220–230. https://doi.org/10.1016/j.clay.2015.03.018.

Baeten, J.; Jervis, B.; De Vos, D.; Waelkens, M. Molecular Evidence for the Mixing of Meat, Fish and Vegetables in Anglo- Saxon Coarseware from Hamwic, UK. *Archaeometry* **2013**, *55* (6), 1150–1174. https://doi.org/10.1111/j.1475-4754.2012.00731.x.

Bakraji, E. H.; Rihawy, M. S.; Castel, C.; Abboud, R. PIXE Multivariate Statistics and OSL Investigation for the Classification and Dating of Archaeological Pottery Excavated at Tell Al-Rawda Site, Syria. *Nucl. Instrum. Methods Phys. Res. Sect. B Beam Interact. Mater. At.* **2015**, *347*, 20–25. https://doi.org/10.1016/j.nimb.2015.01.050.

Barbera, G.; Barone, G.; Crupi, V.; Longo, F.; Maisano, G.; Majolino, D.; Mazzoleni, P.; Teixeira, J.; Venuti, V. Small Angle Neutron Scattering Study of Ancient Pottery from Syracuse (Sicily, Southern Italy). *J. Archaeol. Sci.* **2013**, *40* (2), 983–991. https://doi.org/10.1016/j.jas.2012.09.021.

Barker, A.; Venables, B.; Stevens, S. M.; Seeley, K. W.; Wang, P.; Wolverton, S. An Optimized Approach for Protein Residue Extraction and Identification from Ceramics After Cooking. *J. Archaeol. Method Theory* **2012**, *19* (3), 407–439. https://doi.org/10.1007/s10816-011-9120-5.

Barone, G.; Lo Giudice, A.; Mazzoleni, P.; Pezzino, A.; Barilaro, D.; Crupi, V.; Triscari, M. Chemical Characterization and Statistical Multivariate Analysis of Ancient Pottery from Messina, Catania, Lentini and Siracusa (Sicily). *Archaeometry* **2005**, *47* (4), 745–762. https://doi.org/10.1111/j.1475-4754.2005.00230.x.

Barone, G.; Crupi, V.; Majolino, D.; Mazzoleni, P.; Teixeira, J.; Venuti, V. Small Angle Neutron Scattering as Fingerprinting of Ancient Potteries from Sicily (Southern Italy). *J. Appl. Phys.* **2009**, *106* (5), 054904. https://doi.org/10.1063/1.3204020.

Barone, G.; Crupi, V.; Majolino, D.; Mazzoleni, P.; Teixeira, J.; Venuti, V.; Scandurra, A. Small Angle Neutron Scattering as Fingerprinting of Ancient Potteries from Sicily (Southern Italy). *Appl. Clay Sci.* **2011**, *54* (1), 40-46. https://doi.org/10.1016/j.clay.2011.07.010.

Beltrame, M.; Sitzia, F.; Liberato, M.; Santos, H.; Barata, F. T.; Columbu, S.; Mirão, J. Comparative Pottery Technology between the Middle Ages and Modern Times (Santarém, Portugal). *Archaeol. Anthropol. Sci.* **2020**, *12* (7), 130. https://doi.org/10.1007/s12520-020-01053-x.

Bersani, D.; Lottici, P. P. Raman Spectroscopy of Minerals and Mineral Pigments in Archaeometry. *J. Raman Spectrosc.* **2016**, *47* (5), 499–530. https://doi.org/10.1002/jrs.4914.

Bitetto, A.; Mangone, A.; Mininni, R. M.; Giannossa, L. C. A Nonlinear Principal Component Analysis to Study Archeometric Data. *J. Chemom.* **2016**, *30* (7), 405–415. https://doi.org/10.1002/cem.2807.

Bondetti, M.; Scott, E.; Courel, B.; Lucquin, A.; Shoda, S.; Lundy, J.; Labra-Odde, C.; Drieu, L.; Craig, O. E. Investigating the Formation and Diagnostic Value of ω -(*o* -alkylphenyl)Alkanoic Acids in Ancient Pottery. *Archaeometry* **2021**, *63* (3), 594–608. https://doi.org/10.1111/arcm.12631.

Botticelli, M.; Mignardi, S.; De Vito, C.; Liao, Y.; Montanari, D.; Shakarna, M.; Nigro, L.; Medeghini, L. Variability in Pottery Production at Khalet Al-Jam'a Necropolis, Bethlehem (West Bank): From the Early-Middle Bronze to the Iron Age. *Ceram. Int.* **2020**, *46* (10), 16405–16415. https://doi.org/10.1016/j.ceramint.2020.03.200.

Bouchard, G. P.; Mentzer, S. M.; Riel-Salvatore, J.; Hodgkins, J.; Miller, C. E.; Negrino, F.; Wogelius, R.; Buckley, M. Portable FTIR for On-Site Screening of Archaeological Bone Intended for ZooMS Collagen Fingerprint Analysis. *J. Archaeol. Sci. Rep.* **2019**, *26*, 101862. https://doi.org/10.1016/j.jasrep.2019.05.027.

Brigatti, M. F.; Galan, E.; Theng, B. K. G. Chapter 2 Structures and Mineralogy of Clay Minerals. In *Developments in Clay Science*; Elsevier, 2006; Vol. 1, pp 19–86. https://doi.org/10.1016/S1572-4352(05)01002-0.

Bruni, S.; Longoni, M.; De Filippi, F.; Calore, N.; Bagnasco Gianni, G. External Reflection FTIR Spectroscopy Applied to Archaeological Pottery: A Non-Invasive Investigation about Provenance and Firing Temperature. *Minerals* **2023**, *13*, 1211. https://doi.org/10.3390/min13091211.

Bunaciu, A. A.; Udriştioiu, E. G.; Aboul-Enein, H. Y. X-Ray Diffraction: Instrumentation and Applications. *Crit. Rev. Anal. Chem.* **2015**, *45* (4), 289–299. https://doi.org/10.1080/10408347.2014.949616.

Carrer, F.; Colonese, A. C.; Lucquin, A.; Petersen Guedes, E.; Thompson, A.; Walsh, K.; Reitmaier, T.; Craig, O. E. Chemical Analysis of Pottery Demonstrates Prehistoric Origin for High-Altitude Alpine Dairying. *PLOS ONE* **2016**, *11* (4), e0151442. https://doi.org/10.1371/journal.pone.0151442.

Carter, E. A.; Wood, M. L.; De Waal, D.; Edwards, H. G. M. Porcelain Shards from Portuguese Wrecks: Raman Spectroscopic Analysis of Marine Archaeological Ceramics. *Herit. Sci.* **2017**, *5* (1), 17. https://doi.org/10.1186/s40494-017-0130-9.

Casale, S.; Van Dessel, K.; Hoogland, M. L. P.; Degryse, P.; Hofman, C. L. Technological Persistence in Ceramic Production in the Southeastern Hispaniola. The Case Study of El Cabo (600–1502 CE). *J. Anthropol. Archaeol.* **2022**, *65*, 101387. https://doi.org/10.1016/j.jaa.2021.101387.

Cau Ontiveros, M. A.; Day, P. M.; Montana, G. Secondary Calcite in Archaeological Ceramics: Evaluation of Alteration and Contamination Processes by Thin Section Study. In *Modern Trends in Scientific Studies on Ancient Ceramics*; Kilikoglou, V.; Hein, A.; Maniatis, Y. Eds.; Papers presented at the 5th European Meeting on Ancient Ceramics, Athens 1999; BAR International Series 1011; Archaeopress: Oxford, UK, 2002, pp 9-18.

Cayme, J.-M. C.; Palm, R.; Somelar, P.; Vahur, S.; Leito, I.; Oras, E. Influence of Mineral Composition and Firing Temperature on the Micro- and Mesoporosity of Replicate Archaeological Ceramics. *Clays Clay Miner.* **2024a**, *72*, e13. https://doi.org/10.1017/cmn.2024.18.

Cayme, J.-M. C.; Vahur, S.; Teearu, A.; Oras, E.; Leito, I. The Impact of Mineral Composition on the Yield and Preservation of Selected Fatty Acids in Replicate Archeological Ceramics. *J. Chem. Metrol.* **2024b**, *18* (2), 95–113. https://doi.org/10.25135/jcm.117.2409.3336.

Charters, S.; Evershed, R. P.; Goad, L. J.; Leyden, A.; Blinkhorn, P. W.; Denham, V. Quantification and Distribution of Lipid in Archaeological Ceramics: Implications for Sampling Potsherds for Organic Residue Analysis and the Classification of Vessel Use. *Archaeometry* **1993**, *35* (2), 211–223. https://doi.org/10.1111/j.1475-4754.1993.tb01036.x.

Charters, S.; Evershed, R. P.; Quye, A.; Blinkhorn, P. W.; Reeves, V. Simulation Experiments for Determining the Use of Ancient Pottery Vessels: The Behaviour of Epicuticular Leaf Wax During Boiling of a Leafy Vegetable. *J. Archaeol. Sci.* **1997**, *24* (1), 1–7. https://doi.org/10.1006/jasc.1995.0091.

Charuwat, P.; Boardman, G.; Bott, C.; Novak, J. T. Thermal Degradation of Long Chain Fatty Acids. *Water Environ. Res.* **2018**, *90* (3), 278–287. https://doi.org/10.2175/106143017X15131012152825.

Chasan, R.; Spiteri, C.; Rosenberg, D. Dietary Continuation in the Southern Levant: A Neolithic-Chalcolithic Perspective through Organic Residue Analysis. *Archaeol. Anthropol. Sci.* **2022**, *14* (3), 49. https://doi.org/10.1007/s12520-022-01519-0.

Chatfield, M. Tracing Firing Technology through Clay Properties in Cuzco, Peru. *J. Archaeol. Sci.* **2010**, *37* (4), 727–736. https://doi.org/10.1016/j.jas.2009.11.003.

Chen, S.; Vahur, S.; Teearu, A.; Juus, T.; Zhilin, M.; Savchenko, S.; Oshibkina, S.; Asheichyk, V.; Vashanau, A.; Lychagina, E.; Kashina, E.; German, K.; Dubovtseva, E.; Kriiska, A.; Leito, I.; Oras, E. Classification of archaeological adhesives from Eastern Europe and Urals by ATR-FT-IR spectroscopy and chemometric analysis. *Archaeometry* **2022**, *64* (1), 227–244. https://doi.org/10.1111/ARCM.12686.

Chen, S.; Johanson, K.; Matthews, J. A.; Sammler, S.; Blehner, M. A.; Salmar, S.; Leito, I.; Oras, E. Multi-Proxy Analysis of Starchy Plant Consumption: A Case Study of Pottery Food Crusts from a Late Iron Age Settlement at Pada, Northeast Estonia. *Veg. Hist. Archaeobotany* **2024**, *33* (3), 407–423. https://doi.org/10.1007/s00334-023-00950-0.

Chowdhury, M. P.; Campbell, S.; Buckley, M. Proteomic Analysis of Archaeological Ceramics from Tell Khaiber, Southern Iraq. *J. Archaeol. Sci.* **2021**, *132*, 105414. https://doi.org/10.1016/j.jas.2021.105414.

Cohen, A. S.; Galaty, M. L.; Fisher, C. T. Petrographic Analysis of Ceramics and Clay from Angamuco, Michoacán. *J. Archaeol. Sci. Rep.* **2018**, *19*, 155–165. https://doi.org/10.1016/j.jasrep.2018.02.035.

Coli, V. L.; Gomart, L.; Pisani, D. F.; Cohen, S.; Blanc-Féraud, L.; Leblond, J.; Binder, D. Microcomputed Tomography for Discriminating Between Different Forming Techniques in Ancient Pottery: New Segmentation Method and Pore Distribution Recognition. *Archaeometry* **2022**, *64*, 84-99. https://doi.org/10.1111/arcm.12693.

Colombini, M. P.; Modugno, F.; Ribechini, E. Organic Mass Spectrometry in Archaeology: Evidence for *Brassicaceae* Seed Oil in Egyptian Ceramic Lamps. *J. Mass Spectrom.* **2005a**, *40* (7), 890–898. https://doi.org/10.1002/jms.865.

Colombini, M. P.; Giachi, G.; Modugno, F.; Ribechini, E. Characterisation of Organic Residues in Pottery Vessels of the Roman Age from Antinoe (Egypt). *Microchem. J.* **2005b**, *79* (1–2), 83–90. https://doi.org/10.1016/j.microc.2004.05.004.

Correa-Ascencio, M.; Evershed, R. P. High Throughput Screening of Organic Residues in Archaeological Potsherds Using Direct Acidified Methanol Extraction. *Anal. Methods* **2014**, *6* (5), 1330. https://doi.org/10.1039/c3ay41678j.

Craddock, P. R.; Herron, M. M.; Herron, S. L. Comparison of Quantitative Mineral Analysis By X-Ray Diffraction and Fourier Transform Infrared Spectroscopy. *J. Sediment. Res.* **2017**, *87* (6), 630–652. https://doi.org/10.2110/jsr.2017.34.

Craig, O. E.; Taylor, G.; Mulville, J.; Collins, M. J.; Parker Pearson, M. The Identification of Prehistoric Dairying Activities in the Western Isles of Scotland: An Integrated Biomolecular Approach. *J. Archaeol. Sci.* **2005**, *32* (1), 91–103. https://doi.org/10.1016/j.jas.2004.06.009.

Craig, O. E.; Forster, M.; Andersen, S. H.; Koch, E.; Crombé, P.; Milner, N. J.; Stern, B.; Bailey, G. N.; Heron, C. P. Molecular and Isotopic Demonstration of the Processing of Aquatic Products in Northern European Prehistoric Pottery. *Archaeometry* **2007**, *49* (1), 135–152. https://doi.org/10.1111/j.1475-4754.2007.00292.x.

Craig, O. E.; Steele, V. J.; Fischer, A.; Hartz, S.; Andersen, S. H.; Donohoe, P.; Glykou, A.; Saul, H.; Jones, D. M.; Koch, E.; Heron, C. P. Ancient Lipids Reveal Continuity in Culinary Practices across the Transition to Agriculture in Northern Europe. *Proc. Natl. Acad. Sci.* **2011**, *108* (44), 17910–17915. https://doi.org/10.1073/pnas.1107202108.

Craig, O. E.; Allen, R. B.; Thompson, A.; Stevens, R. E.; Steele, V. J.; Heron, C. Distinguishing Wild Ruminant Lipids by Gas Chromatography/Combustion/Isotope Ratio Mass Spectrometry: Distinguishing Ruminant Lipids. *Rapid Commun. Mass Spectrom.* **2012**, *26* (19), 2359–2364. https://doi.org/10.1002/rcm.6349.

Craig, O. E.; Saul, H.; Lucquin, A.; Nishida, Y.; Taché, K.; Clarke, L.; Thompson, A.; Altoft, D. T.; Uchiyama, J.; Ajimoto, M.; Gibbs, K.; Isaksson, S.; Heron, C. P.; Jordan, P. Earliest Evidence for the Use of Pottery. *Nature* **2013**, *496* (7445), 351–354. https://doi.org/10.1038/nature12109.

Craig, O. E. Prehistoric Fermentation, Delayed-Return Economies, and the Adoption of Pottery Technology. *Curr. Anthropol.* **2021**, *62* (S24), S233–S241. https://doi.org/10.1086/716610.

Cramp, L. J. E.; Jones, J.; Sheridan, A.; Smyth, J.; Whelton, H.; Mulville, J.; Sharples, N.; Evershed, R. P. Immediate Replacement of Fishing with Dairying by the Earliest Farmers of the Northeast Atlantic Archipelagos. *Proc. R. Soc. B Biol. Sci.* **2014**, *281* (1780), 20132372. https://doi.org/10.1098/rspb.2013.2372.

Cramp, L.; Evershed, R. P. Reconstructing Aquatic Resource Exploitation in Human Prehistory Using Lipid Biomarkers and Stable Isotopes. In *Treatise on Geochemistry*; Elsevier, 2014; pp 319–339. https://doi.org/10.1016/B978-0-08-095975-7.01225-0.

Cramp, L. J. E.; Ethier, J.; Urem-Kotsou, D.; Bonsall, C.; Borić, D.; Boroneanţ, A.; Evershed, R. P.; Perić, S.; Roffet-Salque, M.; Whelton, H. L.; Ivanova, M. Regional Diversity in Subsistence among Early Farmers in Southeast Europe Revealed by Archaeological Organic Residues. *Proc. R. Soc. B Biol. Sci.* **2019**, *286* (1894), 20182347. https://doi.org/10.1098/rspb.2018.2347.

Cubas, M.; Lucquin, A.; Robson, H. K.; Colonese, A. C.; Arias, P.; Aubry, B.; Billard, C.; Jan, D.; Diniz, M.; Fernandes, R.; Fábregas Valcarce, R.; Germain-Vallée, C.; Juhel, L.; De Lombera-Hermida, A.; Marcigny, C.; Mazet, S.; Marchand, G.; Neves, C.; Ontañón-Peredo, R.; Rodríguez-Álvarez, X. P.; Simões, T.; Zilhão, J.; Craig, O. E. Latitudinal Gradient in Dairy Production with the Introduction of Farming in Atlantic Europe. *Nat. Commun.* **2020**, *11* (1), 2036. https://doi.org/10.1038/s41467-020-15907-4.

Cultrone, G.; Rodriguez-Navarro, C.; Sebastian, E.; Cazalla, O.; De La Torre, M. J. Carbonate and Silicate Phase Reactions during Ceramic Firing. *Eur. J. Mineral.* **2001**, *13* (3), 621–634. https://doi.org/10.1127/0935-1221/2001/0013-0621.

Cutillas-Victoria, B.; Day, P. M. Pottery Traditions, Consumers' Choices and Exchange Networks at Late Bronze Age Cobatillas La Vieja (Southeast Iberia). *J. Archaeol. Sci. Rep.* **2022**, *45*, 103560. https://doi.org/10.1016/j.jasrep.2022.103560.

Daghmehchi, M.; Rathossi, C.; Omrani, H.; Emami, M.; Rahbar, M. Mineralogical and Thermal Analyses of the Hellenistic Ceramics from Laodicea Temple, Iran. *Appl. Clay Sci.* **2018**, *162*, 146–154. https://doi.org/10.1016/j.clay.2018.06.007.

Daghmehchi, M.; Coletti, C.; Hyeok Moon, D.; Esmaeili Jelodar, M. E.; Omrani, H.; Reka, A. A.; Nematollahzadeh, A.; Emami, M. Mineralogical and Microstructural Characterization of Ceramics from the Fifth and Fourth Millennium BC in the Central Plateau of Iran. *Open Ceram.* **2023**, *15*, 100427. https://doi.org/10.1016/j.oceram.2023.100427.

Damjanović, L.; Bikić, V.; Šarić, K.; Erić, S.; Holclajtner-Antunović, I. Characterization of the Early Byzantine Pottery from Caričin Grad (South Serbia) in Terms of Composition and Firing Temperature. *J. Archaeol. Sci.* **2014**, *46*, 156–172. https://doi.org/10.1016/j.jas.2014.02.031.

De Vito, C.; Medeghini, L.; Mignardi, S.; Orlandi, D.; Nigro, L.; Spagnoli, F.; Lottici, P. P.; Bersani, D. Technological Fingerprints of Black-Gloss Ware from Motya (Western Sicily, Italy). *Appl. Clay Sci.* **2014**, *88–89*, 202–213. https://doi.org/10.1016/j.clay.2013.12.026.

Demirci, Ö.; Lucquin, A.; Çak□lar, C.; Craig, O. E.; Raemaekers, D. C. M. Lipid Residue Analysis on Swifterbant Pottery (c. 5000–3800 Cal BC) in the Lower Rhine-Meuse Area (the Netherlands) and Its Implications for Human-Animal Interactions in Relation to the Neolithisation Process. *J. Archaeol. Sci. Rep.* **2021**, *36*, 102812. https://doi.org/10.1016/j.jasrep.2021.102812.

Derkowski, A.; Kuligiewicz, A. Thermal Analysis and Thermal Reactions of Smectites: A Review of Methodology, Mechanisms, and Kinetics. *Clays Clay Miner.* **2022**, *70* (6), 946–972. https://doi.org/10.1007/s42860-023-00222-y.

Dey, T.; Carter, J. C.; Swift, K. SEM-EDX and FTIR Analysis of Archaeological Ceramic Potteries from Southern Italy. *Microscopy* **2020**, *69* (6), 371–380. https://doi.org/10.1093/jmicro/dfaa034.

Dohrmann, R.; Rüping, K. B.; Kleber, M.; Ufer, K.; Jahn, R. Variation of Preferred Orientation in Oriented Clay Mounts as a Result of Sample Preparation and Composition. *Clays Clay Miner.* **2009**, *57* (6), 686–694. https://doi.org/10.1346/CCMN.2009.0570602.

Dolbunova, E.; Lucquin, A.; McLaughlin, T. R.; Bondetti, M.; Courel, B.; Oras, E.; Piezonka, H.; Robson, H. K.; Talbot, H.; Adamczak, K.; Andreev, K.; Asheichyk, V.; Charniauski, M.; Czekaj-Zastawny, A.; Ezepenko, I.; Grechkina, T.; Gunnarssone, A.; Gusentsova, T. M.; Haskevych, D.; Ivanischeva, M.; Kabaciński, J.; Karmanov, V.; Kosorukova, N.; Kostyleva, E.; Kriiska, A.; Kukawka, S.; Lozovskaya, O.; Mazurkevich, A.; Nedomolkina, N.; Piličiauskas, G.; Sinitsyna, G.; Skorobogatov, A.; Smolyaninov, R. V.; Surkov, A.; Tkachov, O.; Tkachova, M.; Tsybrij, A.; Tsybrij, V.; Vybornov, A. A.; Wawrusiewicz, A.; Yudin, A. I.; Meadows, J.; Heron, C.; Craig, O. E. The Transmission of Pottery Technology among Prehistoric European Hunter-Gatherers. *Nat. Hum. Behav.* **2022**, *7* (2), 171–183. https://doi.org/10.1038/s41562-022-01491-8.

Doliente, J. E.; Langer, S.; Dickinson, M. R.; Cubas, M.; Colonese, A. C.; Penkman, K.; Craig, O. E. Alkylresorcinol Detection and Identification in Archaeological Pottery Using Ultra-high-performance Liquid Chromatography-quadrupole/Orbitrap Mass Spectrometry. *Rapid Commun. Mass Spectrom.* **2024**, *38* (15), e9771. https://doi.org/10.1002/rcm.9771.

Drebushchak, V. A.; Mylnikova, L. N.; Drebushchak, T. N.; Boldyrev, V. V. The Investigation of Ancient Pottery: Application of Thermal Analysis. *J. Therm. Anal. Calorim.* **2005**, *82*, 617-626. https://doi.org/10.1007/s10973-005-0942-9.

Drieu, L.; Horgnies, M.; Binder, D.; Pétrequin, P.; Pétrequin, A. -M.; Peche-Quilichini, K.; Lachenal, T.; Regert, M. Influence of Porosity on Lipid Preservation in the Wall of Archaeological Pottery. *Archaeometry* **2019**, *61* (5), 1081–1096. https://doi.org/10.1111/arcm.12479.

Drieu, L. A Pottery Biography: Considering the Entire Lifecycle of a Pot in Organic Residue Analysis. *ArchéoSciences* **2020**, *44* (2), 129–143. https://doi.org/10.4000/archeosciences.7595.

Drieu, L.; Orecchioni, P.; Capelli, C.; Meo, A.; Lundy, J.; Sacco, V.; Arcifa, L.; Molinari, A.; Carver, M.; Craig, O. E. Chemical Evidence for the Persistence of Wine Production and Trade in Early Medieval Islamic Sicily. *Proc. Natl. Acad. Sci.* **2021**, *118* (10), e2017983118. https://doi.org/10.1073/pnas.2017983118.

Drieu, L.; Regert, M.; Mazuy, A.; Vieugué, J.; Bocoum, H.; Mayor, A. Relationships Between Lipid Profiles and Use of Ethnographic Pottery: An Exploratory Study. *J. Archaeol. Method Theory* **2022**, *29* (4), 1294–1322. https://doi.org/10.1007/s10816-021-09547-1.

Drieu, L.; Lundy, J.; Smith, R. K.; Bergström, E.; Talbot, H.; Primavera, M.; Fiorentino, G.; Craig, O. E.; Thomas-Oates, J. A Medium-throughput Approach for Improved Taxonomic Identification of Lipids Preserved in Ancient Pottery. *Archaeometry* **2024**. https://doi.org/10.1111/arcm.12976.

Dudd, S. N.; Regert, M.; Evershed, R. P. Assessing Microbial Lipid Contributions during Laboratory Degradations of Fats and Oils and Pure Triacylglycerols Absorbed in Ceramic Potsherds. *Org. Geochem.* **1998**, *29* (5–7), 1345–1354. https://doi.org/10.1016/S0146-6380(98)00093-X.

Dumpe, B.; Stivrins, N. Organic Inclusions in Middle and Late Iron Age (5th–12th Century) Hand-Built Pottery in Present-Day Latvia. *J. Archaeol. Sci.* **2015**, *57*, 239–247. https://doi.org/10.1016/j.jas.2015.03.008.

Dunne, J.; Evershed, R. P.; Salque, M.; Cramp, L.; Bruni, S.; Ryan, K.; Biagetti, S.; Di Lernia, S. First Dairying in Green Saharan Africa in the Fifth Millennium BC. *Nature* **2012**, *486* (7403), 390–394. https://doi.org/10.1038/nature11186.

Dunne, J.; Mercuri, A. M.; Evershed, R. P.; Bruni, S.; Di Lernia, S. Earliest Direct Evidence of Plant Processing in Prehistoric Saharan Pottery. *Nat. Plants* **2016**, *3* (1), 16194. https://doi.org/10.1038/nplants.2016.194.

Dunne, J.; Grillo, K. M.; Casanova, E.; Whelton, H. L.; Evershed, R. P. Pastoralist Foodways Recorded in Organic Residues from Pottery Vessels of Modern Communities in Samburu, Kenya. *J. Archaeol. Method Theory* **2019**, *26* (2), 619–642. https://doi.org/10.1007/s10816-018-9384-0.

Dunne, J.; Chapman, A.; Blinkhorn, P.; Evershed, R. P. Fit for Purpose? Organic Residue Analysis and Vessel Specialisation: The Perfectly Utilitarian Medieval Pottery Assemblage from West Cotton, Raunds. *J. Archaeol. Sci.* **2020**, *120*, 105178. https://doi.org/10.1016/j.jas.2020.105178.

Dunne, J.; Höhn, A.; Franke, G.; Neumann, K.; Breunig, P.; Gillard, T.; Walton-Doyle, C.; Evershed, R. P. Honey-Collecting in Prehistoric West Africa from 3500 Years Ago. *Nat. Commun.* **2021**, *12* (1), 2227. https://doi.org/10.1038/s41467-021-22425-4.

El Ouahabi, M.; Daoudi, L.; Hatert, F.; Fagel, N. Modified Mineral Phases During Clay Ceramic Firing. *Clays Clay Miner.* **2015**, *63* (5), 404–413. https://doi.org/10.1346/CCMN.2015.0630506.

Eramo, G. Ceramic Technology: How to Recognize Clay Processing. *Archaeol. Anthropol. Sci.* **2020**, *12* (8), 164. https://doi.org/10.1007/s12520-020-01132-z.

Escalera, E.; Antti, M. L.; Odén, M. Thermal Treatment and Phase Formation in Kaolinite and Illite Based Clays from Tropical Regions of Bolivia. *IOP Conf. Ser. Mater. Sci. Eng.* **2012**, *31*, 012017. https://doi.org/10.1088/1757-899X/31/1/012017.

Espinal, L. Porosity and Its Measurement. In *Characterization of Materials*; Kaufmann, E. N., Ed.; Wiley, 2012; pp 1–10. https://doi.org/10.1002/0471266965.com129.

Evans, M.; Lundy, J.; Lucquin, A.; Hagan, R.; Kowalski, Ł.; Wilczyński, J.; Bickle, P.; Adamczak, K.; Craig, O. E.; Robson, H. K.; Hendy, J. Detection of Dairy Products from Multiple Taxa in Late Neolithic Pottery from Poland: An Integrated Biomolecular Approach. *R. Soc. Open Sci.* **2023**, *10* (3), 230124. https://doi.org/10.1098/rsos.230124.

Evershed, R. P.; Heron, C.; Goad, L. J. Analysis of Organic Residues of Archaeological Origin by High-Temperature Gas Chromatography and Gas Chromatography-Mass Spectrometry. *Analyst* **1990**, *115* (10), 1339-1342. https://doi.org/10.1039/an9901501339.

Evershed, R. P.; Heron, C.; Charters, S.; Goad, L. J. The Survival of Food Residues: New Methods of Analysis, Interpretation and Application. *Proc. Br. Acad.* **1991**, *77*, 187–208.

Evershed, R. P.; Arnot, K. I.; Collister, J.; Eglinton, G.; Charters, S. Application of Isotope Ratio Monitoring Gas Chromatography–Mass Spectrometry to the Analysis of Organic Residues of Archaeological Origin. *The Analyst* **1994**, *119* (5), 909–914. https://doi.org/10.1039/AN9941900909.

Evershed, R. P.; Mottram, H. R.; Dudd, S. N.; Charters, S.; Stott, A. W.; Lawrence, G. J.; Gibson, A. M.; Conner, A.; Blinkhorn, P. W.; Reeves, V. New Criteria for the Identification of Animal Fats Preserved in Archaeological Pottery. *Naturwissenschaften* **1997**, *84* (9), 402–406. https://doi.org/10.1007/s001140050417.

Evershed, R. P.; Dudd, S. N.; Charters, S.; Mottram, H.; Stott, A. W.; Raven, A.; Van Bergen, P. F.; Bland, H. A. Lipids as Carriers of Anthropogenic Signals from Prehistory. *Philos. Trans. R. Soc. Lond. B. Biol. Sci.* **1999**, *354* (1379), 19–31. https://doi.org/10.1098/rstb.1999.0357.

Evershed, R. P.; Dudd, S. N.; Copley, M. S.; Berstan, R.; Stott, A. W.; Mottram, H.; Buckley, S. A.; Crossman, Z. Chemistry of Archaeological Animal Fats. *Acc. Chem. Res.* **2002**, *35* (8), 660–668. https://doi.org/10.1021/ar000200f.

Evershed, R.P. Organic Residue Analysis in Archaeology: The Archaeological Biomarker Revolution. *Archaeometry* **2008a**, *50*(6), 895–924. https://doi.org/10.1111/j.1475-4754.2008.00446.x.

Evershed, R. P. Experimental Approaches to the Interpretation of Absorbed Organic Residues in Archaeological Ceramics. *World Archaeol.* **2008b**, *40* (1), 26–47. https://doi.org/10.1080/00438240801889373.

Evershed, R. P.; Copley, M. S.; Dickson, L.; Hansel, F. A. Experimental Evidence for the Processing of Marine Animal Products and other Commodities Containing Poly-

unsaturated Fatty Acids in Pottery Vessels. *Archaeometry* **2008c**, *50* (1), 101–113. https://doi.org/10.1111/j.1475-4754.2007.00368.x.

Evershed, R. P.; Davey Smith, G.; Roffet-Salque, M.; Timpson, A.; Diekmann, Y.; Lyon, M. S.; Cramp, L. J. E.; Casanova, E.; Smyth, J.; Whelton, H. L.; Dunne, J.; Brychova, V.; Šoberl, L.; Gerbault, P.; Gillis, R. E.; Heyd, V.; Johnson, E.; Kendall, I.; Manning, K.; Marciniak, A.; Outram, A. K.; Vigne, J.-D.; Shennan, S.; Bevan, A.; Colledge, S.; Allason-Jones, L.; Amkreutz, L.; Anders, A.; Arbogast, R.-M.; Bălăşescu, A.; Bánffy, E.; Barclay, A.; Behrens, A.; Bogucki, P.; Carrancho Alonso, Á.; Carretero, J. M.; Cavanagh, N.; Claßen, E.; Collado Giraldo, H.; Conrad, M.; Csengeri, P.; Czerniak, L.; Dębiec, M.; Denaire, A.; Domboróczki, L.; Donald, C.; Ebert, J.; Evans, C.; Francés-Negro, M.; Gronenborn, D.; Haack, F.; Halle, M.; Hamon, C.; Hülshoff, R.; Ilett, M.; Iriarte, E.; Jakucs, J.; Jeunesse, C.; Johnson, M.; Jones, A. M.; Karul, N.; Kiosak, D.; Kotova, N.; Krause, R.; Kretschmer, S.; Krüger, M.; Lefranc, P.; Lelong, O.; Lenneis, E.; Logvin, A.; Lüth, F.; Marton, T.; Marley, J.; Mortimer, R.; Oosterbeek, L.; Oross, K.; Pavúk, J.; Pechtl, J.; Pétrequin, P.; Pollard, J.; Pollard, R.; Powlesland, D.; Pyzel, J.; Raczky, P.; Richardson, A.; Rowe, P.; Rowland, S.; Rowlandson, I.; Saile, T.; Sebők, K.; Schier, W.; Schmalfuß, G.; Sharapova, S.; Sharp, H.; Sheridan, A.; Shevnina, I.; Sobkowiak-Tabaka, I.; Stadler, P.; Stäuble, H.; Stobbe, A.; Stojanovski, D.; Tasić, N.; van Wijk, I.; Vostrovská, I.; Vuković, J.; Wolfram, S.; Zeeb-Lanz, A.; Thomas, M. G. Dairying, Diseases and the Evolution of Lactase Persistence in Europe. *Nature* **2022**, *608* (7922), 336–345. https://doi.org/10.1038/s41586-022-05010-7.

Fabbri, B.; Gualtieri, S.; Shoval, S. The Presence of Calcite in Archeological Ceramics. *J. Eur. Ceram. Soc.* **2014**, *34* (7), 1899–1911. https://doi.org/10.1016/j.jeurceramsoc.2014.01.007.

Fabrizi, L.; Nigro, L.; Ballirano, P.; Guirguis, M.; Spagnoli, F.; Medeghini, L.; De Vito, C. The Phoenician Red Slip Ware from Sulky (Sardinia-Italy): Microstructure and Quantitative Phase Analysis. *Appl. Clay Sci.* **2020**, *197*, 105795. https://doi.org/10.1016/j.clay.2020.105795.

Ferrari, S.; Gualtieri, A. The Use of Illitic Clays in the Production of Stoneware Tile Ceramics. *Appl. Clay Sci.* **2006**, *32* (1–2), 73–81. https://doi.org/10.1016/j.clay.2005.10.001.

Ferri, T.Z.; Rončević, S.; Lipovac Vrkljan, G.; Konestra, A. Post-Depositional Alterations of Terrestrial and Marine Finds of Roman Ceramics from Crikvenica Production Centre (NE Adriatic, Croatia) – A Contribution towards Chemometric Classification. *J. Cult. Herit.* **2020**, *43*, 12–25. https://doi.org/10.1016/j.culher.2019.10.005.

Festa, G.; Andreani, C.; D'Agostino, F.; Forte, V.; Nardini, M.; Scherillo, A.; Scatigno, C.; Senesi, R.; Romano, L. Sumerian Pottery Technology Studied Through Neutron Diffraction and Chemometrics at Abu Tbeirah (Iraq). *Geosciences* **2019**, *9* (2), 74. https://doi.org/10.3390/geosciences9020074.

Forte, V.; Nunziante Cesaro, S.; Medeghini, L. Cooking Traces on Copper Age Pottery from Central Italy: An Integrated Approach Comprising Use Wear Analysis, Spectroscopic Analysis and Experimental Archaeology. *J. Archaeol. Sci. Rep.* **2018**, *18*, 121–138. https://doi.org/10.1016/j.jasrep.2017.12.052.

Frost, R.L.; Vassallo, A.M. The Dehydroxylation of the Kaolinite Clay Minerals Using Infrared Emission Spectroscopy. *Clays Clay Miner.* **1996**, *44* (5), 635–651. https://doi.org/10.1346/CCMN.1996.0440506.

Frost, R. L.; Horváth, E.; Makó, É.; Kristóf, J.; Rédey, Á. Slow Transformation of Mechanically Dehydroxylated Kaolinite to Kaolinite—an Aged Mechanochemically

Activated Formamide-Intercalated Kaolinite Study. *Thermochim. Acta* **2003**, *408* (1–2), 103–113. https://doi.org/10.1016/S0040-6031(03)00316-2.

Gehres, B.; Querré, G. New Applications of LA–ICP–MS for Sourcing Archaeological Ceramics: Microanalysis of Inclusions as Fingerprints of Their Origin. *Archaeometry* **2018**, *60* (4), 750–763. https://doi.org/10.1111/arcm.12338.

Genc Oztoprak, B.; Sinmaz, M. A.; Tülek, F. Composition Analysis of Medieval Ceramics by Laser-Induced Breakdown Spectroscopy (LIBS). *Appl. Phys. A* **2016**, *122* (5), 557. https://doi.org/10.1007/s00339-016-0085-9.

Gilstrap, W. D.; Meanwell, J. L.; Paris, E. H.; López Bravo, R.; Day, P. M. Post-Depositional Alteration of Calcium Carbonate Phases in Archaeological Ceramics: Depletion and Redistribution Effects. *Minerals* **2021**, *11* (7), 749. https://doi.org/10.3390/min11070749.

Giordana, A.; Peacock, E.; McCarthy, M.; Guilbeau, K.; Jacobs, P.; Seger, J. D.; Ramsey, W. G. Estimation of Firing Temperature and Compositional Variability of Archaeological Pottery by Differential Scanning Calorimetry. *Mater. Res. Soc. Symp. Proc.* **2004**, *852*, 240-246. https://doi.org/10.1557/PROC-852-OO8.6.

Gliozzo, E. Ceramic Technology. How to Reconstruct the Firing Process. *Archaeol. Anthropol. Sci.* **2020**, *12* (11), 260. https://doi.org/10.1007/s12520-020-01133-y.

Goldenberg, L.; Neumann, R.; Weiner, S. Microscale Distribution and Concentration of Preserved Organic Molecules with Carbon–Carbon Double Bonds in Archaeological Ceramics: Relevance to the Field of Residue Analysis. *J. Archaeol. Sci.* **2014**, *42*, 509–518. https://doi.org/10.1016/j.jas.2013.11.025.

Golitko, M.; Dudgeon, J. V.; Neff, H.; Terrell, J. E. Identification of Post-depositional Chemical Alteration of Ceramics from the North Coast of Papua New Guinea (Sanduan Province) by Time-of-Flight-Laser Ablation-Inductively Coupled Plasma-Mass Spectrometry (ToF-LA-ICP-MS). *Archaeometry* **2012**, *54* (1), 80–100. https://doi.org/10.1111/j.1475-4754.2011.00612.x.

Gomart, L.; Weiner, A.; Gabriele, M.; Durrenmath, G.; Sorin, S.; Angeli, L.; Colombo, M.; Fabbri, C.; Maggi, R.; Panelli, C.; Pisani, D.F.; Radi, G.; Tozzi, C.; Binder, D. Spiralled Patchwork in Pottery Manufacture and the Introduction of Farming to Southern Europe. *Antiquity* **2017**, *91* (360), 1501–1514. https://doi.org/10.15184/aqy.2017.187.

González-García, F.; Romero-Acosta, V.; García-Ramos, G.; González-Rodríguez, M. Firing Transformations of Mixtures of Clays Containing Illite, Kaolinite and Calcium Carbonate Used by Ornamental Tile Industries. *Appl. Clay Sci.* **1990**, *5* (4), 361–375. https://doi.org/10.1016/0169-1317(90)90031-J.

Gualtieri, A. F.; Ferrari, S. Kinetics of Illite Dehydroxylation. *Phys. Chem. Miner.* **2006**, *33* (7), 490–501. https://doi.org/10.1007/s00269-006-0092-z.

Guggenheim, S.; Martin, R. T. Definition of Clay and Clay Mineral: Joint Report of the Aipea Nomenclature and CMS Nomenclature Committees. *Clays Clay Miner.* **1995**, *43* (2), 255–256. https://doi.org/10.1346/CCMN.1995.0430213.

Hahn, A.; Vogel, H.; Andó, S.; Garzanti, E.; Kuhn, G.; Lantzsch, H.; Schüürman, J.; Vogt, C.; Zabel, M. Using Fourier Transform Infrared Spectroscopy to Determine Mineral Phases in Sediments. *Sediment. Geol.* **2018**, *375*, 27–35. https://doi.org/10.1016/j.sedgeo.2018.03.010.

Hammann, S.; Scurr, D. J.; Alexander, M. R.; Cramp, L. J. E. Mechanisms of Lipid Preservation in Archaeological Clay Ceramics Revealed by Mass Spectrometry Imaging. *Proc. Natl. Acad. Sci.* **2020**, *117* (26), 14688–14693. https://doi.org/10.1073/pnas.1922445117.

Hanein, T.; Thienel, K.-C.; Zunino, F.; Marsh, A. T. M.; Maier, M.; Wang, B.; Canut, M.; Juenger, M. C. G.; Ben Haha, M.; Avet, F.; Parashar, A.; Al-Jaberi, L. A.; Almenares-Reyes, R. S.; Alujas-Diaz, A.; Scrivener, K. L.; Bernal, S. A.; Provis, J. L.; Sui, T.; Bishnoi, S.; Martirena-Hernández, F. Clay Calcination Technology: State-of-the-Art Review by the RILEM TC 282-CCL. *Mater. Struct.* **2022**, *55* (1), 3. https://doi.org/10.1617/s11527-021-01807-6.

Hansel, F. A.; Copley, M. S.; Madureira, L. A. S.; Evershed, R. P. Thermally Produced ω-(o-Alkylphenyl)Alkanoic Acids Provide Evidence for the Processing of Marine Products in Archaeological Pottery Vessels. *Tetrahedron Lett.* **2004**, *45* (14), 2999–3002. https://doi.org/10.1016/j.tetlet.2004.01.111.

Harry, K. G.; Johnson, A. A Non-Destructive Technique for Measuring Ceramic Porosity Using Liquid Nitrogen. *J. Archaeol. Sci.* **2004**, *31* (11), 1567–1575. https://doi.org/10.1016/j.jas.2004.03.020.

Hayes, P. A.; Vahur, S.; Leito, I. ATR-FTIR Spectroscopy and Quantitative Multivariate Analysis of Paints and Coating Materials. *Spectrochim. Acta. A. Mol. Biomol. Spectrosc.* **2014**, *133*, 207–213. https://doi.org/10.1016/j.saa.2014.05.058.

Heath, C.; Pejcic, B.; Delle Piane, C.; Esteban, L. Development of Far-Infrared Attenuated Total Reflectance Spectroscopy for the Mineralogical Analysis of Shales. *Fuel* **2016**, *182*, 771–779. https://doi.org/10.1016/j.fuel.2016.06.056.

Hein, A.; Kilikoglou, V.; Kassianidou, V. Chemical and Mineralogical Examination of Metallurgical Ceramics from a Late Bronze Age Copper Smelting Site in Cyprus. *J. Archaeol. Sci.* **2007**, *34* (1), 141–154. https://doi.org/10.1016/j.jas.2006.04.005.

Hendy, J.; Colonese, A. C.; Franz, I.; Fernandes, R.; Fischer, R.; Orton, D.; Lucquin, A.; Spindler, L.; Anvari, J.; Stroud, E.; Biehl, P. F.; Speller, C.; Boivin, N.; Mackie, M.; Jersie-Christensen, R. R.; Olsen, J. V.; Collins, M. J.; Craig, O. E.; Rosenstock, E. Ancient Proteins from Ceramic Vessels at Çatalhöyük West Reveal the Hidden Cuisine of Early Farmers. *Nat. Commun.* **2018**, *9* (1), 4064. https://doi.org/10.1038/s41467-018-06335-6.

Heron, C.; Evershed, R. P. The Analysis of Organic Residues and the Study of Pottery Use. *Archaeol. Method Theory*, **1993**, *5*, 247-284.

Heron, C.; Craig, O. E. Aquatic Resources in Foodcrusts: Identification and Implication. *Radiocarbon* **2015**, *57* (4), 707–719. https://doi.org/10.2458/azu_rc.57.18454.

Heron, C.; Shoda, S.; Breu Barcons, A.; Czebreszuk, J.; Eley, Y.; Gorton, M.; Kirleis, W.; Kneisel, J.; Lucquin, A.; Müller, J.; Nishida, Y.; Son, J.; Craig, O. E. First Molecular and Isotopic Evidence of Millet Processing in Prehistoric Pottery Vessels. *Sci. Rep.* **2016**, *6* (1), 38767. https://doi.org/10.1038/srep38767.

Herrick, H. M.; Berna, F. A Review of Methods to Analyze Archaeological Lime Production: Investigating Raw Materials Selection and Firing Conditions. *J. Archaeol. Method Theory* **2024**, *31* (4), 1668–1696. https://doi.org/10.1007/s10816-024-09652-x.

Holakooei, P.; De Lapérouse, J.-F.; Carò, F.; Röhrs, S.; Franke, U.; Müller-Wiener, M.; Reiche, I. Non-Invasive Scientific Studies on the Provenance and Technology of Early Islamic Ceramics from Afrasiyab and Nishapur. *J. Archaeol. Sci. Rep.* **2019**, *24*, 759–772. https://doi.org/10.1016/j.jasrep.2019.02.029.

Hopper, C.; Dunne, J.; Dewar, G.; Evershed, R. P. Chemical Evidence for Milk, Meat, and Marine Resource Processing in Later Stone Age Pots from Namaqualand, South Africa. *Sci. Rep.* **2023**, *13* (1), 1658. https://doi.org/10.1038/s41598-023-28577-1.

Irto, A.; Micalizzi, G.; Bretti, C.; Chiaia, V.; Mondello, L.; Cardiano, P. Lipids in Archaeological Pottery: A Review on Their Sampling and Extraction Techniques. *Molecules* **2022**, *27* (11), 3451. https://doi.org/10.3390/molecules27113451.

Işik, İ.; Tarhan, İ. Investigations of the Ancient Ceramic Sherds Excavated from Börükçü Site in Muğla, South-western Turkey, by ATR-FTIR Spectroscopy and Statistical Multivariate Analysis. *Archaeometry* **2021**, *63* (2), 296–311. https://doi.org/10.1111/arcm.12658.

İssi, A.; Kara, A.; Alp, A. O. An Investigation of Hellenistic Period Pottery Production Technology from Harabebezikan/Turkey. *Ceram. Int.* **2011**, *37* (7), 2575–2582. https://doi.org/10.1016/j.ceramint.2011.04.001.

Izadifar, M.; Thissen, P.; Steudel, A.; Kleeberg, R.; Kaufhold, S.; Kaltenbach, J.; Schuhmann, R.; Dehn, F.; Emmerich, K. Comprehensive Examination of Dehydroxylation of Kaolinite, Disordered Kaolinite, and Dickite: Experimental Studies and Density Functional Theory. *Clays Clay Miner.* **2020**, *68* (4), 319–333. https://doi.org/10.1007/s42860-020-00082-w.

Izzo, F.; Germinario, C.; Grifa, C.; Langella, A.; Mercurio, M. External Reflectance FTIR Dataset (4000–400 cm^{-1}) for the Identification of Relevant Mineralogical Phases Forming Cultural Heritage Materials. *Infrared Phys. Technol.* **2020**, *106*, 103266. https://doi.org/10.1016/j.infrared.2020.103266.

Jordá, J. D.; Jordán, M. M.; Ibanco-Cañete, R.; Montero, M. A.; Reyes-Labarta, J. A.; Sánchez, A.; Cerdán, M. Mineralogical Analysis of Ceramic Tiles by FTIR: A Quantitative Attempt. *Appl. Clay Sci.* **2015**, *115*, 1–8. https://doi.org/10.1016/j.clay.2015.07.005.

Kahl, W.-A.; Ramminger, B. Non-Destructive Fabric Analysis of Prehistoric Pottery Using High-Resolution X-Ray Microtomography: A Pilot Study on the Late Mesolithic to Neolithic Site Hamburg-Boberg. *J. Archaeol. Sci.* **2012**, *39* (7), 2206–2219. https://doi.org/10.1016/j.jas.2012.02.029.

Kałużna-Czaplińska, J.; Rosiak, A.; Kwapińska, M.; Kwapiński, W. Different Analytical Procedures for the Study of Organic Residues in Archeological Ceramic Samples with the Use of Gas Chromatography-Mass Spectrometry. *Crit. Rev. Anal. Chem.* **2016**, *46* (1), 67–81. https://doi.org/10.1080/10408347.2015.1008130.

Karunadasa, K. S. P.; Manoratne, C. H.; Pitawala, H. M. T. G. A.; Rajapakse, R. M. G. Thermal Decomposition of Calcium Carbonate (Calcite Polymorph) as Examined by in-Situ High-Temperature X-Ray Powder Diffraction. *J. Phys. Chem. Solids* **2019**, *134*, 21–28. https://doi.org/10.1016/j.jpcs.2019.05.023.

Kilikoglou, V.; Vekinis, G.; Maniatis, Y.; Day, P. M. Mechanical Performance of Quartz-tempered Ceramics: Part I, Strength and Toughness. *Archaeometry* **1998**, *40* (2), 261–279. https://doi.org/10.1111/j.1475-4754.1998.tb00837.x.

Klobes, P.; Meyer, K.; Munro, R. G. *Porosity and Specific Surface Area Measurements for Solid Materials. NIST Recommended Practice Guide*, U.S. Government Printing Office: Washington, 2006.

Knappett, C.; Pirrie, D.; Power, M. R.; Nikolakopoulou, I.; Hilditch, J.; Rollinson, G. K. Mineralogical Analysis and Provenancing of Ancient Ceramics Using Automated SEM-EDS Analysis (QEMSCAN®): A Pilot Study on LB I Pottery from Akrotiri, Thera. *J. Archaeol. Sci.* **2011**, *38* (2), 219–232. https://doi.org/10.1016/j.jas.2010.08.022.

Kozatsas, J.; Kotsakis, K.; Sagris, D.; David, K. Inside out: Assessing Pottery Forming Techniques with Micro-CT Scanning. An Example from Middle Neolithic Thessaly. *J. Archaeol. Sci.* **2018**, *100*, 102–119. https://doi.org/10.1016/j.jas.2018.10.007.

Kramar, S.; Lux, J. Spectroscopic and Porosimetric Analyses of Roman Pottery from an Archaeological Site near Mošnje, Slovenia. *Mater. Tehnol.* **2015**, *49* (4), 503–508. https://doi.org/10.17222/mit.2014.110.

Kriiska, A.; Oras, E.; Lõugas, L.; Meadows, J.; Lucquin, A.; Craig, O. E. Late Mesolithic Narva Stage in Estonia: Pottery, Settlement Types and Chronology. *Est. J. Archaeol.* **2017**, *21* (1), 52. https://doi.org/10.3176/arch.2017.1.03.

Krueger, M.; Wicenciak, U.; Kowarska, Z.; Niedzielski, P.; Kozak, L.; Krueger, M.; Jakubowski, K.; Proch, J.; Mleczek, M.; Waśkiewicz, A. First Results of Organic Residue Analysis on Ceramic Vessels (Jiyeh And Chhîm, Lebanon) By High Perfomance Liquid Chromatography With Tandem Mass Spectrometry. **2018**. https://doi.org/10.5281/zenodo.1165358.

Kubliha, M.; Trnovcová, V.; Ondruška, J.; Štubňa, I.; Bošák, O.; Kaljuvee, T. Comparison of Dehydration in Kaolin and Illite Using DC Conductivity Measurements. *Appl. Clay Sci.* **2017**, *149*, 8–12. https://doi.org/10.1016/j.clay.2017.08.012.

Kuila, U.; Prasad, M. Specific Surface Area and Pore-Size Distribution in Clays and Shales: *Specific Surface Area and Pore-Size Distribution in Clays and Shales*. *Geophys. Prospect.* **2013**, *61* (2), 341–362. https://doi.org/10.1111/1365-2478.12028.

Laita, E.; Bauluz, B. Mineral and Textural Transformations in Aluminium-Rich Clays during Ceramic Firing. *Appl. Clay Sci.* **2018**, *152*, 284–294. https://doi.org/10.1016 / j.clay.2017.11.025.

Langejans, G. H. J. Remains of the Day-Preservation of Organic Micro-Residues on Stone Tools. *J. Archaeol. Sci.* **2010**, *37* (5), 971–985. https://doi.org/10.1016/j.jas.2009.11.030.

Lantos, I.; Chaile, C.; Careaga, V. P.; De Salazar, L.; Maier, M. S. Organic Residue Analysis in Latin American Archaeology: Past, Present, and Future Perspectives. *Archaeometry* **2024**, arcm.12978. https://doi.org/10.1111/arcm.12978.

Larreina-García, D.; Saenz De Buruaga, A.; Vinagre, A. T.; Notario, B. Technical Ceramics for Salt Production in Western Sahara. *Azania Archaeol. Res. Afr.* **2021**, *56* (3), 344–370. https://doi.org/10.1080/0067270X.2021.1966213.

Lindahl, A.; Pikirayi, I. Ceramics and Change: An Overview of Pottery Production Techniques in Northern South Africa and Eastern Zimbabwe during the First and Second Millennium AD. *Archaeol. Anthropol. Sci.* **2010**, *2* (3), 133–149. https://doi.org/10.1007/s12520-010-0031-2.

Liritzis, I.; Xanthopoulou, V.; Palamara, E.; Papageorgiou, I.; Iliopoulos, I.; Zacharias, N.; Vafiadou, A.; Karydas, A. G. Characterization and Provenance of Ceramic Artifacts and Local Clays from Late Mycenaean Kastrouli (Greece) by Means of p-XRF Screening and Statistical Analysis. *J. Cult. Herit.* **2020**, *46*, 61–81. https://doi.org/10.1016/j.culher.2020.06.004.

Liu, G.-L.; Kazarian, S. G. Recent Advances and Applications to Cultural Heritage Using ATR-FTIR Spectroscopy and ATR-FTIR Spectroscopic Imaging. *The Analyst* **2022**, *147* (9), 1777–1797. https://doi.org/10.1039/D2AN00005A.

Lõhmus, M.; Jonuks, T.; Malve, M. Archaeological Salvage Excavations at Kukruse: A Modern Age Road, 13th–15th Century Cemetery. *Archaeological Fieldwork in Estonia* **2011**, *10*, 103–114.

Lucquin, A.; March, R. J.; Cassen, S. Analysis of Adhering Organic Residues of Two "Coupes-à-Socles" from the Neolithic Funerary Site "La Hougue Bie" in Jersey: Evidences of Birch Bark Tar Utilisation. *J. Archaeol. Sci.* **2007**, *34* (5), 704–710. https://doi.org/10.1016/j.jas.2006.07.006.

Lucquin, A.; Robson, H. K.; Oras, E.; Lundy, J.; Moretti, G.; González Carretero, L.; Dekker, J.; Demirci, Ö.; Dolbunova, E.; McLaughlin, T. R.; Piezonka, H.; Talbot, H. M.; Adamczak, K.; Czekaj-Zastawny, A.; Groß, D.; Gumiński, W.; Hartz, S.; Kabaciński, J.; Koivisto, S.; Linge, T. E.; Meyer, A.-K.; Mökkönen, T.; Philippsen, B.; Piličiauskas, G.; Visocka, V.; Kriiska, A.; Raemaekers, D.; Meadows, J.; Heron, C.; Craig, O. E. The Impact of Farming on Prehistoric Culinary Practices throughout Northern Europe. *Proc. Natl. Acad. Sci.* **2023**, *120* (43), e2310138120. https://doi.org/10.1073/pnas.2310138120.

Macchia, A.; Schuberthan, L. M.; Ferro, D.; Colasanti, I. A.; Montorsi, S.; Biribicchi, C.; Barbaccia, F. I.; La Russa, M. F. Analytical Investigations of XIX–XX Century Paints: The Study of Two Vehicles from the Museum for Communications of Frankfurt. *Molecules* **2023**, *28* (5), 2197. https://doi.org/10.3390/molecules28052197.

Madariaga, J. M. Analytical Chemistry in the Field of Cultural Heritage. *Anal. Methods* **2015**, *7* (12), 4848–4876. https://doi.org/10.1039/C5AY00072F.

Mahmoudi, S.; Bennour, A. Characterisation and Ceramic Application of Clays from North Africa. *Appl. Earth Sci.* **2022**, *131* (1), 15–26. https://doi.org/10.1080/25726838.2021.1992815.

Maniatis, Y.; Tite, M. S. Technological Examination of Neolithic-Bronze Age Pottery from Central and Southeast Europe and from the Near East. *J. Archaeol. Sci.* **1981**, *8* (1), 59–76. https://doi.org/10.1016/0305-4403(81)90012-1.

Manoukian, N.; Whelton, H. L.; Dunne, J.; Badalyan, R.; Smith, A. T.; Simonyan, H.; Rothman, M. S.; Bobokhyan, A.; Hovsepyan, R.; Avetisyan, P.; Evershed, R. P.; Pollard, A. M. Diverse Dietary Practices across the Early Bronze Age 'Kura-Araxes Culture' in the South Caucasus. *PLOS ONE* **2022**, *17* (12), e0278345. https://doi.org/10.1371/journal.pone.0278345.

Maritan, L.; Vidale, M.; Mazzoli, C.; Leonardi, G.; Facchi, A. From Clays to Pots: Chaînes Opératoires and Technical Options at a Burnt Late Iron Age Potter's Workshop (North-Eastern Italy). *Archaeol. Anthropol. Sci.* **2019**, *11* (5), 2049–2058. https://doi.org/10.1007/s12520-018-0654-2.

Maritan, L. Ceramic Abandonment. How to Recognise Post-Depositional Transformations. *Archaeol. Anthropol. Sci.* **2020**, *12* (8), 199. https://doi.org/10.1007/s12520-020-01141-y.

Martín-Márquez, J.; Rincón, J. Ma.; Romero, M. Effect of Firing Temperature on Sintering of Porcelain Stoneware Tiles. *Ceram. Int.* **2008**, *34* (8), 1867–1873. https://doi.org/10.1016/j.ceramint.2007.06.006.

Matlova, V.; Roffet-Salque, M.; Pavlu, I.; Kyselka, J.; Sedlarova, I.; Filip, V.; Evershed, R. P. Defining Pottery Use and Animal Management at the Neolithic Site of Bylany (Czech Republic). *J. Archaeol. Sci. Rep.* **2017**, *14*, 262–274. https://doi.org/10.1016/j.jasrep.2017.05.028.

McConville, C. J.; Lee, W. E. Microstructural Development on Firing Illite and Smectite Clays Compared with That in Kaolinite: Communications of the American Ceramic Society. *J. Am. Ceram. Soc.* **2005**, *88* (8), 2267–2276. https://doi.org/10.1111/j.1551-2916.2005.00390.x.

Melessanaki, K.; Mateo, M.; Ferrence, S. C.; Betancourt, P. P.; Anglos, D. The Application of LIBS for the Analysis of Archaeological Ceramic and Metal Artifacts. *Appl. Surf. Sci.* **2002**, *197–198*, 156–163. https://doi.org/10.1016/S0169-4332(02)00459-2.

Ménager, M.; Azémard, C.; Vieillescazes, C. Study of Egyptian Mummification Balms by FT-IR Spectroscopy and GC–MS. *Microchem. J.* **2014**, *114*, 32–41. https://doi.org/10.1016/j.microc.2013.11.018.

Mentesana, R.; Kilikoglou, V.; Todaro, S.; Day, P. M. Reconstructing Change in Firing Technology during the Final Neolithic–Early Bronze Age Transition in Phaistos, Crete. Just the Tip of the Iceberg? *Archaeol. Anthropol. Sci.* **2019**, *11* (3), 871–894. https://doi.org/10.1007/s12520-017-0572-8.

Miller, M. J.; Whelton, H. L.; Swift, J. A.; Maline, S.; Hammann, S.; Cramp, L. J. E.; McCleary, A.; Taylor, G.; Vacca, K.; Becks, F.; Evershed, R. P.; Hastorf, C. A. Interpreting Ancient Food Practices: Stable Isotope and Molecular Analyses of Visible and Absorbed Residues from a Year-Long Cooking Experiment. *Sci. Rep.* **2020**, *10* (1), 13704. https://doi.org/10.1038/s41598-020-70109-8.

Mirabaud, S.; Rolando, C.; Regert, M. Molecular Criteria for Discriminating Adipose Fat and Milk from Different Species by NanoESI MS and MS/MS of Their Triacylglycerols: Application to Archaeological Remains. *Anal. Chem.* **2007**, *79* (16), 6182–6192. https://doi.org/10.1021/ac070594p.

Miras, A.; Galán, E.; González, I.; Romero-Baena, A.; Martín, D. Mineralogical Evolution of Ceramic Clays during Heating. An Ex/in Situ X-Ray Diffraction Method Comparison Study. *Appl. Clay Sci.* **2018**, *161*, 176–183. https://doi.org/10.1016/j.clay.2018.04.003.

Mitkidou, S.; Dimitrakoudi, E.; Urem-Kotsou, D.; Papadopoulou, D.; Kotsakis, K.; Stratis, J. A.; Stephanidou-Stephanatou, I. Organic Residue Analysis of Neolithic Pottery from North Greece. *Microchim. Acta* **2008**, *160* (4), 493–498. https://doi.org/10.1007/s00604-007-0811-2.

Mondelli, C.; Zorzi, S.; Ricci, G.; Galvan, V.; Balliana, E.; Schweins, R.; Cattaruzza, E. Exploring the Porosity in Ceramics at the Nm Scale: From Understanding Historical Ceramics to Innovative Materials Design. *ChemPhysChem* **2020**, *21* (10), 966–970. https://doi.org/10.1002/cphc.202000088.

Monnier, G. F. A Review of Infrared Spectroscopy in Microarchaeology: Methods, Applications, and Recent Trends. *J. Archaeol. Sci. Rep.* **2018**, *18*, 806–823. https://doi.org/10.1016/j.jasrep.2017.12.029.

Moon, D.-H.; Kim, S.-J.; Nam, S.-W.; Cho, H.-G. X-Ray Diffraction Analysis of Clay Particles in Ancient Baekje Black Pottery: Indicator of the Firing Parameters. *Minerals* **2021**, *11* (11), 1239. https://doi.org/10.3390/min11111239.

Moraru, L.; Szendrei, F. Ancient Pottery Analysis using SEM Image Processing. *Eur. J. Sci. Theol.* **2010**, *6* (2), 69-78.

Moraru, L.; Cotoi, O.; Szendrei, F. Euler Number: A Method for Statistical Analysis of Ancient Pottery Porosity. *Eur. J. Sci. Theol.* **2011**, *7* (3), 99-108.

Moropoulou, A.; Bakolas, A.; Bisbikou, K. Thermal Analysis as a Method of Characterizing Ancient Ceramic Technologies. *Thermochim. Acta* **1995**, *269–270*, 743–753. https://doi.org/10.1016/0040-6031(95)02570-7.

Mottram, H. R.; Dudd, S. N.; Lawrence, G. J.; Stott, A. W.; Evershed, R. P. New Chromatographic, Mass Spectrometric and Stable Isotope Approaches to the Classification of Degraded Animal Fats Preserved in Archaeological Pottery. *J. Chromatogr. A* **1999**, *833* (2), 209–221. https://doi.org/10.1016/S0021-9673(98)01041-3.

Msinjili, N. S.; Gluth, G. J. G.; Sturm, P.; Vogler, N.; Kühne, H.-C. Comparison of Calcined Illitic Clays (Brick Clays) and Low-Grade Kaolinitic Clays as Supplementary Cementitious Materials. *Mater. Struct.* **2019**, *52* (5), 94. https://doi.org/10.1617/s11527-019-1393-2.

Müller, C. M.; Pejcic, B.; Esteban, L.; Piane, C. D.; Raven, M.; Mizaikoff, B. Infrared Attenuated Total Reflectance Spectroscopy: An Innovative Strategy for Analyzing

Mineral Components in Energy Relevant Systems. *Sci. Rep.* **2014**, *4* (1), 6764. https://doi.org/10.1038/srep06764.

Musthafa, A. M.; Janaki, K.; Velraj, G. Microscopy, Porosimetry and Chemical Analysis to Estimate the Firing Temperature of Some Archaeological Pottery Shreds from India. *Microchem. J.* **2010**, *95* (2), 311–314. https://doi.org/10.1016/j.microc.2010.01.006.

Namdar, D.; Stacey, R. J.; Simpson, S. J. First Results on Thermally Induced Porosity in Chlorite Cooking Vessels from Merv (Turkmenistan) and Implications for the Formation and Preservation of Archaeological Lipid Residues. *J. Archaeol. Sci.* **2009**, *36* (11), 2507–2516. https://doi.org/10.1016/j.jas.2009.07.003.

Namdar, D.; Shoval, S.; Amrani, A.; Van Den Brink, E. C. M.; Kirzner, D.; Beeri, R. Absorbed Organic Residues in a Late Bronze Age II Clay Coffin with Anthropoid Lid from Tel Shadud, Israel. *J. Archaeol. Sci. Rep.* **2017**, *12*, 726–733. https://doi.org/10.1016/j.jasrep.2017.01.045.

Needham, S.; Evans, J. Honey and Dripping: Neolithic Food Residues from Runnymede Bridge. *Oxf. J. Archaeol.* **1987**, *6* (1), 21–28. https://doi.org/10.1111/j.1468-0092.1987.tb00138.x.

Neumannová, K.; Petřík, J.; Vostrovská, I.; Dvořák, J.; Zikmund, T.; Kaiser, J. Variability in Coiling Technique in LBK Pottery Inferred by Experiments and Pore Structure Micro-Tomography Analysis. *Archeol. Rozhl.* **2017**, *69* (2), 172–186. https://doi.org/10.35686/AR.2017.11.

Oliveira, C.; Araújo, A.; Ribeiro, A.; Delerue-Matos, C. Chromatographic Analysis of Honey Ceramic Artefacts. *Archaeol. Anthropol. Sci.* **2019**, *11* (3), 959–971. https://doi.org/10.1007/s12520-017-0585-3.

Olsson, M.; Isaksson, S. Molecular and Isotopic Traces of Cooking and Consumption of Fish at an Early Medieval Manor Site in Eastern Middle Sweden. *J. Archaeol. Sci.* **2008**, *35* (3), 773–780. https://doi.org/10.1016/j.jas.2007.06.009.

Oras, E.; Vahur, S.; Isaksson, S.; Kaljurand, I.; Leito, I. MALDI-FT-ICR-MS for archaeological lipid residue analysis. *J. Mass Spectrom.* **2017a**, *52* (10), 689-700. https://doi.org/10.1002/jms.3974.

Oras, E.; Lucquin, A.; Lõugas, L.; Tõrv, M.; Kriiska, A.; Craig, O. E. The Adoption of Pottery by North-East European Hunter-Gatherers: Evidence from Lipid Residue Analysis. *J. Archaeol. Sci.* **2017b**, *78*, 112–119. https://doi.org/10.1016/j.jas.2016.11.010.

Oras, E.; Tõrv, M.; Jonuks, T.; Malve, M.; Radini, A.; Isaksson, S.; Gledhill, A.; Kekišev, O.; Vahur, S.; Leito, I. Social Food Here and Hereafter: Multiproxy Analysis of Gender-Specific Food Consumption in Conversion Period Inhumation Cemetery at Kukruse, NE-Estonia. *J. Archaeol. Sci.* **2018**, *97*, 90–101. https://doi.org/10.1016/j.jas.2018.07.001.

Oras, E.; Anderson, J.; Tõrv, M.; Vahur, S.; Rammo, R.; Remmer, S.; Mölder, M.; Malve, M.; Saag, L.; Saage, R.; Teearu-Ojakäär, A.; Peets, P.; Tambets, K.; Metspalu, M.; Lees, D. C.; Barclay, M. V. L.; Hall, M. J. R.; Ikram, S.; Piombino-Mascali, D. Multidisciplinary Investigation of Two Egyptian Child Mummies Curated at the University of Tartu Art Museum, Estonia (Late/Graeco-Roman Periods). *PLOS ONE* **2020**, *15* (1), e0227446. https://doi.org/10.1371/journal.pone.0227446.

Oras, E.; Tõrv, M.; Johanson, K.; Rannamäe, E.; Poska, A.; Lõugas, L.; Lucquin, A.; Lundy, J.; Brown, S.; Chen, S.; Varul, L.; Haferberga, V.; Legzdiņa, D.; Zariņa, G.; Cramp, L.; Heyd, V.; Reay, M.; Pospieszny, Ł.; Robson, H. K.; Nordqvist, K.; Heron, C.; Craig, O. E.; Kriiska, A. Parallel Worlds and Mixed Economies: Multi-Proxy

Analysis Reveals Complex Subsistence Systems at the Dawn of Early Farming in the Northeast Baltic. *R. Soc. Open Sci.* **2023**, *10* (10), 230880. https://doi.org/10.1098/rsos.230880.

Oudemans, T. F. M. Applying Organic Residue Analysis in Ceramic Studies – A Functional Approach. *Leiden J. Pottery Stud.* **2007**, 23, 5-20.

Papageorgiou, I. Ceramic Investigation: How to Perform Statistical Analyses. *Archaeol. Anthropol. Sci.* **2020**, *12* (9), 210. https://doi.org/10.1007/s12520-020-01142-x.

Papakosta, V.; Smittenberg, R. H.; Gibbs, K.; Jordan, P.; Isaksson, S. Extraction and Derivatization of Absorbed Lipid Residues from Very Small and Very Old Samples of Ceramic Potsherds for Molecular Analysis by Gas Chromatography–Mass Spectrometry (GC–MS) and Single Compound Stable Carbon Isotope Analysis by Gas Chromatography–Combustion–Isotope Ratio Mass Spectrometry (GC–C–IRMS). *Microchem. J.* **2015**, *123*, 196–200. https://doi.org/10.1016/j.microc.2015.06.013.

Papakosta, V.; Lopez-Costas, O.; Isaksson, S. Multi-method (FTIR, XRD, PXRF) Analysis of Ertebølle Pottery Ceramics from Scania, Southern Sweden. *Archaeometry* **2020**, *62* (4), 677–693. https://doi.org/10.1111/arcm.12554.

Patrick, M.; De Koning, A. J.; Smith, A. B. Gas Liquid Chromatographic Analysis of Fatty Acids in Food Residues from Ceramics Found in the Southwestern Cape, South Africa. *Archaeometry* **1985**, *27* (2), 231–236. https://doi.org/10.1111/j.1475-4754.1985.tb00366.x.

Pavelka, J.; Smejda, L.; Hynek, R.; Hrdlickova Kuckova, S. Immunological Detection of Denatured Proteins as a Method for Rapid Identification of Food Residues on Archaeological Pottery. *J. Archaeol. Sci.* **2016**, *73*, 25–35. https://doi.org/10.1016/j.jas.2016.07.004.

Pecci, A.; Gabrieli, R. S.; Inserra, F.; Cau, M. A.; Waksman, S. Y. Preliminary Results of the Organic Residue Analysis of 13th Century Cooking Wares from a Household in Frankish Paphos (Cyprus). *STAR Sci. Technol. Archaeol. Res.* **2015**, *1* (2), 99–105. https://doi.org/10.1080/20548923.2016.1183960.

Pecci, A.; Degl'Innocenti, E.; Giorgi, G.; Cau Ontiveros, M. Á.; Cantini, F.; Solanes Potrony, E.; Alós, C.; Miriello, D. Organic Residue Analysis of Experimental, Medieval, and Post-Medieval Glazed Ceramics. *Archaeol. Anthropol. Sci.* **2016**, *8* (4), 879–890. https://doi.org/10.1007/s12520-015-0262-3.

Peets, P.; Leito, I.; Pelt, J.; Vahur, S. Identification and Classification of Textile Fibres Using ATR-FT-IR Spectroscopy with Chemometric Methods. *Spectrochim. Acta. A. Mol. Biomol. Spectrosc.* **2017**, *173*, 175–181. https://doi.org/10.1016/j.saa.2016.09.007.

Peets, P.; Kaupmees, K.; Vahur, S.; Leito, I. Reflectance FT-IR Spectroscopy as a Viable Option for Textile Fiber Identification. *Herit. Sci.* **2019**, *7* (1), 93. https://doi.org/10.1186/s40494-019-0337-z.

Peets, P.; Vahur, S.; Kruve, A.; Haljasorg, T.; Herodes, K.; Pagano, T.; Leito, I. Instrumental Techniques in the Analysis of Natural Red Textile Dyes. *J. Cult. Herit.* **2020**, *42*, 19–27. https://doi.org/10.1016/j.culher.2019.09.002.

Pérez, M.; De Lucio, O. G.; Sobral, H. M.; Márquez-Herrera, C.; Goguitchaichvili, A.; Ortiz, S. Characterization of Traditional Pottery Artifacts from Yucatán Peninsula, México: Implications for Manufacturing Process Based on Elemental Analyses. *Minerals* **2024**, *14* (10), 993. https://doi.org/10.3390/min14100993.

Poulain, M.; Baeten, J.; De Clercq, W.; De Vos, D. Dietary Practices at the Castle of Middelburg, Belgium: Organic Residue Analysis of 16th- to 17th-Century Ceramics. *J. Archaeol. Sci.* **2016**, *67*, 32–42. https://doi.org/10.1016/j.jas.2016.01.006.

Povlsen, K. The Introduction of Ceramics in the Ertebølle Culture. *Dan. J. Archaeol.* **2013**, *2* (2), 146–163. https://doi.org/10.1080/21662282.2013.904127.

Ptáček, P.; Opravil, T.; Šoukal, F.; Wasserbauer, J.; Másilko, J.; Baráček, J. The Influence of Structure Order on the Kinetics of Dehydroxylation of Kaolinite. *J. Eur. Ceram. Soc.* **2013**, *33* (13–14), 2793–2799. https://doi.org/10.1016/j.jeurceramsoc.2013.04.033.

Rageot, M.; Lepère, C.; Henry, A.; Binder, D.; Davtian, G.; Filippi, J.-J.; Fernandez, X.; Guilaine, J.; Jallet, F.; Radi, G.; Thirault, E.; Terradas, X.; Regert, M. Management Systems of Adhesive Materials throughout the Neolithic in the North-West Mediterranean. *J. Archaeol. Sci.* **2021**, *126*, 105309. https://doi.org/10.1016/j.jas.2020.105309.

Rahman, M. S.; Metselaar, H. S. C.; Razak, B. B. A. Mineralogical and Thermal Analysis of Ancient Ceramic Artifacts Based on Modern Techniques of Ceramic Studies. *J. Mediterr. Archaeol.* **2024**, *24* (3), 38-56. https://doi.org/10.5281/zenodo.13383260.

Raven, A. M.; Van Bergen, P. F.; Stott, A. W.; Dudd, S. N.; Evershed, R. P. Formation of Long-Chain Ketones in Archaeological Pottery Vessels by Pyrolysis of Acyl Lipids. *J. Anal. Appl. Pyrolysis* **1997**, *40–41*, 267–285. https://doi.org/10.1016/S0165-2370(97)00036-3.

Ravisankar, R.; Naseerutheen, A.; Rajalakshmi, A.; Raja Annamalai, G.; Chandrasekaran, A. Application of Thermogravimetry–Differential Thermal Analysis (TG–DTA) Technique to Study the Ancient Potteries from Vellore Dist, Tamilnadu, India. *Spectrochim. Acta. A. Mol. Biomol. Spectrosc.* **2014**, *129*, 201–208. https://doi.org/10.1016/j.saa.2014.02.095.

Reber, E. A.; Kerr, M. T.; Whelton, H. L.; Evershed, R.P. Lipid Residues from Low-Fired Pottery. *Archaeometry* **2019**, *61* (1), 131–144. https://doi.org/10.1111/ARCM.12403.

Reedy, C.L.; Reedy, C.L. Micro-Computed Tomography with 3D Image Analysis to Reveal Firing Temperature Effects on Pore Systems in Archaeological and Ethnographic Ceramics. *Appl. Sci.* **2022**, 12, 11448. https://doi.org/10.3390/ app122211448.

Regert, M.; Bland, H. A.; Dudd, S. N.; Bergen, P. F. V.; Evershed, R. P. Free and Bound Fatty Acid Oxidation Products in Archaeological Ceramic Vessels. *Proc. R. Soc. Lond. B Biol. Sci.* **1998**, *265* (1409), 2027–2032. https://doi.org/10.1098/rspb.1998.0536.

Regert, M.; Colinart, S.; Degrand, L.; Decavallas, O. Chemical Alteration and Use of Beeswax Through Time: Accelerated Ageing Tests and Analysis of Archaeological Samples from Various Environmental Contexts. *Archaeometry* **2001**, *43* (4), 549–569. https://doi.org/10.1111/1475-4754.00036.

Regert, M.; Vacher, S.; Moulherat, C.; Decavallas, O. Adhesive Production and Pottery Function During the Iron Age at the Site of Grand Aunay (Sarthe, France). *Archaeometry* **2003**, *45* (1), 101–120. https://doi.org/10.1111/1475-4754.00098.

Regert, M. Analytical Strategies for Discriminating Archeological Fatty Substances from Animal Origin. *Mass Spectrom. Rev.* **2011**, *30* (2), 177–220. https://doi.org/10.1002/mas.20271.

Rella, R.; Sturaro, A.; Parvoli, G.; Ferrara, D.; Casellato, U. Identification of Binding Media in Paintings. *Chromatographia* **2006**, *63* (11–12), 629–631. https://doi.org/10.1365/s10337-006-0803-0.

Rice, P.M. *Pottery Analysis: A Sourcebook*, 2nd Edition; The University of Chicago Press: Chicago and London, 2015.

Roffet-Salque, M.; Regert, M.; Evershed, R. P.; Outram, A. K.; Cramp, L. J. E.; Decavallas, O.; Dunne, J.; Gerbault, P.; Mileto, S.; Mirabaud, S.; Pääkkönen, M.; Smyth, J.; Šoberl, L.; Whelton, H. L.; Alday-Ruiz, A.; Asplund, H.; Bartkowiak, M.; Bayer-Niemeier, E.; Belhouchet, L.; Bernardini, F.; Budja, M.; Cooney, G.; Cubas,

M.; Danaher, E. M.; Diniz, M.; Domboróczki, L.; Fabbri, C.; González-Urquijo, J. E.; Guilaine, J.; Hachi, S.; Hartwell, B. N.; Hofmann, D.; Hohle, I.; Ibáñez, J. J.; Karul, N.; Kherbouche, F.; Kiely, J.; Kotsakis, K.; Lueth, F.; Mallory, J. P.; Manen, C.; Marciniak, A.; Maurice-Chabard, B.; Mc Gonigle, M. A.; Mulazzani, S.; Özdoğan, M.; Perić, O. S.; Perić, S. R.; Petrasch, J.; Pétrequin, A.-M.; Pétrequin, P.; Poensgen, U.; Joshua Pollard, C.; Poplin, F.; Radi, G.; Stadler, P.; Stäuble, H.; Tasić, N.; Urem-Kotsou, D.; Vuković, J. B.; Walsh, F.; Whittle, A.; Wolfram, S.; Zapata-Peña, L.; Zoughlami, J. Widespread Exploitation of the Honeybee by Early Neolithic Farmers. *Nature* **2015**, *527* (7577), 226–230. https://doi.org/10.1038/nature15757.

Roffet-Salque, M.; Dunne, J.; Altoft, D. T.; Casanova, E.; Cramp, L. J. E.; Smyth, J.; Whelton, H. L.; Evershed, R. P. From the inside out: Upscaling Organic Residue Analyses of Archaeological Ceramics. *J. Archaeol. Sci. Rep.* **2017**, *16*, 627–640. https://doi.org/10.1016/j.jasrep.2016.04.005.

Roumie, M.; Oggiano, I.; Reslan, A.; Srour, A.; El-Morr, Z.; Castiglione, M.; Tabbal, M.; Korek, M.; Nsouli, B. PIXE Contribution for a Database of Phoenician Pottery in Lebanon. *Nucl. Instrum. Methods Phys. Res. Sect. B Beam Interact. Mater. At.* **2019**, *450*, 299–303. https://doi.org/10.1016/j.nimb.2018.08.025.

Roumpou, M.; Voskos, I.; Kalogeropoulos, N.; Mantzourani, E. Unfolding Beeswax Use in Neolithic and Chalcolithic Cyprus through Molecular Analysis of Lipids Extracted from Ceramic Containers. *Archaeol. Anthropol. Sci.* **2021**, *13* (5), 73. https://doi.org/10.1007/s12520-021-01322-3.

Roumpou, M.; Vika, E.; Hachtmann, V.; Voutsaki, S. Investigation of Consumption Practices in the Early Mycenaean Period through Biomolecular Analyses: The Case of the Ayios Vasileios North Cemetery (Laconia). *J. Archaeol. Sci. Rep.* **2023**, *48*, 103864. https://doi.org/10.1016/j.jasrep.2023.103864.

Rye, O. S. Keeping Your Temper under Control: Materials and the Manufacture of Papuan Pottery. *Archaeol. Phys. Anthropol. Oceania* **1976**, *11* (2), 106–137.

Salque, M.; Bogucki, P. I.; Pyzel, J.; Sobkowiak-Tabaka, I.; Grygiel, R.; Szmyt, M.; Evershed, R. P. Earliest Evidence for Cheese Making in the Sixth Millennium Bc in Northern Europe. *Nature* **2013**, *493* (7433), 522–525. https://doi.org/10.1038/nature11698.

Sanchez-Garmendia, U.; Iñañez, J. G.; Arana, G. Alterations and Contaminations in Ceramics Deposited in Underwater Environments: An Experimental Approach. *Minerals* **2021**, *11* (7), 766. https://doi.org/10.3390/min11070766.

Sanjurjo-Sánchez, J.; Montero Fenollós, J. L.; Polymeris, G. S. Technological Aspects of Mesopotamian Uruk Pottery: Estimating Firing Temperatures Using Mineralogical Methods, Thermal Analysis and Luminescence Techniques. *Archaeol. Anthropol. Sci.* **2018**, *10* (4), 849–864. https://doi.org/10.1007/s12520-016-0409-x.

Santacreu, D. A. *Materiality, Techniques and Society in Pottery Production: The Technological Study of Archaeological Ceramics through Paste Analysis*; De Gruyter Open Ltd: Warsaw/Berlin, 2014. https://doi.org/10.2478/9783110410204.

Sarmiento, A.; Pérez-Alonso, M.; Olivares, M.; Castro, K.; Martínez-Arkarazo, I.; Fernández, L. A.; Madariaga, J. M. Classification and Identification of Organic Binding Media in Artworks by Means of Fourier Transform Infrared Spectroscopy and Principal Component Analysis. *Anal. Bioanal. Chem.* **2011**, *399* (10), 3601–3611. https://doi.org/10.1007/s00216-011-4677-0.

Schroeder, P. A.; Erickson, G. Kaolin: From Ancient Porcelains to Nanocomposites. *Elements* **2014**, *10* (3), 177–182. https://doi.org/10.2113/gselements.10.3.177.

Schroeder, P.A. *Clays in the Critical Zone*; Cambridge University Press: Cambridge, 2018. https://doi.org/10.1017/9781316480083.

Shoda, S.; Lucquin, A.; Sou, C. I.; Nishida, Y.; Sun, G.; Kitano, H.; Son, J.; Nakamura, S.; Craig, O. E. Molecular and Isotopic Evidence for the Processing of Starchy Plants in Early Neolithic Pottery from China. *Sci. Rep.* **2018**, *8* (1), 17044. https://doi.org/10.1038/s41598-018-35227-4.

Shoval, S. Using FT-IR Spectroscopy for Study of Calcareous Ancient Ceramics. *Opt. Mater.* **2003**, *24* (1–2), 117–122. https://doi.org/10.1016/S0925-3467(03)00114-9.

Shoval, S.; Yadin, E.; Panczer, G. Analysis of Thermal Phases in Calcareous Iron Age Pottery Using FT-IR and Raman Spectroscopy. *J. Therm. Anal. Calorim.* **2011**, *104* (2), 515–525. https://doi.org/10.1007/s10973-011-1518-5.

Shoval, S. Fourier Transform Infrared Spectroscopy (FT-IR) in Archaeological Ceramic Analysis. In *The Oxford Handbook of Archaeological Ceramic Analysis*; Hunt, A., Ed.; Oxford University Press: UK, 2017; pp 509-530. https://doi.org/10.1093/oxfordhb/9780199681532.013.28.

Sing, K.S.W.; Everett, D.H.; Haul, R.A.W.; Moscou, L.; Pierotti, R.A.; Rouquérol, J.; Siemieniewska, T. Reporting Physisorption Data for Gas/Solid Systems with Special Reference to the Determination of Surface Area and Porosity (Recommendations 1984). *Pure Appl. Chem.* **1985**, 57, 603–619. https://doi.org/10.1351/ pac198557040603.

Singh, J.; Sangode, S. J.; Sabale, P. D. Mineral Magnetic and XRD Spectroscopic Studies to Investigate the Firing Temperatures of Archeological Potsherds. *J. Archaeol. Sci. Rep.* **2021**, *35*, 102759. https://doi.org/10.1016/j.jasrep.2020.102759.

Skibo, J. M. Pottery Use-Alteration Analysis. In *Use-Wear and Residue Analysis in Archaeology*; Marreiros, J. M., Gibaja Bao, J. F., Ferreira Bicho, N., Eds.; Manuals in Archaeological Method, Theory and Technique; Springer International Publishing: Switzerland, 2015; pp 189–198. https://doi.org/10.1007/978-3-319-08257-8_10.

Šoberl, L.; Horvat, M.; Žibrat Gašparič, A.; Sraka, M.; Evershed, R.; Budja, M. Neolithic and Eneolithic Activities Inferred from Organic Residue Analysis of Pottery from Mala Triglavca, Moverna Vas and Ajdovska Jama, Slovenia. *Doc. Praehist.* **2014**, *41*, 149–179. https://doi.org/10.4312/dp.41.9.

Sobott, R.; Bente, K.; Kittel, M. Comparative Porosity Measurements on Ceramic Materials. *The Old Potter's Almanack* **2014**, *19* (1), 18–25. https://doi.org/10.11588/opa.2014.1.14853.

Spataro, M.; Oras, E.; Lucquin, A.; Bērziņš, V. Hunter-Fisher-Gatherer Pottery Production and Use at the Neolithic Shell-Midden of Riņņukalns, Latvia. *Antiquity* **2021**, *95* (384), 1446–1463. https://doi.org/10.15184/aqy.2021.127.

Stacey, R. J.; Dunne, J.; Brunning, S.; Devièse, T.; Mortimer, R.; Ladd, S.; Parfitt, K.; Evershed, R.; Bull, I. Birch Bark Tar in Early Medieval England – Continuity of Tradition or Technological Revival? *J. Archaeol. Sci. Rep.* **2020**, *29*, 102118. https://doi.org/10.1016/j.jasrep.2019.102118.

Steele, V. Organic Residues in Archaeology: The Highs and Lows of Recent Research. In *ACS Symposium Series*; Armitage, R. A., Burton, J. H., Eds.; American Chemical Society: Washington, DC, 2013; Vol. 1147, pp 89–108. https://doi.org/10.1021/bk-2013-1147.ch005.

Steele, V. J.; Stern, B. Red Lustrous Wheelmade Ware: Analysis of Organic Residues in Late Bronze Age Trade and Storage Vessels from the Eastern Mediterranean. *J. Archaeol. Sci. Rep.* **2017**, *16*, 641–657. https://doi.org/10.1016/j.jasrep.2017.06.027.

Stern, B.; Heron, C.; Serpico, M.; Bourriau, J. A Comparison of Methods for Establishing Fatty Acid Concentration Gradients Across Potsherds: A Case Study Using Late

Bronze Age Canaanite Amphorae. *Archaeometry* **2000**, *42* (2), 399–414. https://doi.org/10.1111/j.1475-4754.2000.tb00890.x.

Suryanarayan, A.; Cubas, M.; Craig, O. E.; Heron, C. P.; Shinde, V. S.; Singh, R. N.; O'Connell, T. C.; Petrie, C. A. Lipid Residues in Pottery from the Indus Civilisation in Northwest India. *J. Archaeol. Sci.* **2021**, *125*, 105291. https://doi.org/10.1016/j.jas.2020.105291.

Taché, K.; Craig, O. E. Cooperative Harvesting of Aquatic Resources and the Beginning of Pottery Production in North-Eastern North America. *Antiquity* **2015**, *89* (343), 177–190. https://doi.org/10.15184/aqy.2014.36.

Tamilarasi, A.; Chandrasekaran, A. Mineralogical Analysis and Firing Temperature of the Ancient Potteries of Tamil Nadu Using Spectroscopic Techniques. *Vib. Spectrosc.* **2023**, *128*, 103584. https://doi.org/10.1016/j.vibspec.2023.103584.

Tammekivi, E.; Vahur, S.; Kekišev, O.; Van Der Werf, I. D.; Toom, L.; Herodes, K.; Leito, I. Comparison of Derivatization Methods for the Quantitative Gas Chromatographic Analysis of Oils. *Anal. Methods* **2019**, *11* (28), 3514–3522. https://doi.org/10.1039/C9AY00954J.

Tanasi, D.; Tykot, R. H.; Pirone, F.; McKendry, E. Provenance Study of Prehistoric Ceramics from Sicily: A Comparative Study between pXRF and XRF. *Open Archaeol.* **2017**, *3* (1). https://doi.org/10.1515/opar-2017-0013.

Tanasi, D.; Cucina, A.; Cunsolo, V.; Saletti, R.; Di Francesco, A.; Greco, E.; Foti, S. Paleoproteomic Profiling of Organic Residues on Prehistoric Pottery from Malta. *Amino Acids* **2021**, *53* (2), 295–312. https://doi.org/10.1007/s00726-021-02946-4.

Tarhan, İ.; Işık, İ.; Söğüt, B. Application of ATR-FTIR Spectroscopy in Tandem with Chemometrics for Assessing the Firing Conditions of Hellenistic and Roman Ceramic Shards Excavated from the Ancient City of Stratonikeia in South-Western Turkey. *Microchem. J.* **2021**, *162*, 105852. https://doi.org/10.1016/j.microc.2020.105852.

Tarhan, İ.; Derin, Z.; Çelik, B.; Öner, M.; Menteşe, Ş. A Comprehensive and Innovative Chemometric Approach: Archaeometric Analysis of the Sherds from the Neolithic Period to the Chalcolithic and Early Bronze Age with the Full Deployment of FTIR's Molecular Spectroscopic Capabilities. *Vib. Spectrosc.* **2024**, *134*, 103727. https://doi.org/10.1016/j.vibspec.2024.103727.

Thér, R.; Kallistová, A.; Svoboda, Z.; Květina, P.; Lisá, L.; Burgert, P.; Bajer, A. How Was Neolithic Pottery Fired? An Exploration of the Effects of Firing Dynamics on Ceramic Products. *J. Archaeol. Method Theory* **2019**, *26* (3), 1143–1175. https://doi.org/10.1007/s10816-018-9407-x.

Thér, R. Ceramic Technology. How to Reconstruct and Describe Pottery-Forming Practices. *Archaeol. Anthropol. Sci.* **2020**, *12* (8), 172. https://doi.org/10.1007/s12520-020-01131-0.

Tite, M. S.; Kilikoglou, V.; Vekinis, G. Strength, Toughness and Thermal Shock Resistance of Ancient Ceramics, and Their Influence on Technological Choice. *Archaeometry* **2001**, *43* (3), 301–324. https://doi.org/10.1111/1475-4754.00019.

Tite, M. S. Ceramic Production, Provenance and Use—A Review. *Archaeometry* **2008**, *50* (2), 216–231. https://doi.org/10.1111/j.1475-4754.2008.00391.x.

Trindade, M.; Dias, M.; Coroado, J.; Rocha, F. Mineralogical Transformations of Calcareous Rich Clays with Firing: A Comparative Study between Calcite and Dolomite Rich Clays from Algarve, Portugal. *Appl. Clay Sci.* **2009**, *42* (3–4), 345–355. https://doi.org/10.1016/j.clay.2008.02.008.

Trindade, M. J.; Dias, M. I.; Coroado, J.; Rocha, F. Firing Tests on Clay-Rich Raw Materials from the Algarve Basin (Southern Portugal): Study of Mineral Transformations

with Temperature. *Clays Clay Miner.* **2010**, *58* (2), 188–204. https://doi.org/10.1346/CCMN.2010.0580205.

Vahur, S.; Eero, L.; Lehtaru, J.; Virro, K.; Leito, I. Quantitative Non-Destructive Analysis of Paper Fillers Using ATR-FT-IR Spectroscopy with PLS Method. *Anal. Bioanal. Chem.* **2019**, *411* (20), 5127–5138. https://doi.org/10.1007/s00216-019-01888-x.

Vahur, S.; Kiudorv, L.; Somelar, P.; Cayme, J.-M.; Retrato, M. D. C.; Remigio, R. J.; Sharma, V.; Oras, E.; Leito, I. Quantitative Mineralogical Analysis of Clay-Containing Materials Using ATR-FT-IR Spectroscopy with PLS Method. *Anal. Bioanal. Chem.* **2021**, *413* (26), 6535–6550. https://doi.org/10.1007/s00216-021-03617-9.

Van De Velde, T.; Deschepper, E.; Mestdagh, B.; De Clercq, W.; Vandenabeele, P.; Lynen, F. Lipids, Funerals, Gifts and Feasts. Organic Residue Analysis on Merovingian Ceramics from the Elversele Burial Field (Belgium). *J. Archaeol. Sci. Rep.* **2019**, *24*, 30–38. https://doi.org/10.1016/j.jasrep.2018.12.015.

Van Doosselaere, B.; Delhon, C.; Hayes, E. Looking through Voids: A Microanalysis of Organic-Derived Porosity and Bioclasts in Archaeological Ceramics from Koumbi Saleh (Mauritania, Fifth/Sixth–Seventeenth Century AD). *Archaeol. Anthropol. Sci.* **2014**, *6* (4), 373–396. https://doi.org/10.1007/s12520-014-0176-5.

Vannoorenberghe, M.; Van Acker, T.; Belza, J.; Teetaert, D.; Crombé, P.; Vanhaecke, F. Multi-Element LA-ICP-MS Analysis of the Clay Fraction of Archaeological Pottery in Provenance Studies: A Methodological Investigation. *J. Anal. At. Spectrom.* **2020**, *35* (11), 2686–2696. https://doi.org/10.1039/D0JA00286K.

Velde, B.; Meunier, A. *The Origin of Clay Minerals in Soils and Weathered Rocks*; Springer Berlin Heidelberg: Berlin, Heidelberg, 2008. https://doi.org/10.1007/978-3-540-75634-7.

Velsko, I. M.; Overmyer, K. A.; Speller, C.; Klaus, L.; Collins, M. J.; Loe, L.; Frantz, L. A. F.; Sankaranarayanan, K.; Lewis, C. M.; Martinez, J. B. R.; Chaves, E.; Coon, J. J.; Larson, G.; Warinner, C. The Dental Calculus Metabolome in Modern and Historic Samples. *Metabolomics* **2017**, *13* (11), 134. https://doi.org/10.1007/s11306-017-1270-3.

Vieugué, J. Use-Wear Analysis of Prehistoric Pottery: Methodological Contributions from the Study of the Earliest Ceramic Vessels in Bulgaria (6100–5500 BC). *J. Archaeol. Sci.* **2014**, *41*, 622–630. https://doi.org/10.1016/j.jas.2013.09.004.

Volzone, C.; Zagorodny, N. Mercury Intrusion Porosimetry (MIP) Study of Archaeological Pottery from Hualfin Valley, Catamarca, Argentina. *Appl. Clay Sci.* **2014**, *91–92*, 12–15. https://doi.org/10.1016/j.clay.2014.02.002.

Vykukal, R.; Mavridis, F.; Tankosić, Ž. Lipid Analysis of Pottery from the Early Bronze Age II Burials at Ayia Triada Cave, Southern Euboea, Greece: Evidence for Ritualized Consumption? *Archaeometry* **2021**, *63* (6), 1342–1362. https://doi.org/10.1111/arcm.12672.

Warr, L.N. IMA-CNMNC approved mineral symbols. *Mineral. Mag.* **2021**, *85*, 291-320. https://doi.org/10.1180/mgm.2021.43.

Whelton, H. L.; Hammann, S.; Cramp, L. J. E.; Dunne, J.; Roffet-Salque, M.; Evershed, R. P. A Call for Caution in the Analysis of Lipids and Other Small Biomolecules from Archaeological Contexts. *J. Archaeol. Sci.* **2021**, *132*, 105397. https://doi.org/10.1016/j.jas.2021.105397.

Wolters, F.; Emmerich, K. Thermal Reactions of Smectites – Relation of Dehydroxylation Temperature to Octahedral Structure. *Thermochim. Acta* **2007**, *462* (1–2), 80–88. https://doi.org/10.1016/j.tca.2007.06.002.

Woolsey, C. A. Shifting Priorities Apparent in Middle and Late Woodland Ceramics from Nova Scotia. *North Am. Archaeol.* **2018**, *39* (4), 260–291. https://doi.org/10.1177/0197693118806070.

Xiao, J.; Song, Y.; Li, Y. Comparison of Quantitative X-Ray Diffraction Mineral Analysis Methods. *Minerals* **2023a**, *13* (4), 566. https://doi.org/10.3390/min13040566.

Xiao, L.; Wang, S.; Wang, Y.; Wang, B.; Ji, C.; Lin, X.; Liang, H.; Zhang, S.; Xu, X.; Dong, L. Density Functional Theory Studies on the Oleic Acid Thermal Oxidation into Volatile Compounds. *Food Chem. X* **2023b**, *19*, 100737. https://doi.org/10.1016/j.fochx.2023.100737.

Xue, H.; Dong, X.; Fan, Y.; Ma, X.; Yao, S. Study of Structural Transformation and Chemical Reactivity of Kaolinite-Based High Ash Slime during Calcination. *Minerals* **2023**, *13* (4), 466. https://doi.org/10.3390/min13040466.

Zhou, X.; Liu, D.; Bu, H.; Deng, L.; Liu, H.; Yuan, P.; Du, P.; Song, H. XRD-Based Quantitative Analysis of Clay Minerals Using Reference Intensity Ratios, Mineral Intensity Factors, Rietveld, and Full Pattern Summation Methods: A Critical Review. *Solid Earth Sci.* **2018**, *3* (1), 16–29. https://doi.org/10.1016/j.sesci.2017.12.002.

Zouridakis, N.; Tzevelekos, K. Nitrogen Porosimetry on Ancient Ceramics. *J. Eur. Ceram. Soc.* **1999**, *19* (1), 89–92. https://doi.org/10.1016/S0955-2219(98)00109-5.

SUMMARY IN ESTONIAN

Orgaanilised-anorgaanilised interaktsioonid eksperimentaalses ja arheoloogilises keraamikas

Käesoleva doktoritöö peamine eesmärk on tuvastada olulisimad faktorid ja seaduspärasused, mis mõjutavad orgaaniliste ainete, eriti lipiidide (antud juhul täpsemalt $C_{16:0\ ja}$ $C_{18:1}$ rasvhapete) säilimist arheoloogilistes savinõudes. Need faktorid on (1) pooride teke savimassiivis, mis suurendab orgaaniliste jääkide absorptsiooni, ning (2) keemiline ja mineraloogiline koostis, mis hõlmab nii esialgset savi kui ka selle lisandeid. Vastavaid mõjufaktoreid uuriti 44 erineva eksperimentaalse savibriketi abil, mis koosnesid erinevatest savidest (illiitne/illiit-smektiis ja kaoliniitsavi tüübid), erinevatest lisanditest (liiv ja lubjakivi/kriit) ja põletati kahel erineval temperatuuril (600°C ja 800°C). Valikule neist eksperimentaalsetest brikettidest lisati $C_{16:0}$ ja $C_{18:1}$ rasvhappeid, kusjuures ühe rühma puhul lasti neil adsorbeeruda ja kuivada õhu käes ilma edasise töötlemiseta (lagundamata), samas kui teist rühma lagundati 100°C juures 14 tundi, et jäljendada kuumutamisprotsessi (lagundatud materjal). Eksperimentaal-materjali analüüside tulemusi ja korrelatsioone võrreldi ja testiti kolme arheoloogilise, 12.–13. sajandi Kukruse matmispaigast pärineva arheoloogilise savinõu analüüsidega.

Eksperimentaalsete savibrikettide poorsuse analüüsi põhjal tuvastati, et mikro- ja mesopooride tekkimist mõjutab otseselt tooraine ehk savi algne poorsus, mida täiendavalt mõjutavad lisandite tüüp ja põletustemperatuurist tulenevad mineraloogilised muutused. Liiva lisandina kasutamine avaldab poorsusele vähe mõju, samas kui lubjakivi, eriti selle saviseguna põletamine 800°C juures, võib sõltuvalt illitilisest/illite-smektitilisest või kaoliniitsavist muuta mikro- ja mesopooride moodustumist olulisel määral. Need on olulised faktorid, mis mõjutavad mikro- ja mesopooride teket ja on olulised arheoloogilise keraamika kui uurimismaterjali valikul orgaaniliste jäägianalüüside kontekstis.

Valitud savibrikettidele lisatud $C_{16:0}$ ja $C_{18:1}$ rasvhappe ekstraheerimise saagis oli samuti märkimisväärselt mõjutatud savi ja täiteaine koostisest. Täpsema kvantifitseerimise eesmärgil kasutati $C_{16:0}$ ja $C_{18:1}$ rasvhapete metüülestrite (ingl. k. FAME) põhiseid kalibreerimiskõveraid. Tulemused näitavad, et küllastumata $C_{18:1}$ saagist mõjutas liiva osakaal eksperimentaalsetes brikettides, kusjuures lagundamiseksperimendis illitilise saviga toimus ka selle komponendi isomeeriseerumine. Liiva lisandina kasutamine avaldas küllastunud $C_{16:0}$ saagisele minimaalset mõju. Seevastu lubjakivi/kriidi kõrge osakaal suurendas nii $C_{16:0}$ kui ka $C_{18:1}$ sidumist savimaatriksis, sõltumata sellest, kas rasvhapped olid eksperimentaalselt lagundatud või mitte. Lagunenud $C_{18:1}$ rasvhappega proovide puhul näidati, et see komponent seondub mineraalmaatriksisse tugevamalt korrelatsioonis lisatud lubjakivi/kriidi hulgaga. See on tingitud rasvhappe kaltsiumsoolade moodustumisest, mis parandab muuhulgas lipiidide säilimist.

Töö käigus tuvastati, et peamised mineraalkomponendid, mis võivad mõjutada orgaaniliste jääkide säilimist keraamikas, on savimineraalid, liivast pärinev kvarts ja lubjakivist/kriidist pärinev $CaCO_3$. Vastavate mineraalide tuvastamiseks

kasutati ATR-FT-IR-PLS meetodit, mida kasutati Kukruse arheoloogilises keraamika kolme savinõu (Kukruse V, Kukruse XXXVIII ja Kukruse XLIII) analüüsiks. Nende savinõude proovides mõõdeti suures hulgas mikro- ja meso-poorsuse väärtusi, mis olid võrreldavad eksperimentaalsete brikettide pooride parameetritega, milles tuvastati vastavalt näiteks suurem $CaCO_3$ osakaal (Kukruse V), savi osakaal (Kukruse XXXVIII) ja liiva lisandi osakaal (Kukruse XLIII).

Kukruse proovidest $C_{16:0}$ ja $C_{18:1}$ esktraheerimise saagise kindlakstegemiseks kasutati samuti rasvhapete metüülestrite põhiseid kalibreerimiskõveraid ja leiti, et tulemused olid kooskõlas eksperimentaalbrikettidest mõõdetud tulemustega. Kukruse V, mida iseloomustab kõrgeim $CaCO_3$ sisaldus, näitas madalamat rasvhapete saagist, samal ajal kui suhteliselt suurema savisisaldusega proovide (Kukruse XXXVII ja Kukruse XLIII) rasvhapete saagised olid suuremad. Lisaks kvantifitseeriti Kukruse proovide puhul ka teisi rasvhappeid, nagu müristiin- ja steariinhape, ning ka nende saagised leiti olevat mineraloogilise koostisega korrelatsioonis.

Käesoleva uuringu tulemused näitavad, et eri liiki savide ja nende lisanditega täiendatud segude kuumutamisel toimuvad savimaatriksis erinevad mineraloogilised muutused, sealhulgas käesoleva töö seisukohast oluline mikro- ja meso-pooride teke, mis omakorda mõjutab keraamikast ekstraheeritavate $C_{16:0}$ ja $C_{18:1}$ rasvhappe saagist. Need füüsikalised ja keemilised muutused savimaatriksis ja nende mõju orgaaniliste komponentide ekstraheerimisele mõjutavad oluliselt arheoloogilise orgaanilise jäägianalüüsi proovide valikuid ja tõlgendusi ning tulevikus peaks orgaanilise jäägianalüüsi metoodikad võtma arvesse ka savimaatriksi mineroloogilise koostise mõju orgaaniliste ühendite säilimisele ja ekstraheerimise saagisele.

ACKNOWLEDGEMENTS

I would like to express my heartfelt gratitude to Dr. Ester Oras, Dr. Signe Vahur and Dr. Ivo Leito, who have been very generous with their time, expertise, and knowledge. Their patience and understanding, especially when things are not happening as planned, have meant the world for me. I am deeply grateful for their genuine concern for both my personal well-being and professional growth. Their unwavering support and encouragement made this dissertation possible, and I feel truly blessed to have them as my mentors.

Special thanks to my co-authors, Dr. Rasmus Palm, Dr. Peeter Somelar and Dr. Anu Teearu for the insightful discussions and feedback, which significantly improved my publications in this PhD journey. Thank you to my thesis opponent, Dr. Léa Drieu, for scrutinizing my work and whose publications have inspired me to tackle some of the most fundamental unanswered questions in organic residue analysis.

I also appreciate Tõiv Haljasorg and Dr. Siim Salmar for their assistance during the early stages of my GC-MS work, and to Eliise Tammekivi, who is always ready to help with any lab-related concerns.

To my Archemy family – Ester Oras, Mari Tõrv, Eve Rannamäe, Kristiina Johanson, Shidong Chen, Holar Sepp, Alessandra Morrone, Sandra Sammler, Agnes Unt, Mairi Kaseorg, Raivo Suni and Helery Hindriksoo – I am truly grateful to them for creating a welcoming and comfortable environment, for the encouragement, for fostering a sense of camaraderie, and giving me a true sense of home in Estonia.

To my friends here in Estonia – Shidong, Shrikant, Ernesto, Oey, Ngan, Vinh, Pau, Christian, Hans, Carlo, Joanna Mae – thank you for making PhD life more bearable. To my Philippine friends – Mike, Jeanne, Noy Noy, Eric, Maria, Stach, and Aldrin – I appreciate all of you for always staying in touch. To my brothers and sisters in Christ in the Philippines, who are always praying for my PhD success, my health, and my protection – Kuya Noah, Ate Doris, Ate Janely, Tita Malou, Tita Corrie, Pastor Obet, Bro. Bob, Ate Maris, Ate Nora and Pastor Ed – thank you so much.

To my lovely parents Joey and Fe, my family – Kuya Jay, Jackie, Ate Mirriam, Kiddo, Iya, and my aunt Ate Balbina, thank you for the love, support, prayers and for always being there for me. To my wonderful uyab Cha, thank you for always warming my heart and for being my source of inspiration during hard times.

I extend my deep gratitude to the Estonian Research Council for their funding (Grant PSG492, PRG1198), as well as the ASTRA project PER ASPERA Graduate School of Functional Materials and Technologies, supported by the European Regional Development Fund under the University of Tartu. Additionally, I acknowledge the Estonian Ministry of Education and Research (TK210) for their invaluable contributions. This work was carried out using the instrumentation at the Estonian Center of Analytical Chemistry (TT4, https://www.akki.ee) and Centers of Excellence, TK141 'Advanced materials and high-technology devices for energy recuperation systems'.

To my Lord and Messiah Jesus to whom "*I can do all things through Him who gives me strength and power* (Philippians 4:13)"

PUBLICATIONS

CURRICULUM VITAE

Name: Jan-Michael C. Cayme
Date of birth: August 19, 1976, Quezon City, Manila, Philippines
Citizenship: Filipino
Contact: Institute of Chemistry, University of Tartu, Ravila 14a, Tartu, 50411, Estonia
E-mail: jan-michael.cayme@ut.ee
jm.cayme@gmail.com

Education:

2020–… University of Tartu, Institute of Chemistry, Estonia, PhD student
De La Salle University-Manila, Chemistry Department, Philippines, M.Sc. in Chemistry
De La Salle University-Manila, Chemistry Department, Philippines, B.Sc. in Chemistry

Professional employment:

2020–… Team member, Archemy Lab, University of Tartu, Estonia

Research grants and scholarships:

- Doctoral scholarship from University of Tartu, Estonia

Scientific publications:

1. Vahur, S., Kiudorv, L., Somelar, P., **Cayme, J.-M.**, Retrato, M.D.C., Remigio, R.J., Sharma, V., Oras, E., Leito, I. (2021). Quantitative mineralogical analysis of clay-containing materials using ATR-FT-IR spectroscopy with PLS method. *Analytical and Bioanalytical Chemistry*, 413, 6535–6550. https://doi.org/10.1007/s00216-021-03617-9
2. **Cayme, J.-M.C.**, Palm, R., Somelar, P., Vahur, S., Leito, I., Oras, E. (2024). Influence of mineral composition and firing temperature on the micro and mesoporosity of replicate archaeological ceramics. *Clays and Clay Minerals*, 72, e13, 1–14. https://doi.org/10.1017/cmn.2024.18
3. **Cayme, J.-M.C.**, Vahur, S., Teearu, A., Oras, E., Leito, I. (2024). The impact of mineral composition on the yield and preservation of selected fatty acids in replicate archaeological ceramics. *Journal of Chemical Metrology*, 18(2), 95–113. http://doi.org/10.25135/jcm.117.2409.3336

Conference presentation:

- **Cayme, J.-M.C.**, Palm, R., Somelar, P., Vahur, S., Leito, I., Oras, E. (2023) "Influence of clay composition and firing temperature on pore formation of model pottery samples" 16th European Meeting on Ancient Ceramics (EMAC) conference at Pisa, Italy (14–16.06.12.2023). Oral presentation.

ELULOOKIRJELDUS

Nimi: Jan-Michael C. Cayme
Sünniaeg: 19. august 1976, Quezon Linn, Manila, Filipiinid
Kodakonsus: Filipiinlane
Kontakt: Tartu Ülikool keemia instituut, Ravila 14a, Tartu, 50411, Eesti
E-post: jan-michael.cayme@ut.ee
jm.cayme@gmail.com

Haridus:

2020–… Tartu Ülikool, keemia eriala doktoriõpe
De La Salle Ülikool-Manila, Keemia Osakond, Filipiinid, Magistriõpe keemia
De La Salle Ülikool-Manila, Keemia Osakond, Filipiinid, Bakalaureuseõpe keemia

Töökogemus:

2020–… Rühmaliige, Archemy labor, Tartu Ülikool, Eesti

Teadustoetused ja stipendiumid

- Tartu Ülikool doktorandistipendium.

Teaduspublikatsioonid:

1. Vahur, S., Kiudorv, L., Somelar, P., **Cayme, J.-M.**, Retrato, M.D.C., Remigio, R.J., Sharma, V., Oras, E., Leito, I. (2021). Quantitative mineralogical analysis of clay-containing materials using ATR-FT-IR spectroscopy with PLS method. *Analytical and Bioanalytical Chemistry*, 413, 6535–6550. https://doi.org/10.1007/s00216-021-03617-9
2. **Cayme, J.-M.C.**, Palm, R., Somelar, P., Vahur, S., Leito, I., Oras, E. (2024). Influence of mineral composition and firing temperature on the micro and mesoporosity of replicate archaeological ceramics. *Clays and Clay Minerals*, 72, e13, 1-14. https://doi.org/10.1017/cmn.2024.18
3. **Cayme, J.-M.C.**, Vahur, S., Teearu, A., Oras, E., Leito, I. (2024). The impact of mineral composition on the yield and preservation of selected fatty acids in replicate archaeological ceramics. *Journal of Chemical Metrology*, 18(2), 95-113. http://doi.org/10.25135/jcm.117.2409.3336

Osalemine konverentsidel:

- **Cayme, J.-M.C.**, Palm, R., Somelar, P., Vahur, S., Leito, I., Oras, E. (2023) "Influence of clay composition and firing temperature on pore formation of model pottery samples" 16th European Meeting on Ancient Ceramics (EMAC) conference at Pisa, Italy (14-16.06.12.2023). Suuline ettekanne

DISSERTATIONES CHIMICAE UNIVERSITATIS TARTUENSIS

1. **Toomas Tamm.** Quantum-chemical simulation of solvent effects. Tartu, 1993, 110 p.
2. **Peeter Burk.** Theoretical study of gas-phase acid-base equilibria. Tartu, 1994, 96 p.
3. **Victor Lobanov.** Quantitative structure-property relationships in large descriptor spaces. Tartu, 1995, 135 p.
4. **Vahur Mäemets.** The ^{17}O and ^{1}H nuclear magnetic resonance study of H_2O in individual solvents and its charged clusters in aqueous solutions of electrolytes. Tartu, 1997, 140 p.
5. **Andrus Metsala.** Microcanonical rate constant in nonequilibrium distribution of vibrational energy and in restricted intramolecular vibrational energy redistribution on the basis of slater's theory of unimolecular reactions. Tartu, 1997, 150 p.
6. **Uko Maran.** Quantum-mechanical study of potential energy surfaces in different environments. Tartu, 1997, 137 p.
7. **Alar Jänes.** Adsorption of organic compounds on antimony, bismuth and cadmium electrodes. Tartu, 1998, 219 p.
8. **Kaido Tammeveski.** Oxygen electroreduction on thin platinum films and the electrochemical detection of superoxide anion. Tartu, 1998, 139 p.
9. **Ivo Leito.** Studies of Brønsted acid-base equilibria in water and non-aqueous media. Tartu, 1998, 101 p.
10. **Jaan Leis.** Conformational dynamics and equilibria in amides. Tartu, 1998, 131 p.
11. **Toonika Rinken.** The modelling of amperometric biosensors based on oxidoreductases. Tartu, 2000, 108 p.
12. **Dmitri Panov.** Partially solvated Grignard reagents. Tartu, 2000, 64 p.
13. **Kaja Orupõld.** Treatment and analysis of phenolic wastewater with microorganisms. Tartu, 2000, 123 p.
14. **Jüri Ivask.** Ion Chromatographic determination of major anions and cations in polar ice core. Tartu, 2000, 85 p.
15. **Lauri Vares.** Stereoselective Synthesis of Tetrahydrofuran and Tetrahydropyran Derivatives by Use of Asymmetric Horner-Wadsworth-Emmons and Ring Closure Reactions. Tartu, 2000, 184 p.
16. **Martin Lepiku.** Kinetic aspects of dopamine D_2 receptor interactions with specific ligands. Tartu, 2000, 81 p.
17. **Katrin Sak.** Some aspects of ligand specificity of P2Y receptors. Tartu, 2000, 106 p.
18. **Vello Pällin.** The role of solvation in the formation of iotsitch complexes. Tartu, 2001, 95 p.
19. **Katrin Kollist.** Interactions between polycyclic aromatic compounds and humic substances. Tartu, 2001, 93 p.

20. **Ivar Koppel.** Quantum chemical study of acidity of strong and superstrong Brønsted acids. Tartu, 2001, 104 p.
21. **Viljar Pihl.** The study of the substituent and solvent effects on the acidity of OH and CH acids. Tartu, 2001, 132 p.
22. **Natalia Palm.** Specification of the minimum, sufficient and significant set of descriptors for general description of solvent effects. Tartu, 2001, 134 p.
23. **Sulev Sild.** QSPR/QSAR approaches for complex molecular systems. Tartu, 2001, 134 p.
24. **Ruslan Petrukhin.** Industrial applications of the quantitative structure-property relationships. Tartu, 2001, 162 p.
25. **Boris V. Rogovoy.** Synthesis of (benzotriazolyl)carboximidamides and their application in relations with *N*- and *S*-nucleophyles. Tartu, 2002, 84 p.
26. **Koit Herodes.** Solvent effects on UV-vis absorption spectra of some solvatochromic substances in binary solvent mixtures: the preferential solvation model. Tartu, 2002, 102 p.
27. **Anti Perkson.** Synthesis and characterisation of nanostructured carbon. Tartu, 2002, 152 p.
28. **Ivari Kaljurand.** Self-consistent acidity scales of neutral and cationic Brønsted acids in acetonitrile and tetrahydrofuran. Tartu, 2003, 108 p.
29. **Karmen Lust.** Adsorption of anions on bismuth single crystal electrodes. Tartu, 2003, 128 p.
30. **Mare Piirsalu.** Substituent, temperature and solvent effects on the alkaline hydrolysis of substituted phenyl and alkyl esters of benzoic acid. Tartu, 2003, 156 p.
31. **Meeri Sassian.** Reactions of partially solvated Grignard reagents. Tartu, 2003, 78 p.
32. **Tarmo Tamm.** Quantum chemical modelling of polypyrrole. Tartu, 2003. 100 p.
33. **Erik Teinemaa.** The environmental fate of the particulate matter and organic pollutants from an oil shale power plant. Tartu, 2003. 102 p.
34. **Jaana Tammiku-Taul.** Quantum chemical study of the properties of Grignard reagents. Tartu, 2003. 120 p.
35. **Andre Lomaka.** Biomedical applications of predictive computational chemistry. Tartu, 2003. 132 p.
36. **Kostyantyn Kirichenko.** Benzotriazole – Mediated Carbon–Carbon Bond Formation. Tartu, 2003. 132 p.
37. **Gunnar Nurk.** Adsorption kinetics of some organic compounds on bismuth single crystal electrodes. Tartu, 2003, 170 p.
38. **Mati Arulepp.** Electrochemical characteristics of porous carbon materials and electrical double layer capacitors. Tartu, 2003, 196 p.
39. **Dan Cornel Fara.** QSPR modeling of complexation and distribution of organic compounds. Tartu, 2004, 126 p.
40. **Riina Mahlapuu.** Signalling of galanin and amyloid precursor protein through adenylate cyclase. Tartu, 2004, 124 p.

41. **Mihkel Kerikmäe.** Some luminescent materials for dosimetric applications and physical research. Tartu, 2004, 143 p.
42. **Jaanus Kruusma.** Determination of some important trace metal ions in human blood. Tartu, 2004, 115 p.
43. **Urmas Johanson.** Investigations of the electrochemical properties of polypyrrole modified electrodes. Tartu, 2004, 91 p.
44. **Kaido Sillar.** Computational study of the acid sites in zeolite ZSM-5. Tartu, 2004, 80 p.
45. **Aldo Oras.** Kinetic aspects of dATPαS interaction with $P2Y_1$ receptor. Tartu, 2004, 75 p.
46. **Erik Mölder.** Measurement of the oxygen mass transfer through the air-water interface. Tartu, 2005, 73 p.
47. **Thomas Thomberg.** The kinetics of electroreduction of peroxodisulfate anion on cadmium (0001) single crystal electrode. Tartu, 2005, 95 p.
48. **Olavi Loog.** Aspects of condensations of carbonyl compounds and their imine analogues. Tartu, 2005, 83 p.
49. **Siim Salmar.** Effect of ultrasound on ester hydrolysis in aqueous ethanol. Tartu, 2006, 73 p.
50. **Ain Uustare.** Modulation of signal transduction of heptahelical receptors by other receptors and G proteins. Tartu, 2006, 121 p.
51. **Sergei Yurchenko.** Determination of some carcinogenic contaminants in food. Tartu, 2006, 143 p.
52. **Kaido Tämm.** QSPR modeling of some properties of organic compounds. Tartu, 2006, 67 p.
53. **Olga Tšubrik.** New methods in the synthesis of multisubstituted hydrazines. Tartu. 2006, 183 p.
54. **Lilli Sooväli.** Spectrophotometric measurements and their uncertainty in chemical analysis and dissociation constant measurements. Tartu, 2006, 125 p.
55. **Eve Koort.** Uncertainty estimation of potentiometrically measured ph and pK_a values. Tartu, 2006, 139 p.
56. **Sergei Kopanchuk.** Regulation of ligand binding to melanocortin receptor subtypes. Tartu, 2006, 119 p.
57. **Silvar Kallip.** Surface structure of some bismuth and antimony single crystal electrodes. Tartu, 2006, 107 p.
58. **Kristjan Saal.** Surface silanization and its application in biomolecule coupling. Tartu, 2006, 77 p.
59. **Tanel Tätte.** High viscosity $Sn(OBu)_4$ oligomeric concentrates and their applications in technology. Tartu, 2006, 91 p.
60. **Dimitar Atanasov Dobchev**. Robust QSAR methods for the prediction of properties from molecular structure. Tartu, 2006, 118 p.
61. **Hannes Hagu**. Impact of ultrasound on hydrophobic interactions in solutions. Tartu, 2007, 81 p.
62. **Rutha Jäger.** Electroreduction of peroxodisulfate anion on bismuth electrodes. Tartu, 2007, 142 p.

63. **Kaido Viht.** Immobilizable bisubstrate-analogue inhibitors of basophilic protein kinases: development and application in biosensors. Tartu, 2007, 88 p.
64. **Eva-Ingrid Rõõm.** Acid-base equilibria in nonpolar media. Tartu, 2007, 156 p.
65. **Sven Tamp.** DFT study of the cesium cation containing complexes relevant to the cesium cation binding by the humic acids. Tartu, 2007, 102 p.
66. **Jaak Nerut.** Electroreduction of hexacyanoferrate(III) anion on Cadmium (0001) single crystal electrode. Tartu, 2007, 180 p.
67. **Lauri Jalukse.** Measurement uncertainty estimation in amperometric dissolved oxygen concentration measurement. Tartu, 2007, 112 p.
68. **Aime Lust.** Charge state of dopants and ordered clusters formation in CaF_2:Mn and CaF_2:Eu luminophors. Tartu, 2007, 100 p.
69. **Iiris Kahn**. Quantitative Structure-Activity Relationships of environmentally relevant properties. Tartu, 2007, 98 p.
70. **Mari Reinik.** Nitrates, nitrites, N-nitrosamines and polycyclic aromatic hydrocarbons in food: analytical methods, occurrence and dietary intake. Tartu, 2007, 172 p.
71. **Heili Kasuk.** Thermodynamic parameters and adsorption kinetics of organic compounds forming the compact adsorption layer at Bi single crystal electrodes. Tartu, 2007, 212 p.
72. **Erki Enkvist.** Synthesis of adenosine-peptide conjugates for biological applications. Tartu, 2007, 114 p.
73. **Svetoslav Hristov Slavov**. Biomedical applications of the QSAR approach. Tartu, 2007, 146 p.
74. **Eneli Härk.** Electroreduction of complex cations on electrochemically polished Bi(*hkl*) single crystal electrodes. Tartu, 2008, 158 p.
75. **Priit Möller.** Electrochemical characteristics of some cathodes for medium temperature solid oxide fuel cells, synthesized by solid state reaction technique. Tartu, 2008, 90 p.
76. **Signe Viggor.** Impact of biochemical parameters of genetically different pseudomonads at the degradation of phenolic compounds. Tartu, 2008, 122 p.
77. **Ave Sarapuu.** Electrochemical reduction of oxygen on quinone-modified carbon electrodes and on thin films of platinum and gold. Tartu, 2008, 134 p.
78. **Agnes Kütt.** Studies of acid-base equilibria in non-aqueous media. Tartu, 2008, 198 p.
79. **Rouvim Kadis.** Evaluation of measurement uncertainty in analytical chemistry: related concepts and some points of misinterpretation. Tartu, 2008, 118 p.
80. **Valter Reedo.** Elaboration of IVB group metal oxide structures and their possible applications. Tartu, 2008, 98 p.
81. **Aleksei Kuznetsov.** Allosteric effects in reactions catalyzed by the cAMP-dependent protein kinase catalytic subunit. Tartu, 2009, 133 p.

82. **Aleksei Bredihhin.** Use of mono- and polyanions in the synthesis of multisubstituted hydrazine derivatives. Tartu, 2009, 105 p.
83. **Anu Ploom.** Quantitative structure-reactivity analysis in organosilicon chemistry. Tartu, 2009, 99 p.
84. **Argo Vonk.** Determination of adenosine A_{2A}- and dopamine D_1 receptor-specific modulation of adenylate cyclase activity in rat striatum. Tartu, 2009, 129 p.
85. **Indrek Kivi.** Synthesis and electrochemical characterization of porous cathode materials for intermediate temperature solid oxide fuel cells. Tartu, 2009, 177 p.
86. **Jaanus Eskusson.** Synthesis and characterisation of diamond-like carbon thin films prepared by pulsed laser deposition method. Tartu, 2009, 117 p.
87. **Marko Lätt.** Carbide derived microporous carbon and electrical double layer capacitors. Tartu, 2009, 107 p.
88. **Vladimir Stepanov.** Slow conformational changes in dopamine transporter interaction with its ligands. Tartu, 2009, 103 p.
89. **Aleksander Trummal.** Computational Study of Structural and Solvent Effects on Acidities of Some Brønsted Acids. Tartu, 2009, 103 p.
90. **Eerold Vellemäe.** Applications of mischmetal in organic synthesis. Tartu, 2009, 93 p.
91. **Sven Parkel.** Ligand binding to 5-HT_{1A} receptors and its regulation by Mg^{2+} and Mn^{2+}. Tartu, 2010, 99 p.
92. **Signe Vahur.** Expanding the possibilities of ATR-FT-IR spectroscopy in determination of inorganic pigments. Tartu, 2010, 184 p.
93. **Tavo Romann**. Preparation and surface modification of bismuth thin film, porous, and microelectrodes. Tartu, 2010, 155 p.
94. **Nadežda Aleksejeva.** Electrocatalytic reduction of oxygen on carbon nanotube-based nanocomposite materials. Tartu, 2010, 147 p.
95. **Marko Kullapere.** Electrochemical properties of glassy carbon, nickel and gold electrodes modified with aryl groups. Tartu, 2010, 233 p.
96. **Liis Siinor.** Adsorption kinetics of ions at Bi single crystal planes from aqueous electrolyte solutions and room-temperature ionic liquids. Tartu, 2010, 101 p.
97. **Angela Vaasa.** Development of fluorescence-based kinetic and binding assays for characterization of protein kinases and their inhibitors. Tartu 2010, 101 p.
98. **Indrek Tulp.** Multivariate analysis of chemical and biological properties. Tartu 2010, 105 p.
99. **Aare Selberg.** Evaluation of environmental quality in Northern Estonia by the analysis of leachate. Tartu 2010, 117 p.
100. **Darja Lavõgina.** Development of protein kinase inhibitors based on adenosine analogue-oligoarginine conjugates. Tartu 2010, 248 p.
101. **Laura Herm.** Biochemistry of dopamine D_2 receptors and its association with motivated behaviour. Tartu 2010, 156 p.

102. **Terje Raudsepp.** Influence of dopant anions on the electrochemical properties of polypyrrole films. Tartu 2010, 112 p.
103. **Margus Marandi.** Electroformation of Polypyrrole Films: *In-situ* AFM and STM Study. Tartu 2011, 116 p.
104. **Kairi Kivirand.** Diamine oxidase-based biosensors: construction and working principles. Tartu, 2011, 140 p.
105. **Anneli Kruve.** Matrix effects in liquid-chromatography electrospray mass-spectrometry. Tartu, 2011, 156 p.
106. **Gary Urb.** Assessment of environmental impact of oil shale fly ash from PF and CFB combustion. Tartu, 2011, 108 p.
107. **Nikita Oskolkov.** A novel strategy for peptide-mediated cellular delivery and induction of endosomal escape. Tartu, 2011, 106 p.
108. **Dana Martin.** The QSPR/QSAR approach for the prediction of properties of fullerene derivatives. Tartu, 2011, 98 p.
109. **Säde Viirlaid.** Novel glutathione analogues and their antioxidant activity. Tartu, 2011, 106 p.
110. **Ülis Sõukand.** Simultaneous adsorption of Cd^{2+}, Ni^{2+}, and Pb^{2+} on peat. Tartu, 2011, 124 p.
111. **Lauri Lipping.** The acidity of strong and superstrong Brønsted acids, an outreach for the "limits of growth": a quantum chemical study. Tartu, 2011, 124 p.
112. **Heisi Kurig.** Electrical double-layer capacitors based on ionic liquids as electrolytes. Tartu, 2011, 146 p.
113. **Marje Kasari.** Bisubstrate luminescent probes, optical sensors and affinity adsorbents for measurement of active protein kinases in biological samples. Tartu, 2012, 126 p.
114. **Kalev Takkis.** Virtual screening of chemical databases for bioactive molecules. Tartu, 2012, 122 p.
115. **Ksenija Kisseljova**. Synthesis of aza-β^3-amino acid containing peptides and kinetic study of their phosphorylation by protein kinase A. Tartu, 2012, 104 p.
116. **Riin Rebane.** Advanced method development strategy for derivatization LC/ESI/MS. Tartu, 2012, 184 p.
117. **Vladislav Ivaništšev.** Double layer structure and adsorption kinetics of ions at metal electrodes in room temperature ionic liquids. Tartu, 2012, 128 p.
118. **Irja Helm.** High accuracy gravimetric Winkler method for determination of dissolved oxygen. Tartu, 2012, 139 p.
119. **Karin Kipper.** Fluoroalcohols as Components of LC-ESI-MS Eluents: Usage and Applications. Tartu, 2012, 164 p.
120. **Arno Ratas.** Energy storage and transfer in dosimetric luminescent materials. Tartu, 2012, 163 p.
121. **Reet Reinart-Okugbeni**. Assay systems for characterisation of subtype-selective binding and functional activity of ligands on dopamine receptors. Tartu, 2012, 159 p.

122. **Lauri Sikk.** Computational study of the Sonogashira cross-coupling reaction. Tartu, 2012, 81 p.
123. **Karita Raudkivi.** Neurochemical studies on inter-individual differences in affect-related behaviour of the laboratory rat. Tartu, 2012, 161 p.
124. **Indrek Saar.** Design of GalR2 subtype specific ligands: their role in depression-like behavior and feeding regulation. Tartu, 2013, 126 p.
125. **Ann Laheäär.** Electrochemical characterization of alkali metal salt based non-aqueous electrolytes for supercapacitors. Tartu, 2013, 127 p.
126. **Kerli Tõnurist.** Influence of electrospun separator materials properties on electrochemical performance of electrical double-layer capacitors. Tartu, 2013, 147 p.
127. **Kaija Põhako-Esko.** Novel organic and inorganic ionogels: preparation and characterization. Tartu, 2013, 124 p.
128. **Ivar Kruusenberg.** Electroreduction of oxygen on carbon nanomaterial-based catalysts. Tartu, 2013, 191 p.
129. **Sander Piiskop.** Kinetic effects of ultrasound in aqueous acetonitrile solutions. Tartu, 2013, 95 p.
130. **Ilona Faustova**. Regulatory role of L-type pyruvate kinase N-terminal domain. Tartu, 2013, 109 p.
131. **Kadi Tamm.** Synthesis and characterization of the micro-mesoporous anode materials and testing of the medium temperature solid oxide fuel cell single cells. Tartu, 2013, 138 p.
132. **Iva Bozhidarova Stoyanova-Slavova.** Validation of QSAR/QSPR for regulatory purposes. Tartu, 2013, 109 p.
133. **Vitali Grozovski**. Adsorption of organic molecules at single crystal electrodes studied by *in situ* STM method. Tartu, 2014, 146 p.
134. **Santa Veikšina**. Development of assay systems for characterisation of ligand binding properties to melanocortin 4 receptors. Tartu, 2014, 151 p.
135. **Jüri Liiv.** PVDF (polyvinylidene difluoride) as material for active element of twisting-ball displays. Tartu, 2014, 111 p.
136. **Kersti Vaarmets.** Electrochemical and physical characterization of pristine and activated molybdenum carbide-derived carbon electrodes for the oxygen electroreduction reaction. Tartu, 2014, 131 p.
137. **Lauri Tõntson**. Regulation of G-protein subtypes by receptors, guanine nucleotides and Mn^{2+}. Tartu, 2014, 105 p.
138. **Aiko Adamson.** Properties of amine-boranes and phosphorus analogues in the gas phase. Tartu, 2014, 78 p.
139. **Elo Kibena**. Electrochemical grafting of glassy carbon, gold, highly oriented pyrolytic graphite and chemical vapour deposition-grown graphene electrodes by diazonium reduction method. Tartu, 2014, 184 p.
140. **Teemu Näykki.** Novel Tools for Water Quality Monitoring – From Field to Laboratory. Tartu, 2014, 202 p.
141. **Karl Kaupmees.** Acidity and basicity in non-aqueous media: importance of solvent properties and purity. Tartu, 2014, 128 p.

142. **Oleg Lebedev**. Hydrazine polyanions: different strategies in the synthesis of heterocycles. Tartu, 2015, 118 p.
143. **Geven Piir.** Environmental risk assessment of chemicals using QSAR methods. Tartu, 2015, 123 p.
144. **Olga Mazina.** Development and application of the biosensor assay for measurements of cyclic adenosine monophosphate in studies of G protein-coupled receptor signalinga. Tartu, 2015, 116 p.
145. **Sandip Ashokrao Kadam.** Anion receptors: synthesis and accurate binding measurements. Tartu, 2015, 116 p.
146. **Indrek Tallo.** Synthesis and characterization of new micro-mesoporous carbide derived carbon materials for high energy and power density electrical double layer capacitors. Tartu, 2015, 148 p.
147. **Heiki Erikson.** Electrochemical reduction of oxygen on nanostructured palladium and gold catalysts. Tartu, 2015, 204 p.
148. **Erik Anderson.** *In situ* Scanning Tunnelling Microscopy studies of the interfacial structure between Bi(111) electrode and a room temperature ionic liquid. Tartu, 2015, 118 p.
149. **Girinath G. Pillai.** Computational Modelling of Diverse Chemical, Biochemical and Biomedical Properties. Tartu, 2015, 140 p.
150. **Piret Pikma.** Interfacial structure and adsorption of organic compounds at Cd(0001) and Sb(111) electrodes from ionic liquid and aqueous electrolytes: an *in situ* STM study. Tartu, 2015, 126 p.
151. **Ganesh babu Manoharan.** Combining chemical and genetic approaches for photoluminescence assays of protein kinases. Tartu, 2016, 126 p.
152. **Carolin Siimenson**. Electrochemical characterization of halide ion adsorption from liquid mixtures at Bi(111) and pyrolytic graphite electrode surface. Tartu, 2016, 110 p.
153. **Asko Laaniste.** Comparison and optimisation of novel mass spectrometry ionisation sources. Tartu, 2016, 156 p.
154. **Hanno Evard.** Estimating limit of detection for mass spectrometric analysis methods. Tartu, 2016, 224 p.
155. **Kadri Ligi.** Characterization and application of protein kinase-responsive organic probes with triplet-singlet energy transfer. Tartu, 2016, 122 p.
156. **Margarita Kagan.** Biosensing penicillins' residues in milk flows. Tartu, 2016, 130 p.
157. **Marie Kriisa.** Development of protein kinase-responsive photoluminescent probes and cellular regulators of protein phosphorylation. Tartu, 2016, 106 p.
158. **Mihkel Vestli.** Ultrasonic spray pyrolysis deposited electrolyte layers for intermediate temperature solid oxide fuel cells. Tartu, 2016, 156 p.
159. **Silver Sepp**. Influence of porosity of the carbide-derived carbon on the properties of the composite electrocatalysts and characteristics of polymer electrolyte fuel cells. Tartu, 2016, 137 p.
160. **Kristjan Haav**. Quantitative relative equilibrium constant measurements in supramolecular chemistry. Tartu, 2017, 158 p.

161. **Anu Teearu**. Development of MALDI-FT-ICR-MS methodology for the analysis of resinous materials. Tartu, 2017, 205 p.
162. **Taavi Ivan**. Bifunctional inhibitors and photoluminescent probes for studies on protein complexes. Tartu, 2017, 140 p.
163. **Maarja-Liisa Oldekop**. Characterization of amino acid derivatization reagents for LC-MS analysis. Tartu, 2017, 147 p.
164. **Kristel Jukk**. Electrochemical reduction of oxygen on platinum- and palladium-based nanocatalysts. Tartu, 2017, 250 p.
165. **Siim Kukk**. Kinetic aspects of interaction between dopamine transporter and *N*-substituted nortropane derivatives. Tartu, 2017, 107 p.
166. **Birgit Viira**. Design and modelling in early drug development in targeting HIV-1 reverse transcriptase and Malaria. Tartu, 2017, 172 p.
167. **Rait Kivi**. Allostery in cAMP dependent protein kinase catalytic subunit. Tartu, 2017, 115 p.
168. **Agnes Heering**. Experimental realization and applications of the unified acidity scale. Tartu, 2017, 123 p.
169. **Delia Juronen**. Biosensing system for the rapid multiplex detection of mastitis-causing pathogens in milk. Tartu, 2018, 85 p.
170. **Hedi Rahnel.** ARC-inhibitors: from reliable biochemical assays to regulators of physiology of cells. Tartu, 2018, 176 p.
171. **Anton Ruzanov.** Computational investigation of the electrical double layer at metal–aqueous solution and metal–ionic liquid interfaces. Tartu, 2018, 129 p.
172. **Katrin Kestav.** Crystal Structure-Guided Development of Bisubstrate-Analogue Inhibitors of Mitotic Protein Kinase Haspin. Tartu, 2018, 166 p.
173. **Mihkel Ilisson.** Synthesis of novel heterocyclic hydrazine derivatives and their conjugates. Tartu, 2018, 101 p.
174. **Anni Allikalt.** Development of assay systems for studying ligand binding to dopamine receptors. Tartu, 2018, 160 p.
175. **Ove Oll.** Electrical double layer structure and energy storage characteristics of ionic liquid based capacitors. Tartu, 2018, 187 p.
176. **Rasmus Palm.** Carbon materials for energy storage applications. Tartu, 2018, 114 p.
177. **Jörgen Metsik.** Preparation and stability of poly(3,4-ethylenedioxythiophene) thin films for transparent electrode applications. Tartu, 2018, 111 p.
178. **Sofja Tšepelevitš.** Experimental studies and modeling of solute-solvent interactions. Tartu, 2018, 109 p.
179. **Märt Lõkov.** Basicity of some nitrogen, phosphorus and carbon bases in acetonitrile. Tartu, 2018, 104 p.
180. **Anton Mastitski**. Preparation of α-aza-amino acid precursors and related compounds by novel methods of reductive one-pot alkylation and direct alkylation. Tartu, 2018, 155 p.
181. **Jürgen Vahter**. Development of bisubstrate inhibitors for protein kinase CK2. Tartu, 2019, 186 p.

182. **Piia Liigand.** Expanding and improving methodology and applications of ionization efficiency measurements. Tartu, 2019, 189 p.
183. **Sigrid Selberg.** Synthesis and properties of lipophilic phosphazene-based indicator molecules. Tartu, 2019, 74 p.
184. **Jaanus Liigand.** Standard substance free quantification for LC/ESI/MS analysis based on the predicted ionization efficiencies. Tartu, 2019, 254 p.
185. **Marek Mooste.** Surface and electrochemical characterisation of aryl film and nanocomposite material modified carbon and metal-based electrodes. Tartu, 2019, 304 p.
186. **Mare Oja.** Experimental investigation and modelling of pH profiles for effective membrane permeability of drug substances. Tartu, 2019, 306 p.
187. **Sajid Hussain.** Electrochemical reduction of oxygen on supported Pt catalysts. Tartu, 2019, 220 p.
188. **Ronald Väli.** Glucose-derived hard carbon electrode materials for sodium-ion batteries. Tartu, 2019, 180 p.
189. **Ester Tee.** Analysis and development of selective synthesis methods of hierarchical micro- and mesoporous carbons. Tartu, 2019, 210 p.
190. **Martin Maide.** Influence of the microstructure and chemical composition of the fuel electrode on the electrochemical performance of reversible solid oxide fuel cell. Tartu, 2020, 144 p.
191. **Edith Viirlaid.** Biosensing Pesticides in Water Samples. Tartu, 2020, 102 p.
192. **Maike Käärik.** Nanoporous carbon: the controlled nanostructure, and structure-property relationships. Tartu, 2020, 162 p.
193. **Artur Gornischeff.** Study of ionization efficiencies for derivatized compounds in LC/ESI/MS and their application for targeted analysis. Tartu, 2020, 124 p.
194. **Reet Link.** Ligand binding, allosteric modulation and constitutive activity of melanocortin-4 receptors. Tartu, 2020, 108 p.
195. **Pilleriin Peets.** Development of instrumental methods for the analysis of textile fibres and dyes. Tartu, 2020, 150 p.
196. **Larisa Ivanova.** Design of active compounds against neurodegenerative diseases. Tartu, 2020, 152 p.
197. **Meelis Härmas.** Impact of activated carbon microstructure and porosity on electrochemical performance of electrical double-layer capacitors. Tartu, 2020, 122 p.
198. **Ruta Hecht.** Novel Eluent Additives for LC-MS Based Bioanalytical Methods. Tartu, 2020, 202 p.
199. **Max Hecht.** Advances in the Development of a Point-of-Care Mass Spectrometer Test. Tartu, 2020, 168 p.
200. **Ida Rahu.** Bromine formation in inorganic bromide/nitrate mixtures and its application for oxidative aromatic bromination. Tartu, 2020, 116 p.
201. **Sander Ratso**. Electrocatalysis of oxygen reduction on non-precious metal catalysts. Tartu, 2020, 371 p.
202. **Astrid Darnell.** Computational design of anion receptors and evaluation of host-guest binding. Tartu, 2021, 150 p.

203. **Ove Korjus.** The development of ceramic fuel electrode for solid oxide cells. Tartu, 2021, 150 p.
204. **Merit Oss.** Ionization efficiency in electrospray ionization source and its relations to compounds' physico-chemical properties. Tartu, 2021, 124 p.
205. **Madis Lüsi**. Electroreduction of oxygen on nanostructured palladium catalysts. Tartu, 2021, 180 p.
206. **Eliise Tammekivi.** Derivatization and quantitative gas-chromatographic analysis of oils. Tartu, 2021, 122 p.
207. **Simona Selberg.** Development of Small-Molecule Regulators of Epi-transcriptomic Processes. Tartu, 2021, 122 p.
208. **Olivier Etebe Nonga.** Inhibitors and photoluminescent probes for in vitro studies on protein kinases PKA and PIM. Tartu, 2021, 189 p.
209. **Riinu Härmas.** The structure and H2 diffusion in porous carbide-derived carbon particles. Tartu, 2022, 123 p.
210. **Maarja Paalo.** Synthesis and characterization of novel carbon electrodes for high power density electrochemical capacitors. Tartu, 2022, 144 p.
211. **Jinfeng Zhao.** Electrochemical characteristics of Bi(hkl) and micro-meso-porous carbon electrodes in ionic liquid based electrolytes. Tartu, 2022, 134 p.
212. **Alar Heinsaar.** Investigation of oxygen electrode materials for high-temperature solid oxide cells in natural conditions. Tartu, 2022, 120 p.
213. **Jaana Lilloja.** Transition metal and nitrogen doped nanocarbon cathode catalysts for anion exchange membrane fuel cells. Tartu, 2022, 202 p.
214. **Maris-Johanna Tahk.** Novel fluorescence-based methods for illuminating transmembrane signal transduction by G-protein coupled receptors. Tartu, 2022, 200 p.
215. **Eerik Jõgi.** Development and Applications of E. coli Immunosensor. Tartu, 2022, 103 p.
216. **Alo Rüütel.** Design principles of synthetic molecular receptors for anion-selective electrodes. Tartu, 2022, 109 p.
217. **Tanel Sõrmus.** Development of stimuli-responsive and covalent bisubstrate inhibitors of protein kinases. Tartu, 2022, 148 p.
218. **Oleg Artemchuk.** Autotrophic nitrogen removal processes for nutrient removal from sidestream and mainstream wastewater. Tartu, 2022, 115 p.
219. **Andre Leesment.** Quantitative studies of Brønsted acidity in biphasic systems and gas-phase. Tartu, 2023, 83 p.
220. **Meeli Arujõe-Sado.** Structural effects in aza-peptide bond formation reaction. Tartu, 2023, 83 p.
221. **Jonas Mart Linge.** Electrochemical reduction of oxygen on silver-based catalysts. Tartu, 2023, 269 p.
222. **Tõnis Laasfeld.** Integrating Image Analysis and Quantitative Modeling for a Holistic View of GPCR Ligand Binding Dynamics. Tartu, 2023, 226 p.
223. **Ernesto de Jesus Zapata Flores.** Derivatization Reagents used in negative mode electrospray LC-MS. Tartu, 2023, 107 p.

224. **Patrick Teppor.** Obtaining platinum-free oxygen reduction catalysts through biomass valorization: a case study of peat. Tartu, 2023, 161 p.
225. **Peeter Valk.** Methanol Oxidation on Platinum-Rare-Earth Metal Oxide Activated Catalysts. Tartu, 2023, 162 p.
226. **Shidong Chen.** Unravelling prehistoric plant exploitation in eastern Baltic: organic residue analysis of plant-based materials by multi-method approach. Tartu, 2023, 245 p.
227. **Yogesh Kumar.** M-N_4 macrocycle-based catalysts for electrocatalysis of oxygen reduction and oxygen evolution. Tartu, 2023, 224 p.
228. **Kerli Martin.** Recognition of carboxylates by synthetic receptors – from structure-affinity studies to solid-contact anion-selective electrode prototyping. Tartu, 2024, 130 p.
229. **Huy Quí Vinh Nguyen.** Development of Carbon Supported Pt–CeO_2 Catalysts for Proton Exchange Membrane Fuel Cells. Tartu, 2024, 198 p.
230. **Heigo Ers**. Adsorption and Structuring Processes at Single Crystal Electrode – Ionic Liquid Interface – Insights from Simulations and *in situ* Studies. Tartu, 2024, 137 p.
231. **Ritums Cepitis.** Modelling Structural and Geometrical Effects in Carbon Dioxide and Oxygen Electrocatalysis. Tartu, 2024, 99 p.
232. **Kaarel Kisand.** Resorcinol-derived carbon-based catalysts for polymer electrolyte fuel cell cathodes. Tartu, 2024, 205 p.
233. **Akmal Kosimov**. Template-assisted Mechanosynthesis (TAMS) for the production of bifunctional transition metal-based catalysts. Tartu, 2024, 123 p.
234. **Larissa Silva Macieli.** Derivatization-targeted LC-MS analysis of compounds containing amino group. Tartu, 2024, 157 p.
235. **Silvester Jürjo.** Separation of rare earth elements from Estonian phosphorite ore using liquid extraction followed by electrochemical reduction. Tartu, 2024, 99 p.